UCLA
UCLA Electronic Theses and Dissertations

Title

Functional Delivery of Proteins Using Engineered Degradable Polymeric Nanocapsules

Permalink

https://escholarship.org/uc/item/8x84m363

Author

Biswas, Anuradha

Publication Date

2013

Peer reviewed|Thesis/dissertation

UNIVERSITY OF CALIFORNIA

Los Angeles

Functional Delivery of Proteins Using

Engineered Degradable Polymeric Nanocapsules

A dissertation submitted in partial satisfaction

of the requirements for the degree Doctor of Philosophy

in Chemical Engineering

by

Anuradha Biswas

2013

ABSTRACT OF THE DISSERTATION

Functional Delivery of Proteins Using

Engineered Degradable Polymeric Nanocapsules

by

Anuradha Biswas

Doctor of Philosophy in Chemical Engineering

University of California at Los Angeles, 2013

Professor Yi Tang, Chair

Proteins have distinct intracellular roles which can have widespread therapeutic value in various biological applications. Particularly, transcription factors (TFs) are specialized proteins with the unique ability to direct cell fate which can have important applications in regenerative medicine and design of patient-specific disease models. Polymeric nanocarriers can be used to maintain protein structure and functional integrity while transporting proteins into the cytosol of cells and can be engineered to be intracellularly degradable. The development of a endoprotease-degradable intracellular protein delivery vehicle is described which draws biomimetic inspiration from natural phenomena occurring in response to the intracellular actions of furin. Both *in situ* and microemulsion polymerization were explored to synthesize degradable NCs. Furin-degradable nanocapsules (NCs) were further optimized to incorporate biologically-compatible polymers which exhibited minimal cytotoxicity in mice and human cell lines. Several nuclear and cytosolic proteins were delivered in active form to various cell lines using furin-degradable or redox-responsive NCs. NCs exhibited stability in response to protease treatment, acidic conditions and storage and high temperatures and retained encapsulated protein as well as mRNA. To demonstrate delivery of an active nuclear protein, the myogenic differentiation TF MyoD was encapsulated in NCs and delivered to myoblast cells. NC-treated cells exhibited differentiation of myoblast cells into myotubes which displayed morphological development and

activated gene expression of downstream markers. Active delivery of MyoD confirmed the ability of NCs to retain the activity of encapsulated protein to allow complex downstream actions including DNA binding and association with co-activators. For treatment of type I diabetes, the generation of pancreatic β-cells using a TF, Pdx1, is a feasible therapeutic option. Pdx1 degradable NCs were delivered to liver and exocrine pancreatic cells to induce transdifferentiation to pancreatic β-cells. Enhanced nuclear delivery and biological assays indicated functional delivery of Pdx1 to the nuclei of target cells. Morphological differences between untreated and treated exocrine cells indicated that Pdx1 delivered by NCs was able to induce changes in cells. Gene expression analysis also demonstrated slight activation of downstream β-cell markers. This work represents development of a robust polymeric nanocarrier platform for intracellular delivery and exhibits several examples of functional delivery of proteins to various cell lines.

The dissertation of Anuradha Biswas is approved.

James Liao

Tatiana Segura

Guoping Fan

Yi Tang, Committee Chair

University of California, Los Angeles

2013

Table of Contents

List of Figures and Tables

CHAPTER 1

CHAPTER 2

CHAPTER 3

Acknowledgements

There are several people that I want to thank for their continued guidance and support during my Ph.D. education. Firstly, I want to thank my Ph.D. advisor, Dr. Yi Tang, for giving me the opportunity to work on this research project. My work on intracellular protein delivery has sparked a passion for biomaterials and regenerative medicine which I hope to pursue professionally. Dr. Tang's innovation and enthusiasm have helped fuel a nascent project into a robust display of applications using developed technology. The training I have received from Dr.

ANURADHA BISWAS

EDUCATION

University of California at Los Angeles   **2008-Present**

       Ph.D. Candidate in Chemical Engineering; Expected Graduation June 2013

       M.S. in Chemical Engineering; June 2010; *GPA: 3.827/4.000*

       Thesis: Development of a Furin-Mediated Intracellular Protein Delivery System

University of Illinois at Urbana-Champaign   **2004-2008**

       B.S. in Chemical and Biomolecular Engineering; *GPA: 3.58/4.00*

       Minor in Biomolecular Bioengineering

       Thesis: Structure-Function Analysis of 2'-Oxoalkylresorcylic Acid Synthase

HONORS AND AWARDS

UCLA Graduate Division Dissertation Year Fellowship, 2012

American Association of University Women Dissertation Fellowship, 2012

AIChE Women's Initiatives Committee Travel Award, 2011

UCLA Engineering Outstanding Master's Student Departmental Award, 2010

National Science Foundation Graduate Research Fellow, 2009-2012

Merck Engineering and Technology Fellow, 2007-2008

BP America Scholarship, 2006

Proctor and Gamble Leadership Award, 2005

Intel Research Scholar, 2004-2006

UIUC Women in Engineering Scholarship, 2004

PUBLICATIONS (*: equal contribution)

6. Anuradha Biswas, Ying Liu, Tianfei Liu, Guoping Fan, Yi Tang, "Polyethylene Glycol-based Protein Nanocapsules for Functional Delivery of a Differentiation Transcription Factor" ***Biomaterials****,* 33(5459), 2012*.

5. Anuradha Biswas*, Zhen Gu*, Muxun Zhao, Yi Tang, "Tailoring Nanocarriers for Protein Intracellular Delivery" ***Chemical Society Reviews***, 40(3638), 2011 (invited manuscript).

4. Muxun Zhao, Anuradha Biswas, Biliang Hu, Kye-Il Joo, Pin Wang, Zhen Gu, Yi Tang, "Redox-Responsive Nanocapsules for Intracellular Protein Delivery" ***Biomaterials***, 32(5223), 2011.

3. Anuradha Biswas, Kye-Il Joo , Jing Liu , Muxun Zhao , Guoping Fan , Pin Wang , Zhen Gu , Yi Tang, "Endoprotease-Mediated Intracellular Protein Delivery Using Nanocapsules" ***ACS Nano***, 5(1385), 2011.

2. Zhen Gu, Anuradha Biswas, Kye-Il Joo, Biliang Hu, Pin Wang, Yi Tang, "Probing Protease Activity by Single-Fluorescent-Protein Nanocapsules" ***Chemical Communications***, 46(6467), 2010.

1. Zhen Gu, Ming Yan, Biliang Hu, Kye-Il Joo, Anuradha Biswas, Yu Huang, Yunfeng Lu, Pin Wang, Yi Tang, "Protein Nanocapsule Weaved with Enzymatically Degradable Polymeric Network" ***Nano Letters***, 12(4533), 2009.

PATENT APPLICATIONS

1. Yi Tang, Zhen Gu, Anuradha Biswas, Guoping Fan. "Endoprotease-Mediated Protein Intracellular Delivery" 2010, UCLA-Case#-014.

PROFESSIONAL AFFILIATIONS: California NanoSystems Institute (CNSI), American Institute of Chemical Engineers (AIChE), American Chemical Society (ACS), International Society for Stem Cell Research (ISSCR), Society for Biomaterials (SFB), American Association for University Women (AAUW)

<u>PRESENTATIONS AND POSTERS</u>

6. <u>Anuradha Biswas</u>, Guoping Fan, Yi Tang, "Intracellular Delivery of Transcription Factors Using Polymeric Nanocapsules" ***Society for Biomaterials. 2013 Annual Meeting***, Apr. 10-13, 2013, Boston, MA, USA. (**Oral Presentation**)

5. <u>Anuradha Biswas</u>, Guoping Fan, Yi Tang, "Intracellular Delivery of Transcription Factors Using Polymeric Nanocapsules" ***2011 AICHE Annual Meeting***, Sep. 17-21, 2011, Minneapolis, MN, USA. (**Oral Presentation**)

4. <u>Anuradha Biswas</u>, Zhen Gu, Muxun Zhao, Yi Tang, "Endoprotease-Mediated Intracellular Protein Delivery Using Nanocapsules" ***9th Annual ISSCR Meeting***, June 15-18, 2011, Toronto, Canada. (Poster)

3. <u>Anuradha Biswas</u>, Zhen Gu, Muxun Zhao, Yi Tang, "Endoprotease-Mediated Intracellular Protein Delivery" ***Society for Biomaterials, 2011 Annual Meeting***, Apr. 13-16, 2011, Orlando, FL, USA. (**Oral Presentation**)

2. <u>Anuradha Biswas</u>, Zhen Gu, Muxun Zhao, Yi Tang, "Endoprotease-Mediated Intracellular Protein Delivery Using Nanocapsules" ***241th ACS National Meeting***, Mar. 27-31, 2011, Anaheim, CA, USA. (Poster)

1. <u>Anuradha Biswas</u>, Zhen Gu, Muxun Zhao, Yi Tang, "Development of a Proteolytically Triggered Intracellular Protein Delivery System" ***2010 AICHE Annual Meeting***, Nov. 7-12, 2010, Salt Lake City, UT, USA. (**Oral Presentation**)

<u>RESEARCH EXPERIENCE</u>

Graduate Student Researcher, University of California, Los Angeles   2009-Present
Advisor: Dr. Yi Tang, Chemical and Biomolecular Engineering

- Engineered novel degradable polymeric nanocapsule for active delivery of various proteins including transcription factors and anticancer agents, characterized efficacy of delivery using chemical analysis, biological assays and imaging

- Led multidisciplinary collaborations with material scientists, bio and chemical engineers and geneticists

Undergraduate Researcher, University of Illinois, Urbana Champaign   2005-2008
Advisor: Dr. Huimin Zhao, Chemical and Biomolecular Engineering

- Performed various steps in protein engineering projects including cloning, site-directed mutagenesis, heterologous expression, protein purification and characterization of protein activity, substrate specificity and product profile

<u>Selected Technical Skills:</u> Tissue culture, DNA/RNA isolation, PCR primer construction and cloning, Transfection, Protein expression and purification, Gel electrophoresis, Fluorescence microscopy, ELISA, Immunocytochemistry, Immunohistochemistry, Chromatographic Techniques, Nanomaterial synthesis and analysis, Peptide Synthesis, Gene Expression Analysis, Statistical Analysis

<u>INDUSTRIAL EXPERIENCE</u>

Summer Intern, Merck & Co.; West Point, PA *Pharmaceutical Commercialization Dept*   **2007**

- Developed platform lyophilization process to complement monoclonal antibody formulations in early stage by compiling scientific data from various departments and presented comprehensive conclusions to the Sterile/Liquids Commercialization team

Summer Intern, PepsiCo; Barrington, IL   *Gatorade® Process Development Dept*   **2006**

- Developed basis for testing product portfolio for a cost-saving process opportunity, assessed technical feasibility hurdles, evaluated final beverage produced with the new process and presented results to upper management while answering technical questions.

1. BACKGROUND AND SIGNIFICANCE

1.1. Polymeric Nanocarriers for Intracellular Protein Delivery

Proteins are indispensable components of life as they perform essential functions such as catalysis, cellular signaling, gene regulation, and maintaining the delicate balance between cell survival and programmed death.[1] Many diseases arise from alterations in the functions of intracellular proteins.[2] Consequently, intracellular delivery of functional proteins to specific cells and organs in living organisms has significant therapeutic implications in various biological applications including disease therapies, regenerative medicine, vaccination, and imaging. [3] From a therapeutic perspective, transient protein-based delivery approaches may be safer than gene therapy due to the lack of risk of random or permanent genetic changes in transduced cells. However, most native proteins are unable to penetrate the cell membrane and often suffer from loss of function due to proteolysis or aggregation in serum.[4] Due to the tremendous potential of protein therapeutics, general methods for intracellular protein delivery are highly desirable.

The main barriers of delivering target proteins to the intracellular space result from intrinsic properties of most proteins, including the large sizes, varying surface charges and the fragile tertiary structures.[5] When administered into serum, native proteins can suffer from serum instability and can be rapidly degraded or inactivated. Most native proteins are also membrane impermeable due to electrostatic repulsions. To address these challenges, appropriate delivery vehicles for transporting proteins to the cytosol are essential, just as drug, DNA or siRNA delivery systems.[6-9] Intracellular protein delivery carriers often need to assist the protein cargo in endolysosomal escape. Figure 1 displays a schematic process of typical endocytic pathway for protein delivery vehicles. For targeted delivery to the cytosol, nuclei or mitochondria, the delivery carrier must escape the endosomal pathway to avoid

trafficking through endomembrane compartments and eventual clearance and degradation by lysosomes.[10]

Currently, the most commonly used approach for intracellular protein delivery is the genetic fusion of the target protein to protein transduction domains (PTDs) or cell-penetrating peptides
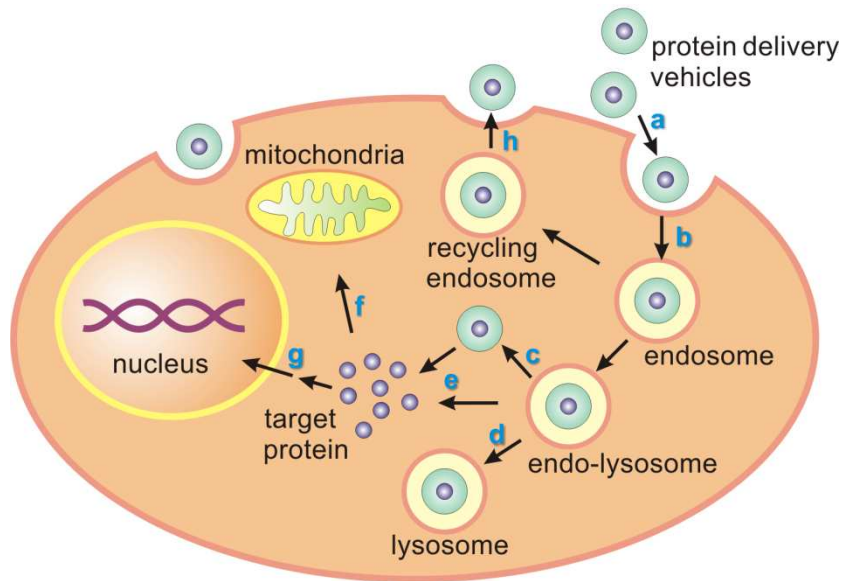
Figure 1. Schematic process of a typical endocytic pathway for nanocarriers of protein cargoes. (a) cell-surface attachment of protein delivery vehicles; (b) internalization of delivery vehicles via endocytosis; (c) endosomal escape of delivery vehicles or (d) lysosomal degradation; (e) target protein diffuses into cytoplasm; (f) transport of target proteins to specific organelle; (g) participate in cellular functions such as signal transduction; (h) exocytosis of delivery vehicles.

(CPPs), such as the HIV-1 transactivator of transcription (TAT) peptide, oligoarginines, and the *Drosophila* Antennapedia-derived penetratin peptide.[11] Commonly used PTDs are displayed in Table 1. PTDs are short peptide sequences which help penetrate the cell membrane and have been isolated from natural viruses or proteins such as the TAT peptide from HIV, as well as synthetic derivatives typically containing positively charged amino acids such as polyarginines.[12] Despite many practical advantages of the protein transduction technology, the main bottleneck of this method is the inefficient escape of protein from the endosome to the cytosol, leading to CPP-tagged proteins sequestered in intracellular vesicles.[13, 14] In several PTD systems, less than 1% of the protein cargo may be released in PTD systems and proteins often become degraded and inactive during the cellular uptake process.[15]

In the past decade, promising nanocarrier-based[6, 16] intracellular protein delivery approaches have generated considerable interest. Nanocarriers for intracellular delivery include lipid-containing colloidal systems such as liposomes and solid lipid nanoparticles,

Table 1. Protein transduction domains have been utilized for intracellular protein delivery. Representative examples of conjugation to proteins to allow intracellular delivery are mentioned.

PTD	Amino acid sequence	Examples of intracellular protein delivery
TAT$_{49-57}$	RKKRRQRRR	Hsp70-TAT treatment increased survival of NPCs in mice and decreased infarct size to 25% of the original size[17]
Penetratin	RQIKIWFQNRRMKWKK	Radiolabeled-Fab fragments conjugated to penetratin showed concentration in the spleen, adrenal gland, and liver of rats [18]
HSV VP22	DAATATRGRSAASRPT ERPRAPARSASRPRRP VE	Thymidine kinase delivery was enhanced and showed desired suicide therapy for cancer cells in cell culture [19]
Pep-1	KETWWETWWTEWSQ PKKKRKV	Pep-1-SOD1 showed improved cardiac function of the left ventricle, decreased infarct size, reduced level of malondialdehyde, creatine kinase, and lactate dehydrogenase (LDH), and decreased cardiomyocyte apoptosis in rats [20]
Polyarginine	RRRRRRRRR	R$_9$-OVA conjugates were able to effectively transduce dendritic cells and enhance antitumor immunity, and elicit complete rejection of tumors when co-administered with adjuvants [21]
Transportan	VQRKRQKLMP	Streptavidin intracellular delivery was very efficient though most protein was trapped in endosomal compartments in cell culture [22]

polymeric nanocarriers, inorganic nanoparticles/nanotubes and protein-based carriers.[23] Target protein cargos can be loaded into various polymeric nanocarriers using different strategies, including direct conjugation through either chemical or genetic modifications, physical adsorption and covalent/noncovalent encapsulation. One key role of nanocarriers is the ability to shield proteins from premature degradation and various denaturing interactions with the biological environment.[6, 24, 25] Nanocarriers can increase the stealth of the delivered protein by concealing antigenic and immunogenic epitopes and attenuating receptor-

mediated uptake by the reticuloendothelial system (RES).[26] Furthermore, nanocarriers can prevent protein proteolysis and can increase the size of the delivered cargo *in vivo,* thereby reducing renal filtration. The high surface
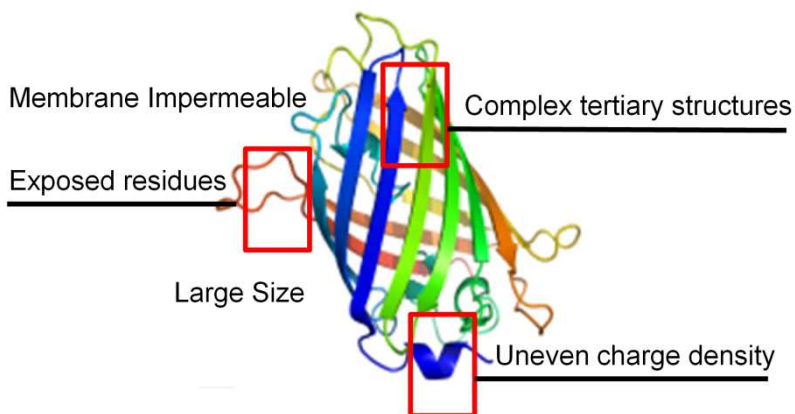
Figure 2. Challenges to delivering proteins result from inherent properties of proteins including their large size, membrane impermeability, uneven charge density and complex and exposed residues which can lead to degradation and loss of activity.

area to volume ratio of nanocarriers also leads to improved pharmacokinetics and biodistribution of payload.[6, 27, 28] Another crucial feature of polymeric nanocarrier-based delivery system is the increased flexibility of tailoring the chemical and physical properties of the vehicle through controlled synthesis, assembly, and facile biocompatible chemical modifications.[4, 29] Key particle properties such as size, surface charge and displayed ligands[30] can be customized to facilitate cell penetration and endolysosomal escape, and to optimize stability, targeting specificity and cargo release kinetics, which can address many of the challenges associated with native protein delivery as shown in Figure 2 . There are several recent methodologies developed using nanocarriers to deliver proteins intracellularly including lipid-based nanocarriers, inorganic nanocarriers, protein-mediated carriers and polymeric nanocarriers. Polymeric nanocarriers for protein delivery can be classified based on the protein loading method for nanocarrier synthesis as shown in Figure 3.

1.1.1. Direct attachment

The direct conjugation of polymers, such as poly(ethyleneglycol) (PEG), to proteins has been widely explored as a means to increase the systemic circulation of serum-based protein drugs. To date, various antibodies, cytokines and growth factors have been PEGylated[31] and the resulting polymer/protein conjugates have received Food and Drug

Administration (FDA) approval for clinical use.[32] Attachment of polymers to protein surfaces can be accomplished using well-established bioconjugation methods in literature. Reactive side chains on protein surfaces, such as amines, thiols, carboxylic acids and hydroxyl groups can all serve as the tethering site, depending on the coupling chemistry. Several methods using direct polymer attachment have also been developed to achieve intracellular delivery of target proteins.

Yamada and coworkers have widely explored intracellular protein transduction by chemically conjugating polyethylenimine (PEI) to the surface of various proteins to create cationized macromolecules.[33, 34] The authors were able to deliver a diverse array of proteins including ribonuclease (RNase), enhanced green fluorescent protein (eGFP) and IgG to the cytosol of murine and human fibroblast cells without observing significant differences in protein function. Proteins were internalized via receptor or transporter-independent endocytosis.[35] When PEI-eGFP was injected both intraportally and intraperitoneally *in vivo* in mice, cellular internalization was observed within 8 hours which was absent from mice treated with native eGFP. The system was further expanded by reversibly cationizing proteins by incorporating disulfide bonds which can reduce under cytosolic conditions. Denatured human tumor-suppressor p53 was delivered to human osteogenic sarcoma-derived Saos-2 cells through a reversibly cationized complex. Subsequent reduction of disulfide bonds in the cytosol and refolding into tetramers *in vitro* resulted in downstream intracellular events such as nuclear localization and induction of p53 target genes and eventual apotosis.[36] The authors have since extended the direct PEI-attachment system to synthesize platform protein transduction carrier molecules for biotinylated proteins or antibodies by synthesizing PEI-cationized strepatividin, avidin or protein G.[37] They showed the utility of their engineered system by delivering functional protein simian virus 40 large T-antigen (SVLT-N), which inactivates retinoblastoma family proteins, by reversible biotinylation and complexation with PEI-cationized avidin.[38] Delivery of the complex to 3T3

fibroblast cells resulted in nuclear delivery of SVLT-N, interaction with cellular machinery and subsequent induction of cell proliferation.

Lackey *et al.* constructed a model system with an antibody conjugated to a pH-sensitive poly(propylacrylic acid) (PPAAc) (Table 2), which can disrupt the endosomal membrane and aid delivery of the protein cargo to the cytosol.[39] Both the anti-CD3 antibody and the PPAAc polymer were first biotinylated, and complexed together in the presence of streptavidin. Confocal microscropy was used to determine receptor-mediated endocytosis as the mechanism of cellular internalization for both the polymer-protein complex and the antibody itself. Visualization of the internalized ternary polymer-protein complex showed

Direct Attachment   Physical Adsorption   Microemulsion-based Encapsulation

In situ Polymerization   Polymeric Micelles   Layer by Layer Encapsulation
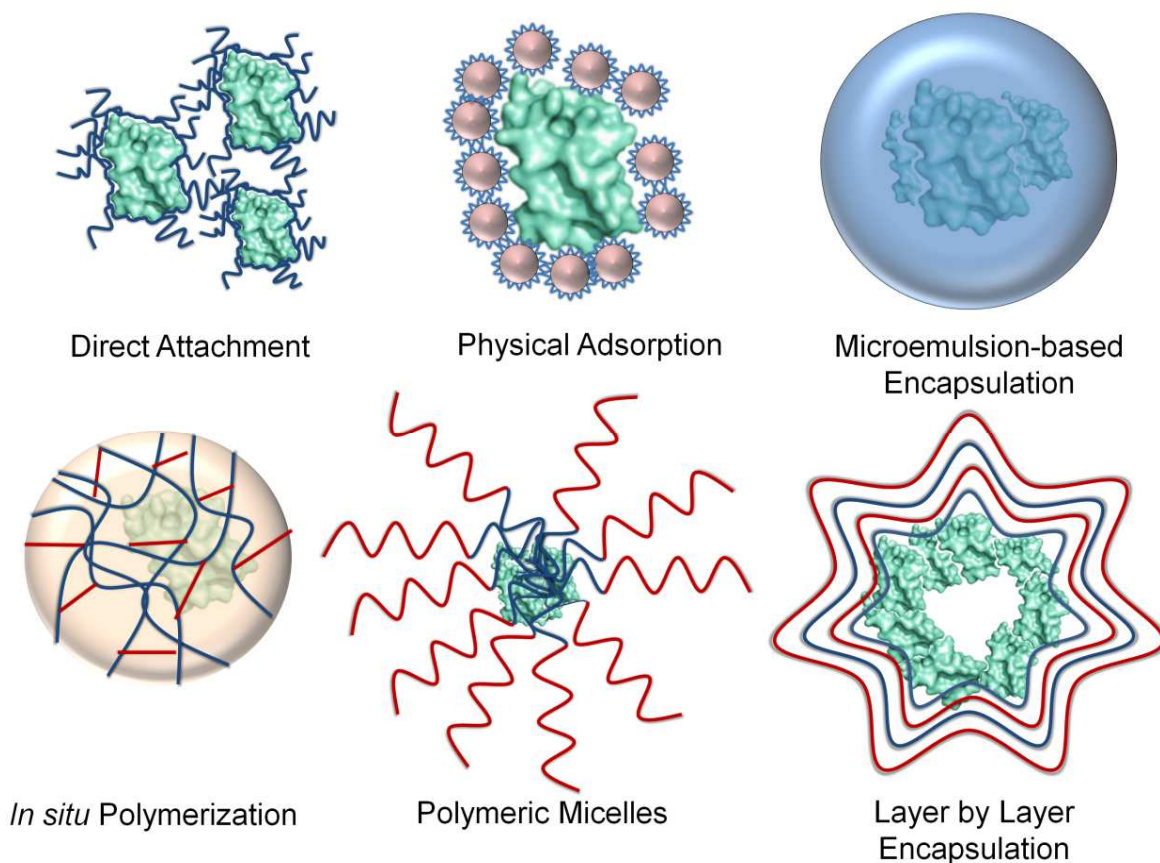
Figure 3. Schematic of various polymeric nanocarriers used for protein intracellular delivery. Nanocarriers can be classified by the synthesis method as shown above. Synthesis methods can include both covalent and non-covalent conjugation techniques to conjugate, adsorb or encapsulate target protein

6

diffuse staining in the cytosol indicating endosomal escape, whereas antibody without conjugation of PPAAc showed punctate fluorescence, indicating no release from lysosomal or endosomal compartments. Recently the authors extended this strategy *in vivo* by directly conjugating PPAAc to the model antigen ovalbumin (OVA).[40] When the conjugates were delivered *in vivo* to an EG.7-OVA mouse tumor protection model, production of specific CD8+ T lymphocytes and antiovalbumin IgG increased 8-fold and 11-fold, respectively, resulting in robust inhibition of tumor growth.

Recently, Park and coworkers used glucose-coated polymeric beads to demonstrate delivery of eGFP into mouse embryonic stem (mES) cells and HeLa cells.[41] The glucose coating was applied to establish interactions between beads and the cell membrane. The monodispersed beads with a size of ~150 nm were obtained by dispersion polymerization in the presence of 6-*O*-glucosyl methacrylate, styrene, and acrylic acid (Table 3). The protein was then conjugated to the beads using the coupling agent EDC (1-ethyl-3-(3-dimethylaminopropyl) carbodiimide). Neither native eGFP alone nor eGFP-conjugated beads without glucose coating was found to be internalized into cells. However, the eGFP-conjugated, glucose-coated beads were clearly internalized into cells as visualized by fluorescence microscopy and transmission electron microscopy (TEM). The transduction was inhibited at 4^oC, indicating that the internalization process involved an endocytic pathway.

Wagner and co-workers developed a system in which protein cargo was covalently linked to a three arm cationic oligomer polymer to assist intracellular delivery.[42, 43] The attachment polymer was developed to enhance plasmid DNA and siRNA delivery and has the sequence [C-Stp-Stp-Stp)$_2$]K-Stp-Stp-Stp-C in which K is a lysine with branching at the α,ε-amino groups, C is cysteine and Stp is an artificial amino acid.[44] For intracellular protein delivery, the authors conjugated the oligomer with a bio-reversible disulfide bond to yield positively-charged particles ~30 nm. The resulting protein carrier with precise and low

7

molecular weight exhibited cellular uptake and efficient endosomal escape of protein cargo. Nuclear eGFP and β-galactosidase were transduced with resulting respective nuclear subcellularization and enzymatic activity, indicating that the protein retained its biological function.

Zimmerman and co-workers enhanced the ability of superoxide dismutase 1 (SOD1) to be delivered across the blood brain barrier (BBB) by conjugating free amine groups on the enzyme with poly(2-oxazoline) (POx) block copolymers, P(MeOx-b-BuOx) or P(EtOx-b-BuOx), composed of (1) hydrophilic 2-methyl-2-oxazoline (MeOx) or 2-ethyl-2-oxazoline (EtOx) and (2) hydrophobic-butyl-2-oxazoline (BuOx) repeating units.[45] The conjugates formed 8 or 20 nm aggregates in aqueous solution and retained 30-50% of SOD1 activity. Conjugates did not display toxicity to neurons and were internalized through lipid raft/caveolae. Studies in mice indicated that the SOD1-POx conjugates showed increased half life and enhanced penetration to the BBB to accumulate in brain parenchyma. The conjugates maintained high stability both in the serum and brain of mice, further validating SOD1-POx conjugates as promising candidates as macromolecular antioxidant therapies for superoxide-associated diseases such as Ang II-induced neurocardiovascular disease.

1.1.2. Physical adsorption and interaction

One major disadvantage of covalent conjugation of carrier to protein is that the cargo is chemically modified, often in a nonspecific fashion. This may lead to deleterious effects on the activities of the cargo. An alternate, commonly used method without covalent modification is the self-assembly between the protein and the nanocarrier. The spontaneous assembly is typically facilitated by physical adsorption, which is driven by electrostatic forces or van der Waals interactions. For example, PEI-protein complexes were used to deliver fluorescently-labeled avidin and a functional lamin antibody to the cytosol of fibroblast cells which localized at the lamin site and induced morphological changes.[46]

Hu *et al.* have utilized emulsion polymerization to generate pH-responsive core-shell

nanostructures to load and deliver small molecules and proteins.[47] The pH-sensitive core of nanoparticles was formed by a tertiary amine monomer (2-diethylamino ethyl methacrylate (DEAEMA); pK_b ~ 7.0-7.3) (Table 3) and a crosslinker (poly(ethylene glycol) dimethacrylate (PEGDMA; pK_b ~ 11); while the pH-insensitive hydrophilic shell layer was formed by the addition of a primary amine monomer (2-aminoethyl methacrylate (AEMA)). Highly monodisperse particles were synthesized with a diameter of ~205 nm at pH 7.4. Remarkably, these particles exhibited an abrupt size change between pH 7.0 and 6.8. The diameter increased by 2.8-fold upon moving from buffer solution with pH 7.4 (extracellular/cytosolic environment) to pH 5 (endolysosomal environment) at 37°C, corresponding to a ~22-fold volume change. OVA was mixed with core-shell nanoparticles via electrostatic adsorption. After incubation of protein-containing nanoparticles with bone marrow-derived dendritic cells (BMDCs) for 1h at 37°C, fluorescently-tagged OVA was clearly observed in the cytosol and nucleus in BMDCs. As expected, DCs treated with OVA-loaded pH-responsive nanoparticles elicited 4-fold more cytokine interferon-γ (IFN-γ) secretion compared to free OVA without carriers.

Akiyoshi and coworkers demonstrated effective intracellular delivery of anionic proteins using self-assembled cationic nanogels.[48] The cationic nanogel matrix stabilized encapsulated protein molecules and prevented aggregation (Table 2). To enhance the cationic properties of the nanogel, the authors functionalized cholesteryl group-bearing pullulan (CHP) with an ethylenediamine group to form $CHPNH_2$. This in turn resulted in strong interaction with anionic FITC-BSA, and led to the formation of <50 nm nanoparticles by self-assembly in water. Flow cytometry analysis showed more efficient intracellular uptake into HeLa cells using $CHPNH_2$ nanogels compared to cationic liposomes and protein transduction domain-based carriers, both in the presence and absence of serum. Nanogels were observed to undergo macropinocytosis, escape into the cytosol, and dissociate into protein and $CHPNH_2$. Dissociation of the nanogel complex was attributed to an exchange

mechanism resulting from substitution of protein with other intracellular hydrophobic substrates. Cell viability did not decrease after 24 h incubation of 100 nM nanogels, indicating the polymer vehicle is biocompatible. Sub-cellular delivery of target protein into nuclei by CHPNH$_2$ nanogels was also demonstrated using nuclear localization signal (NLS) tagged GFP. Recently, Kiyono and coworkers extended cationic CHP nanogels to construct an intranasal antigen-delivery vehicle for adjuvant-free vaccination.[49] A non-toxic receptor-binding fragment of *C. botulinum* type-A neurotoxin subunit antigen Hc (BoHc/A) was selected as a prototype vaccine antigen. They successfully demonstrated that CHP nanogels loaded with BoHc/A continuously attached to the nasal epithelium and were effectively internalized by CD11c$^+$ dendritic cells. A strong botulinum-neurotoxin-A-specific mucosal IgA antibody and serum IgG and secretory responses was effectively induced in the absence of co-administration of the mucosal adjuvant, whereas responses were not observed in mice immunized with naked BoHc/A or control PBS. Moreover, the authors validated that [^{111}In]-labelled BoHc/A nanogels did not accumulate in the olfactory bulbs or brain, which eliminated safety concerns of the potential internalization of antigens to the central nervous system (CNS). CHP nanogels were also engineered to be degradable in acidic conditions.[50]

Zimmerman and coworkers demonstrated effective intracellular delivery of copper/zinc superoxide dismutase (CuZnSOD), which can scavenge O_2^- intermediates resulting from aberrant AngII signaling in the central nervous system in a multitude of cardiovascular diseases.[51] "Nanozymes" were created by complexing CuZnSOD with a copolymer of PEI and PEG to create polyion complexes. When the nanozymes were delivered to mouse catecholaminergic CATH neurons, the increase in O_2^- intermediates caused by AngII was significantly inhibited compared to untreated neurons or neurons treated with native CuZnSOD. When CuZnSOD nanozymes were injected *in vivo* using an intracarotid injection into rabbits along with intracerebroventricular-delivered AngII, the

responses of AngII were significantly inhibited without any toxic effects. In comparison, intracarotid injection of free CuZnSOD or PEI-PEG copolymer did not exhibit inhibition of AngII responses.

Table 2. Summary of recently reported polymeric nanocarriers for intracellular protein delivery

Types of Nanocarriers	Physical Properties	Delivered Protein	Cell Lines Used	Refs
PEI-cationized proteins through chemical conjugation	positively charged	RNase; eGFP; IgG; anti-S100C; p53; simian virus 40 large T-antigen	NIH-3T3; KMS-6; OUMS-36; HEK293; HeLa; K562; HFL-1; Saos-2	33-38
PPAAc-NH$_2$/Streptavidin		biotinylated anti-CD3 antibody	Jurkat	39
Glucose-coated beads	size: ~ 150 nm	EGFP	mES; Hela	41
Cationic oligomer-conjugated proteins	size~30 nm; positively charged	nuclear EGFP, β-Galactosidase	HeLa; 3T3; NeuroDA	42, 43
Protein-POx conjugates	size~8 or 20 nm	SOD1	CATHa, Mouse brain cells	45
PEI-self assembled protein conjugates	positively charged	Avidin, anti-lamin antibody	U87; HCA2 fibroblasts	46
Self-assembled cationic nanogels	size: ~ 20-40 nm; positively charged	BSA; β-Galactosidase; Tat-NLS-GFP; BoHc/A	CHO-K1; cos-7;NIH-3T3; HeLa; Nasal mucosal dendritic cells	48-50
Acid-degradable particles by inverse emulsion polymerization	size: 200~500 nm	OVA	RAW309.1 CR macrophage	52
Acid-degradable particles by double emulsion evaporation	size: ~250 nm	OVA	RAW309.1 CR macrophage	53, 54
PLGA particles by emulsion/solvent evaporation	size~300 nm	polyIC; OVA	mice lymph nodes	55
Single-protein nanocapsules	size: 8-20 nm; positively charged	GFP;BSA;HRP;SOD;Caspase-3; Klf4	HeLa; MCF-7; CHO; MEF	56-58
Charge-conversional polyion complex (PIC) micelles	size: ~ 50 nm; positively charged	Cytochrome c; anti-NPC mouse IgG	HuH-7	59, 60
Amphiphilic poly(amino acid) derivatives	size: 250-300 nm; negatively charged	OVA	Immature DCs	61
Layer by Layer PMA$_{SH}$ and PVPON capsules	size: ~500 nm	KP9	blood cells from simian immunodefiency virus model ex vivo	62, 63

Yang and coworkers exploited biodegradable, cationic and amphiphilic copolymer poly(*N*-methyldietheneamine sebacate)-*co*-[(cholesteryl oxocarbonylamido ethyl) methyl bis(ethylene) ammonium bromide] sebacate) (P(MDS-*co*-CES)) (Table 3) to deliver lectin A-chain, an anticancer glycoprotein.[64] The nano-complexes had an average size of ~ 150 nm and ζ-potential of ~ +30 mV. Cytotoxicity assays of lectin A-chain delivered by polymeric nanoparticles were performed towards various cell lines. The IC_{50} values were 20, 50, 40 and 100 ppm for MDA-MB-231, HeLa, HepG2 and 4T1 cells, respectively. In comparison, lipid-based BioPorter/lectin A-chain complexes showed significantly weaker cytotoxicity indicating less efficient intracellular delivery of lectin A-chain. The difference can be attributed to greater cellular uptake, stability and endosomal buffering capacity of nanoparticle/lectin A-chain complexes.

Hasadsri *et al.* utilized polybutylcyanoacrylate (PBCA) as an effective carrier to deliver specific proteins to neurons.[65] PBCA nanoparticles undergo degradation *in vivo* due to enzymatic ester hydrolysis which produces a primary alcohol, butanol, and water soluble poly(2-cyanoacrylic acid). The nanoparticles (200-250 nm) were synthesized using anionic polymerization with dextran as a stabilizer. Incubation of nanoparticles with protein led to formation of the loaded delivery vehicle via adsorption. Effective delivery of three different proteins to neuronal cultures were demonstrated: recombinant *E.coli β*-galactosidase, recombinant human Myc-tagged rhoG and anti-α-synuclein mouse monoclonal antibody H3C. Each of the three protein cargo were shown to be successfully delivered indicated by positive staining for β-gal activity, morphological changes in response to rhoG and immunostaining of α-synuclein. Notably, the nanoparticle delivery of rhoG led to neurite outgrowth and differentiation on PC12 cells after only 2 days whereas genetic transfection of rhoG required 4 days.

1.1.3. Emulsion-based encapsulation

Fréchet and colleagues have widely explored protein intracellular delivery through emulsion-based encapsulation that can degrade in the acidic environment of endosomes. Murthy *et al.* encapsulated OVA in particles sized from 200-500 nm using acrylamide as the monomer and an acid degradable crosslinker containing a hydrophilic triglyme moiety as shown in Table 3.[52] Particles were prepared using an inverse microemulsion technique where the aqueous phase (monomer, protein, and crosslinker) was dispersed via sonication in the organic phase (hexane and surfactants, Tween 80 and Span 80). After free radical initiator was added, polymerization around the protein formed water-soluble microparticles. Whereas only 10% protein was released over 5 hours at pH 7.4, 80% of encapsulated protein was released at an acidic, endosomal pH 5.0. Acid-degradable protein nanoparticles activated three times more OVA-specific cytotoxic lymphocytes after delivery to antigen presenting cells compared to native OVA and showed 75% viability at 5 mg/mL. This study demonstrated acid-degradable nanoparticles as promising carriers for protein-based vaccines. To investigate the effect of particle size on the activation of T-cells with the treatment by antigen-presenting cells, Cohen *et al.* prepared OVA particles with mean diameters of 35 nm and 3.5 μm by emulsion and microemulsion based polymerization.[66] *In vivo* studies suggested that there was no significant difference for both sizes of particles in stimulating the proliferation of T-cells and both were able to generate antigen-specific cytotoxic T-cell response upon coadministration with immunostimulatory DNA. Furthermore, the double emulsion water/oil/water evaporation method was also explored, by incorporating biocompatible and degradable polymers, such as acetalated-dextran[54, 67] and polyurethane[53] with acetal moieties. In order to achieve high cell-penetrating ability and enhance subsequent activity, protein nanoparticles were conjugated with unmethylated CpG oligonucleotide ligands[68] or cell-penetrating peptides[67, 69].

Irvine and co-workers also utilized emulsion methods to fabricate nanoparticles for intracellular delivery. Emulsion-solvent evaporation was used using lipids as surfactants for particle synthesis to yield lipid-containing biodegradable poly(D,L-lactide-co-glycolide PLGA particles.[55, 70] PLGA nanoparticles ~300 nm were loaded with the Toll-like receptor-3 ligand poly(inosinic:cytidylic acid) (polyIC) and were injected into the lymph nodes of mice. Intranodal injection of the PLGA nanoparticles were able to increase the persistance of polyIC in lymph nodes, thereby increasing the accumulation of Toll-like receptor agonist in lymph node resident antigen presenting cells and increase activation of dendritic cells. When coupled with ovalbumin as an adjuvant, PLGA-polyIC particles enhanced the humoral response and expanded OVA-specific T cells.

Generally, microencapsulation techniques require multiple steps that may deteriorate protein stability and activity, including exposure to organic and aqueous interfaces, shear stress during homogenization of phases, and lyophilization. To combat these issues, Diwan *et al.* enhanced protein stability during encapsulation in PLGA microspheres by PEGylating the surface amine groups of lysozyme with methoxy-polyethylene glycol succinimidyl succinate.[71] PEGylated lysozyme formed less aggregates during the encapsulation process and exhibited a near complete, sustained release of protein over 85 days compared to native lysozyme which suffered aggregation and a 65% burst release *in vitro*. Utama *et al.* also aimed to modify the emulsion nanoparticle synthesis to avoid denaturation of the protein by radicals.[72] A reverse mini-emulsion procedure was used to fabricate hollow polymeric nanoparticles with methyl methacrylate monomer and ethylene glycol dimethacrylate crosslinker using periphery RAFT polymerization to ensure that the protein remained within the reaction-free aqueous phase. The ~200 nm nanoparticles showed spherical structure and displayed controlled release of encapsulated BSA over three days.

1.1.4. *In situ* polymerization

Different from emulsion-assisted encapsulation, *in situ* polymerization-based

encapsulation occurs on the surface of core materials, similar to interfacial polymerization. Yan *et al.* have developed an intracellular delivery strategy based on nanocapsules that consist of a single-protein core and thin polymer shell anchored covalently to the protein core.[56] Briefly, polymerizable vinyl groups are covalently linked to the protein; subsequently, polymerization is performed in an aqueous solution containing monomers and crosslinker to wrap each protein core with a thin polymer shell that can protect the protein content from denaturation and proteolysis. This scheme enabled the synthesis of protein nanocapsules with non-degradable or degradable shells by using non-degradable or degradable crosslinker (Table 3), respectively. TEM and AFM images of horseradish peroxidase (HRP) indicated these nanocapsules were spherical with uniform diameter around 15 nm. By labeling each HRP molecule with a single 1.4 nm gold nanoparticle, most nanocapsules observed contained only one single gold nanoparticle, further confirming a single-protein core-shell structure. Nanocapsules encapsulating a wide variety of reporter and functional proteins including eGFP, HRP, BSA, superoxide dismutase (SOD), and caspase-3. Non-degradable nanocapsules exhibited long-term intracellular stability while degradable nanocapsules dissociated in the acidic environment in the endosome. The cells treated with eGFP nanocapsules showed significantly higher fluorescence intensity than those with native eGFP and TAT-fused eGFP. Further cellular internalization studies suggested that the eGFP nanocapsule uptake was through a clathrin/caveolae-mediated endocytosis pathway. The authors also demonstrated *in vivo* stability of nanocapsules. eGFP nanocapsules remained intense fluorescence even 50 h after injection to nude mice, while HRP nanocapsules showed enzymatic activity 8 h after injection. Recently, Du *et al.* utilized the "single protein nanocapsule" concept to encapsulate HRP and decorate the polymeric shell of nanocapsules with quantum dots (QDs) for a bioluminescence study.[73] The bioluminescence generated from HRP-mediated oxidation of luminol can well-overlap with the absorbance wavelengths of QDs, which enables their effective bioluminescence

15

resonance energy transfer (BRET). The maximum BRET efficiency can be achieved by adjusting the enzyme/QD conjugation ratio. Furthermore, Gu *et al.* developed a fluorescence resonance energy transfer (FRET)-based protease detection strategy, using a single-fluorescent-protein nanogel as donor and a dark quencher as acceptor linked by a photolabile caged-peptide.[74] Utilizing caspase-3 as a target protease, the authors demonstrated this design can be used for on-demand probing of protease activity within cells in a UV-responsive fashion.

Gu and Tang *et al.* conceived a new approach for preparation of single protein nanocapsules in which the protein was encapsulated by an enzymatically degradable polymeric network.[57] Instead of irreversible, pre-modification of protein surface, the protein cargo was reversibly encapsulated within a thin polymer shell through physical adsorption of monomers/crosslinkers and followed *in situ* polymerization. The crosslinker that interconnected the polymeric matrix was a peptide linker that can be cleaved by a specific
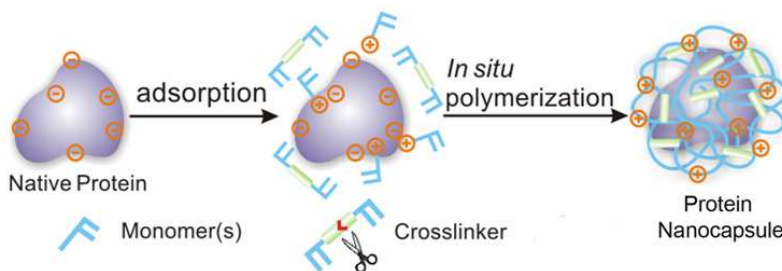
Figure 4. Schematic diagram of protein nanocapsule synthesis as described by Gu and Tang, 2009. Protein nanocapsules were prepared using *in situ* free radical polymerization in a "one-pot" fashion.

protease. Caspase-3 was selected as the model protein and bisacrylated peptide crosslinker containing Asp-Glu-Val-Asp (DEVD), which is the substrate of caspase 3, was used to synthesize a self-degradable nanocapsule. The self-degradation progress was monitored in cell-free systems to occur at 37℃ compared to negligible degradation at 4℃. Degradable nanogels were shown to induce apoptosis when delivered to a variety of mammalian cells in comparison to nanogels constructed with non-degradable crosslinker or native protein. To

achieve a spatiotemporal control of caspase-3 nanocapsule degradation, the P1 aspartic acid was conjugated to a photolabile *o*-nitrobenzyl ester moiety. Only after decaging of the aspartic acid was caspase-3 able to recognize the peptide substrate and cleave the polymeric shell. In comparison, cells treated with only caspase-3 nanocapsules without UV or cells treated with only UV did not show significant cell death. Nanocapsules for intracellular protein delivery were generalized through engineered crosslinkers including a redox-responsive moeity[75] as well as an endoprotease-degradable crosslinker, which will be discussed in more detail later.

1.1.5. Polymeric micelles

In 2009, Lee *et al.* reported a new delivery strategy based on 50 nm core-shell structured polyionic complex (PIC) micelles, which are formed via electrostatic interactions. Block copolymers were synthesized to incorporate both ionic and neutral regions and were subsequently allowed to associate with counterions of the charged region thereby creating micelles.[59] In this study, the cationic protein cytochrome *c* was modified with citraconic and *cis*-aconitic anhydrides to invert the surface charge and subsequently decrease the pI value. Next PIC micelles were formed between charge-inverted cytochrome *c* and cationic block copolymer PEG-pAsp(DET) (Table 3). The micelles displayed a charge-conversional property since citraconic amides and *cis*-aconitic amides are stable at the physiological pH 7.4 but dissociate at endosome pH 5.5. PIC micelles showed efficient cytochrome *c* endosomal escape and subsequent diffusion to cytosol compared to non-charge-conversion control micelles which contained succinic amide modifications. The authors also demonstrated that the activity of cytochrome *c* was not compromised upon modification of the surface amine groups. This method demonstrated a stable PIC micelle protein delivery system without the use of cross-linking. Most recently, the authors have extended this technique to deliver a bioactive antibody, anti-NPC (nuclear pore complex) mouse IgG to

human hepatoma cells.[60] They confirmed that the charge-conventional PIC micelles can successfully deliver IgG into cytosol and the IgG recognition toward NPC was highly retained, further promoting applications in cellular imaging and therapeutic targeting of specific antigens. Murthy and co-workers used PIC micelles composed of the block copolymer PEG-poly(L-lysine-dithiopyridine) (PEG-PLDTP) which is grafted with dithiopyridine groups.[76] The resulting core-shell micelles were then cross-linked with a dithiol thereby generating degradable disulfide-crosslinked polyion micelles (DCPM). A model vaccine formulation of OVA and immunostimulatory CpG-DNA protein was incorporated into DCPMs and yielded stable nanoparticles ~50-100 nm. The enzyme catalase was encapsulated in DPCMs and confirmed the ability of PIC micelles to preserve enzyme activity in the core.

Polymeric micelles were also synthesized by Kim *et al.* in which a positively-charged di-block copolymer conjugate of poly(L-lysine)-poly(ethylene glycol)-folate (PLL-PEG-FOL) was complexed to negatively charged FITC-BSA (Table 3).[77] This method targets specific cells which possess a folate receptor which is a marker for several cancers and could be used for tumor-selective drug delivery. Intracellular uptake was greatly enhanced for the 25 nm complexes made using PLL-PEG-FOL compared to PLL-PEG. To confirm the uptake was due to folate receptor mediated endocytosis, a folate receptor deficient cell line (A549) and folate overexpressing line (KB) were compared. The comparative study showed only an enhanced cellular uptake for the KB cell line upon complexation of FITC-BSA and PLL-PEG-FOL versus PLL-PEG or native FITC-BSA.

Akagi *et al.* selected biodegradable poly(γ-glutamic acid) (γ-PGA) (Table 3) to deliver target proteins.[61] The β-carboxylate side chains of γ-PGA were modified with hydrophobic amino acid derivatives such as L-phenylalanine ethylester and L-tryptophan methylester. The resulting block copolymer was added to an equal volume of hydrophilic OVA or

18

recombinant human immunodeficiency virus-1 gp120 to create 250-300 nm protein-loaded nanoparticles. When γ-PGA-gp120 nanoparticles were delivered intranasally to mice, antigen-specific immune responses were detected through induction of IFN-γ -producing splenocytes and antigen-specific CTL activity.

<u>1.1.6. Layer-by-layer encapsulation</u>
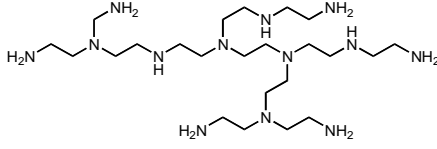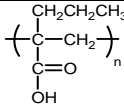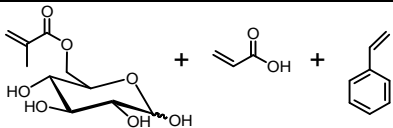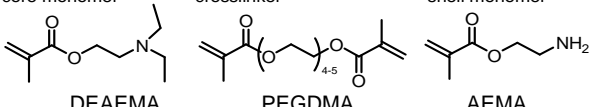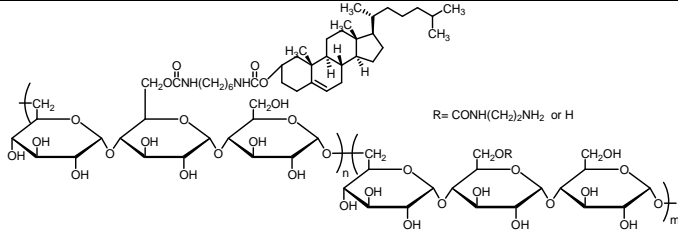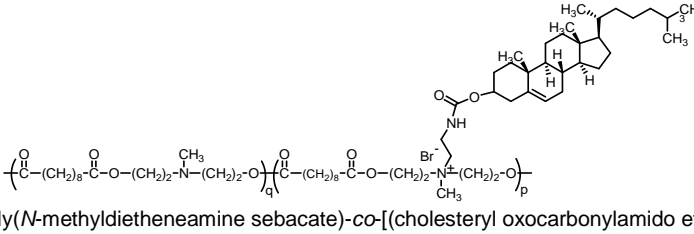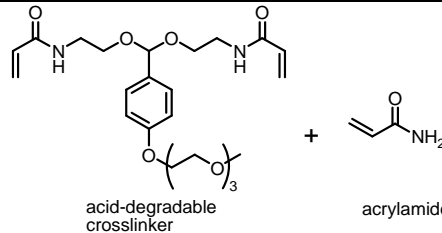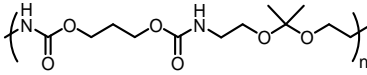
Layer-by-layer (LbL) encapsulation is based on the consecutive adsorption of oppositely charged polyelectrolytes around a sacrificial template core, which is followed by chemically dissolution. De Rose *et al.* applied the LbL strategy to load nanoengineered capsules with an oligopeptide vaccine (KP9 epitope).[63] The pair of polyelectrolytes included biodegradable thiolatedpoly(methacrylic acid) (PMA$_{SH}$) and poly(vinylpyrrolidone) (PVPON). The cysteine modified KP9 was first conjugated to PMA$_{SH}$ through disulfide linkage, which can be cleaved inside cells for release of KP9. The resulting KP9 carried polymer was adsorbed onto the amine-grafted silica template particles. PVPON and PMA$_{SH}$ were then alternately assembled. Finally, KP9 encapsulated hollow particles were formed upon the removal of the template. The authors demonstrated that the intracellular delivery of KP9 capsules stimulated a significant proportion of the KP9-specific CD8 T cells, which simultaneously expressed cytokines of IFN-γ and TFN-α. The authors further optimized the LbL capsules to deliver to APCs and demonstrated specific activation of CTLs in a non-human primate model of simian immunodeficiency virus infection *ex vivo.*[62]
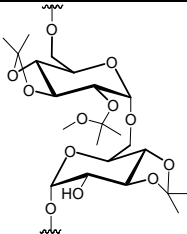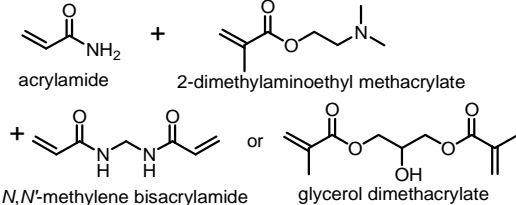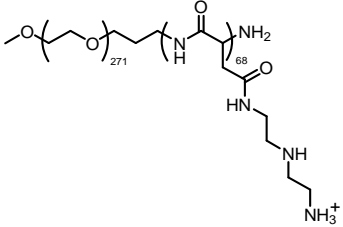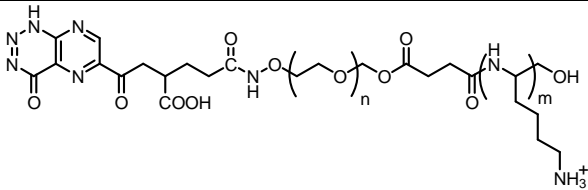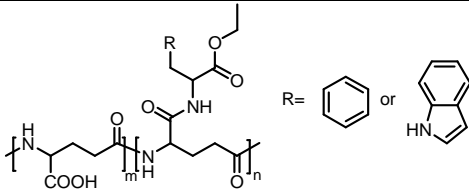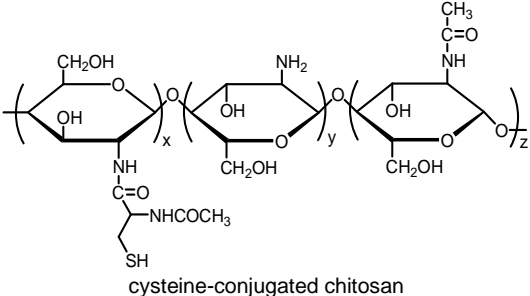
Using the LbL method, Parak and coworkers developed enzymatically degradable capsules for OVA delivery.[78] CaCO$_3$ particles coprecipitated with BODIPY dye conjugated OVA were selected as the core template. Two bilayers, dextran sulfate/ poly-L-arginine (DEXS/pARG) and sodium poly(styrenesulfonate)/ poly(allylamine hydrochloride) (PSS/PAH) were selected to form degradable and nondegradable shells respectively. Because of the close proximity of dye molecules, the green fluorescence of BODIPY was self-quenched in the

capsule cavity and displayed red excimers. The authors presented that in the case of nondegradable capsules delivered towards embryonic NIH/3T3 fibroblasts, such red emission remained over incubation periods up to several days. In contrast, when using biodegradable DEXS/pARG capsules, the self-quenching of dyes was relieved and bright green emission appeared, indicating effective release of proteins upon harnessing of intracellular enzymes.

Recently, Shu *et al.* employed gradient shell cross-linked hollow polyelectrolyte nanocapsules for protein intracellular delivery.[79] The protein loaded polymeric outer shell consisting of dextran sulfate and chitosan decorated with cysteamine was formed by four steps: 1) loading target protein to the β-cyclodextrin functionalized silica spheres through physical adsorption; 2) LbL assembling polymers (Table 3) on silica spheres; 3) cross-linking thiols to generate polymeric matrix; and 4) removal of silica core-based templates. The authors demonstrated this disulfide bond gradient cross-linked nanocapsules had both reduction and pH sensitivity. Using BSA as a model protein, the release of protein from nanocapsules was performed in the buffer solution of pH 1.4 (simulating the pH in the stomach) and 6.8 (simulating the extracellular pH). The authors demonstrated that the cross-linked nanocapsules can remain stable in physiological pH levels and protect the loss of protein in the gastric cavity. It is noteworthy that this approach can not only reduce the loss of protein in acidic environments, but also achieve the sustained release of protein in the cytosol.

Table 3. Selected polymers and monomers used for polymeric nanocarriers used for protein delivery

Loading Methods	Polymer or Monomers	Ref.
Direct attachment	polyethyleneimine (PEI)	33
	poly(propylacrylic acid) (PPAAc)	39
	6-*O*-glucosyl methacrylate, acrylic acid and styrene	41
Physical adsorption	core monomer DEAEMA, crosslinker PEGDMA, shell monomer AEMA	47
	cholesteryl group-bearing pullulans (CHPNH$_2$) R= CONH(CH$_2$)$_2$NH$_2$ or H	48
	Poly(*N*-methyldietheneamine sebacate)-*co*-[(cholesteryl oxocarbonylamido ethyl) methyl bis(ethylene) ammonium bromide] sebacate) (P(MDS-*co*-CES))	64
Microemulsion -based encapsulation	acid-degradable crosslinker + acrylamide	52
	Polyurethane with acetal	53

Acetyl-derivatized dextran | 54 |
| *In situ* polymerization |

acrylamide   2-dimethylaminoethyl methacrylate

N,N'-methylene bisacrylamide   glycerol dimethacrylate | 56 |
| Polymeric micelles |

polyethylene glycol-poly(*N*-[*N'*-(2-aminoethyl)-2-aminoethyl]aspartamide) (PEG-pAsp(DET)) | 59 |
| |

poly(L-lysine)-poly(ethylene glycol)-folate (PLL- PEG-FOL) | 77 |
| |

(*γ*-PGA)-poly(L-phenylalanine ethylester) or (*γ*-PGA)-poly(L-tryptophan methylester) | 61 |
| Layer-by-layer encapsulation |

cysteine-conjugated chitosan | 79 |

1.2. Transcription Factor-Mediated Cell Therapy

Transcription factors (TFs) are modular proteins that include one or more DNA binding domains capable of attaching to specific sequences and regulating transcription of specific genes.[80, 81] As such, TFs are the primary regulatory components of cells and can determine the expression of all genes, including those imperative for cellular development and cell cycle control. The expression of specific TFs is also regulated by elaborate control mechanisms in response to different intracellular and extracellular signals.[82, 83] The discovery that the diversity of different cell lineages can result from the varying combinations of TF expression has enormously impacted the field of regenerative medicine, which aims to replace diseased cells with healthy, functional cells of the same type. [84, 85]

<u>1.2.1. Delivery of TFs for pluripotency</u>

Embryonic stem cells (ESCs) are cells which derive from the inner cell mass of an early-stage embryo or blastocyst.[86] ESCs are pluripotent, meaning that they possess the ability to differentiate into cells of all three germ layers: the endoderm, mesoderm and ectoderm which make up all cell types in the human body. Furthermore, ESCs have the ability for indefinite self-renewal in specific conditions which allows expansion to many cells *in vitro.*[87] Due to their unlimited self-renewal and pluripotent properties, ESCs have widespread therapeutic potential for research applications and regenerative therapies.[88] For example, ESCs have been used to derive healthy cell types to treat diseases such as Parkinson's[89], diabetes[90], muscular dystrophy[91] and sickle cell anemia[92], to name a few. However, ethical concerns regarding the source of embryonic stem cells have plagued the advancement of research.[93] Embryos reach the blastocyst stage 4 to 5 days after being fertilized; as a result, isolating the ESCs from the inner cell mass of the blastocyst results in destruction of a fertilized human embryo, thereby raising ethical and moral issues.

For these reasons, the discovery that terminally differentiated cells can be reprogrammed into induced pluripotent stem (iPS) cells using ectopic expression of four specific

TFs has shown great promise for medical applications while avoiding the ethical controversies associated with ESCs.[94] The first production of iPS cells were obtained by exogenous delivery of four TFs, *Oct4, Sox2, Klf4* and *c-Myc,* into mouse embryonic or adult fibroblast cells which then displayed the capability to differentiate into healthy functional cells of all three germ layers.[95] The generation of iPS cells suggested the possibility of disease and patient-specific regenerative medicine therapies. That is, iPS cells created from a patient and subsequently differentiated into specific cell types for disease therapy could avoid immunological rejection, a primary concern arising from transplantation with ESCs.[96] Furthermore, iPS cells can serve as a powerful means to create disease models in culture and to screen the efficacy and safety of drugs. Since the first discovery of iPS cells, researchers displayed the ability of iPS cells to form adult cells when injected into mouse embryos.[97-99] The first human iPS cells were soon generated by three research groups[100-102] and were followed by iPS cell formation from a variety of human tissues including neurons,[103, 104] stomach and liver,[105] pancreatic[106] and immune
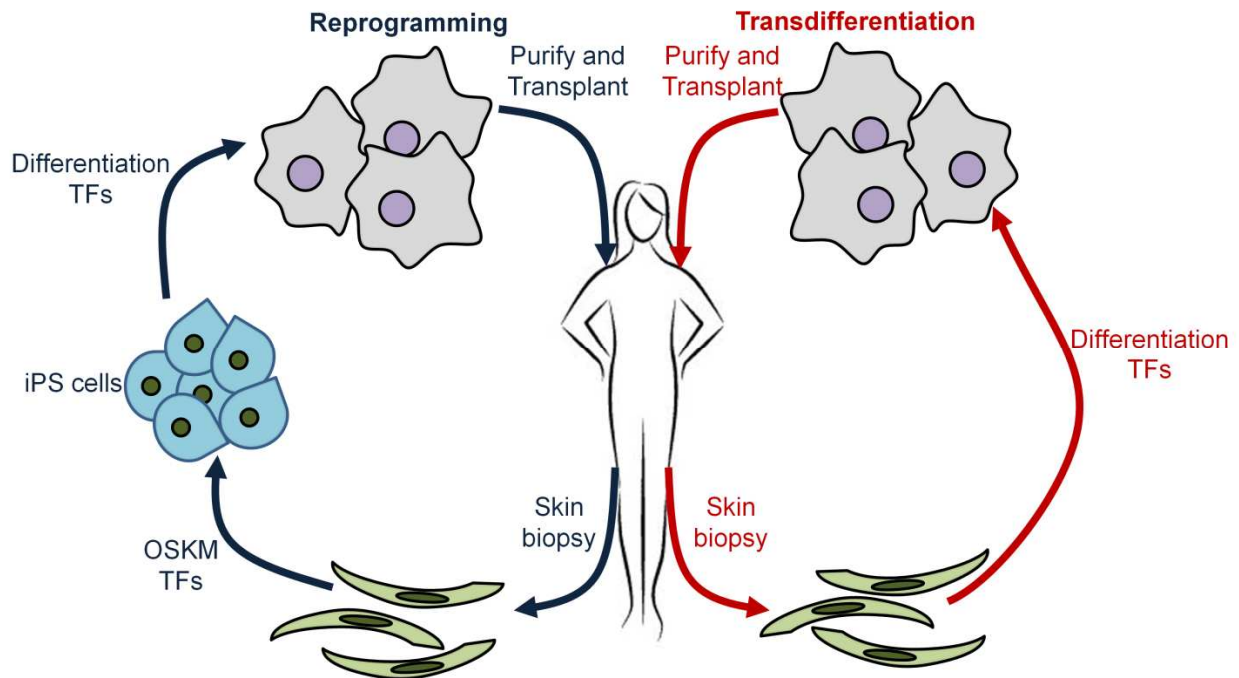
Figure 5. Schematic demonstrating patient-specific therapy process for reprogramming and transdifferentiation. Skin cells extracted from the patient can be reprogrammed into induced pluripotent (iPS) cells for subsequent differentiation into target cells such as macrophages. Macrophages can then be transplanted into the patient's lymph nodes. In transdifferentiation, skin cells can be directly differentiated into macrophages with specific TFs that can be transplanted into the patient.

cells.[107] Several additional TFs and small molecules which can enhance the efficiency and formation of iPS cells have also been identified.[108] Scientists have used iPS cells to cure mice with sickle cell anemia[109], Parkinson's disease[110] and hemophilia[111]. Models to study diseases such as amyotrophic lateral sclerosis, Huntington's disease, spinal muscular atrophy and type I diabetes have been created[112-114] as well as fully three dimensional intestinal tissue models[115]. In one landmark study, researchers used reprogrammed cells to produce living mice by transplanting iPS cells into the embryo of mother mice.[116]

Despite the abundance of promising studies to promote iPS cells as tools to treat and study diseases, there are several studies suggesting that iPS cells and ES cells are significantly different despite their similar phenotypes. ES and iPS cells have varying gene expression,[117, 118] differentiation[119] and proliferation[120] profiles as well as differences in disease modeling[121]. It is difficult to reprogram certain cells into iPS cells and erase epigenetic memory from the original cell type.[122, 123] Furthermore, the generation of iPS cells remains lengthy, complex and expensive, posing a challenge for large scale cell therapies. Evaluation of lab-generated iPS cells remains a source of discussion as criteria can vary between various laboratories.[108] Additionally, difficulties with transplantation of iPS cells into the body and efficient integration of the generated tissue without generation of tumors remains challenging. A method to circumvent these issues is to directly reprogram differentiated cells into different lineages by using transdifferentiation.

1.2.2. TF delivery for Transdifferentiation of Cells

Transdifferentiation refers to the process in which differentiated adult cells of one type are directly and efficiently converted into functional cells of another type, excluding the need to reprogram cells into a pluripotent state first.[84] Several studies have demonstrated transdifferentiation of cells to convert cell lineages producing cells relevant for treatment of various diseases which could be used for creating disease models, studying TF action and lineage determination and patient-specific cell transplantation. In addition, cell division is not

required for direct lineage conversion as is the case with iPS cell reprogramming. In addition to one less step in the conversion process, cell transdifferentiation is much faster, has higher efficiency and allows screening of numerous individuals in contrast to iPS cell reprogramming. The differences between cell reprogramming and transdifferentiation are outlined in Figure 5.

TFs can be ectopically introduced into cells to induce transdifferentiation into different cell types. Specific TFs can also dedifferentiate cells into immature forms as evidenced by the demyelination of Schwann cells when *c-Jun* expression is increased, thereby allowing cell proliferation for replacement of damaged cells after nerve injuries [124, 125]. Key TFs for transdifferentiation from different cell lineages have been identified as shown in Table 4. The first example of transdifferentiation occurred from the muscle TF, *MyoD* which was able to convert fibroblasts into muscle cells.[126, 127] Further studies elucidated the ability of *MyoD* to convert a diverse array of cell lines such as melanoma, neuroblastoma, liver, retinal pigmented epithelia and adipose-derived cells.[128, 129] Several TFs have also been identified which allow one blood type to differentiate into another. For example, *GATA-1* displayed the ability to reprogram monocytic precursors to eosinophils, thromboblasts and erythroblasts.[130] Additionally, the conversion of B cells to macrophages has been demonstrated using *CCAAT-enhancer-binding*

Table 4. Summary of recent efforts using TFs to transdifferentiate adult cells to different lineages

Starting Cells	TFs	Target Cell Type	Disease Application	References
Fibroblasts	MyoD	Muscle Cells	Muscular Dystrophy	126-129
	Oct4	Blood progenitors	Blood Loss	131
	PU.1., CEBPα and β	Macrophage	Immunodeficiencies, Infection Susceptibility	132
	Ascl1, Brn2 and Myt1l	Neurons	Motor neuron disease, spinal cord injury	133
	Gata4, Mef2c, Tbx5	Cardiomyocytes	Myocardial infarction	134
	Prdm16, CEBPβ	Brown Fat	Hypothermia	135
	Gata4, Hnf1α,	Hepatocytes	Liver Damage	136

	Foxa3, p19ARF knockdown			
Pigment, Nerve, Fat, Liver, and Cells	MyoD	Myotube cells	Myocardial Infarction	[128]
Chondroblasts, Smooth-Muscle, and Retinal Pigmented Epithelial-Cells	MyoD	Myotube and Myoblast cells	Muscular Dystrophy	[129]
Monocytic precursors	GATA1	Erythroid-megakaryocytic cells, eosinophils	Blood loss, sickle cell anemia	[130]
B cells	CEBPα and β	Macrophages	Immune Deficiencies	[137]
	Pax 5 ablation	T cells	Immune Deficiencies	[138]
naive/pre T cells	CEPα or β	Macrophages	Immune Deficiencies	[139]
	PU.1.	Dendritic Cells	Allergy and Autoimmune Diseases	[139]
	Foxp3	Regulatory T cells	Autoimmune diseases	[140]
Hepatocytes	Pdx1	Pancreatic β-cells	Diabetes	[141]
Pancreatic Exocrine Cells	Pdx1, Ngn3, Mafa	Pancreatic β-cells	Diabetes	[142]
	CEBPα and β	Hepatocytes	Liver Failure	[143]
B Cell lymphoma	CEB-α	Macrophage	Cancer Therapy	[144]

protein-α (*CEBPα*) and *CEBPβ*.[137] B cells can be converted to T cells by ablation of the *Pax5* TF which can then undergo transdifferentiation to macrophages by using *CEBPα* and *β*.[138, 139] The order of hematopoietic TFs used for transdifferentiation is a crucial variable for the target cell outcome.[145] *Foxp3* has been identified as a key TF to transdifferentiate naive T cells into regulatory T cells.[140] Lineage switch to blood progenitors has also been demonstrated by delivery of *Oct4* into human fibroblasts[131] or *PU.1* and *CEBPα* and *β* into macrophage-like

cells[132]. *Pdx1* has been elucidated as a master transcription factor necessary for the development of pancreatic β-cells and several experiments overexpressing *Pdx1* in liver cells demonstrated conversion of adult hepatocytes into pancreatic β-cells.[146] *Pdx1* along with *Ngn3* and *Mafa* were used to transdifferentiate pancreatic exocrine cells into β-cells *in vivo.*[142] It is also possible to transdifferentiate mouse fibroblasts into functional neurons using three TFs: *Ascl1, Brn2 and Myt1l* for neurons.[133] Fibroblasts have also been transdifferentiated into cardiomyocytes using 13 TFs and epigenetic remodeling factors in knockout mice; three critical TFs, *Gata4, Mef2c* and *Tbx5* were found to be critical in the transdifferentiation process.[134]

As discussed above, controlling intracellular levels of specific TFs is a powerful method to redirect cellular fate and produce healthy functioning cells of desired lineages. The production of specific cell types can lead to clinically relevant cell sources such as healthy neural cells for Parkinson's disease or spinal cord injuries, islet β-cells for diabetes, cardiomyocytes for myocardial infarction and blood cells for immune deficiencies, for example. Transdifferentiation of diseased cells may also impair the resilience of the disease as was demonstrated by a study in which *CEBPα* induced transdifferentiation of B lymphoma and leukemia cell lines into macrophages weakened tumorigenicity.[144] Developing tools to directly deliver TFs to specific cells can therefore have widespread therapeutic value in regenerative medicine.
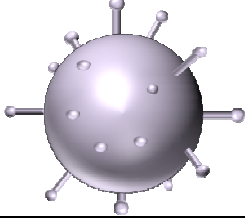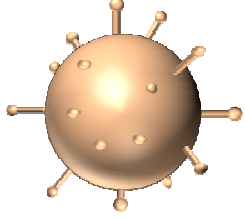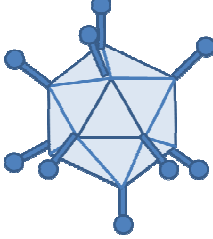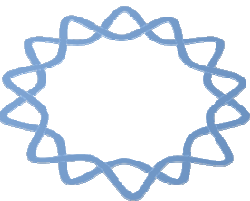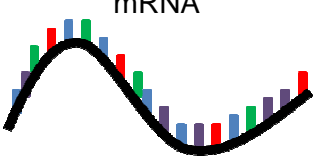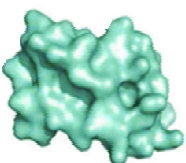
1.2.3. Delivery of TFs for Cell Therapies

Delivery of TFs to redirect cell fate has been explored primarily through retroviral or lentiviral methods [108, 147, 148]. These methods have raised safety concerns due to the incidence of viral integration within endogenous genomes leading to unintended gene activation. When human patients with X-linked severe combined immunodeficiency were treated with retroviral gene therapy, the protooncogene LMO2 was activated and resulted in leukemia.[149] Another safety risk for retroviral or lentiviral delivery is transgene reactivation. When retroviral OSKM factors were used to produce iPS cells and subsequently implanted in chimeric mice, ~50%

28

mice formed tumors.[97] Another study found the formation of iPS cells with viruses without OSKM factors, suggesting that the genotoxicity of lentiviral vectors alone may alone play a role in somatic cell reprogramming derivation.[150] To address these concerns, TF delivery for generation of iPS cells has been explored using adenoviruses[151], plasmids[152, 153] and transposons followed by transgene removal using Cre-mediated excision[154]. However safety issues of delivering TFs using genetic methods remain widespread due to the potential for unexpected genetic modifications by the exogenous sequences in target cells. Furthermore, extensive analysis of produced cells using Southern blotting, PCR analysis and/or sequencing is necessary to confirm the absence of integration into the host genome. Advantages and disadvantages of each delivery vehicle are summarized in Table 5.

Several groups have identified chemicals or small molecules which can replace virus-delivered TFs during iPS cell formation. For example, DNA methyltransferase and histone deacetylase (HDAC) inhibitors such as valproic acid can improve reprogramming efficiency while avoiding the use of the oncogene, c-Myc.[155, 156] Other studies have delivered TFs by introducing mRNA into cells instead of DNA which avoids the need for nuclear delivery and results in high reprogramming efficiency.[157] To avoid the introduction of foreign genetic material into the cell, TFs can be introduced directly as recombinant proteins fused with protein transduction domain (PTD) tags [158, 159]. However as mentioned earlier, PTD-tagged proteins suffer from inefficient escape of transduced protein from endosomes to the cytosol, degradation and inactivation of protein during the cellular uptake process.[15] TF delivery using proteins remains very inefficient due to several challenges of protein-mediated delivery as outlined in Table 5. For patient-specific therapies and development of disease models, safety precautions of cellular reprogramming are extremely important. As such, the need for efficacious and transient technologies for TF delivery remains a critical aim for cell-based therapies to achieve their full potential.

Table 5. Summary of delivery vehicles used for TF delivery in recent years. Advantages and disadvantages of all methods are outlined.

TF Delivery Vehicle	Advantages	Disadvantages
Retrovirus	• Low immunogenicity • Possible to shuttle large DNA fragments (8 kb) • High transfection efficiency	• Does not transduce non-dividing cells • Insertional mutagenesis
Lentivirus	• Able to transduce non-dividing cells • Low immunogenicity • Possible to shuttle large DNA fragments (8 kb) • High transfection efficiency	• Site of integration is unpredictable
Adenovirus	• High titer and easy propogation • Infects both replicating and non-dividing cells • Insertion of large DNA • Non -integrative • No replication during cell division	• High immunogenecity inducing humoral immune responses that can be fatal • Viral proteins can be expressed after vector administration • Lower efficiency
plasmid DNA	• No genomic integration • Limitation of delivered DNA size • Low immunological reactions	• Low efficiency • Nuclear delivery is challenging
mRNA	• Only cytosolic delivery is required • High efficiency • Protein produced endogenously • Transient process	• mRNA instability • High cost of *in vitro* transcription • High immune response
Protein	• No genetic material • Transient process • Safest therapeutic option for delivery	• Instability of protein • Low efficiency • Exogenous protein purification optimization procedures required

2. DEVELOPMENT OF AN INTRACELLULAR PROTEIN DELIVERY SYSTEM

2.1. Endoprotease-Mediated Intracellular Protein Delivery Using Nanocapsules

To achieve delivery of native proteins, we recently reported a strategy to first protect, and then remove the protective coating intracellularly without affecting protein function.[160] We demonstrated intracellular delivery of apoptotic protease caspase-3 (CP3) encapsulated in polymer nanocapsules (NCs) that are crosslinked with peptides that can be degraded by CP3 from within. Although effective as an apoptosis-inducing NC, the strategy is specialized by the requirement that the cargo itself must be proteolytically active to degrade the protective shell. In order to deliver a wide assortment of functional proteins that can interact with different cellular targets, a general mechanism for enzymatic degradation of the NC and release of the protein cargo is needed. Towards this end, we sought to design the NC that can disintegrate and release proteins in response to the essential endoprotease furin (53 kDa), which is a ubiquitous proprotein convertase expressed in all eukaryotic organisms and many mammalian cells.[161, 162]

2.1.1. Furin: An Endoprotease for Inspiration of a Biomimetic Delivery Vehicle

Furin is localized in various intracellular locations and has a preferred substrate in the form RX(K/R)R↓ (R: arginine; K: lysine, X: any amino acid; ↓: the cleavage site).[163]. Interestingly, furin processes its own cleavage sites to transform its pro-enzyme into a mature form by first cleaving itself in the neutral pH environment of the endoplasmic reticulum followed by a second cleavage in acidic conditions in the trans-Golgi network (TGN) and endosomal system. [164] After self-activation through cleavage *cis*, furin becomes primed to act on its many substrates in *trans*.

Furin has many essential embryogenesis and homeostasis roles which are supported by the lethality observed in mice upon knockout of the furin gene.[165] (Figure 6) Furin processes a diverse group of endogenous proproteins including growth factors, plasma proteins, dementia-related secretases and cancer-associated extracellular matrix proteinases in which cleavage may lead to homeostasis or abnormalities.[166] The 16 kDa β-nerve growth factor (β-NGF)

31

precursor is cleaved by furin to allow binding to Trk receptors leading to neuron innervations and survival; in contrast, unprocessed β-NGF binds to neuroptrophin receptor p75[NTR] which leads to apoptosis.[167] The BRI gene codes for a type-II transmembrane precursor
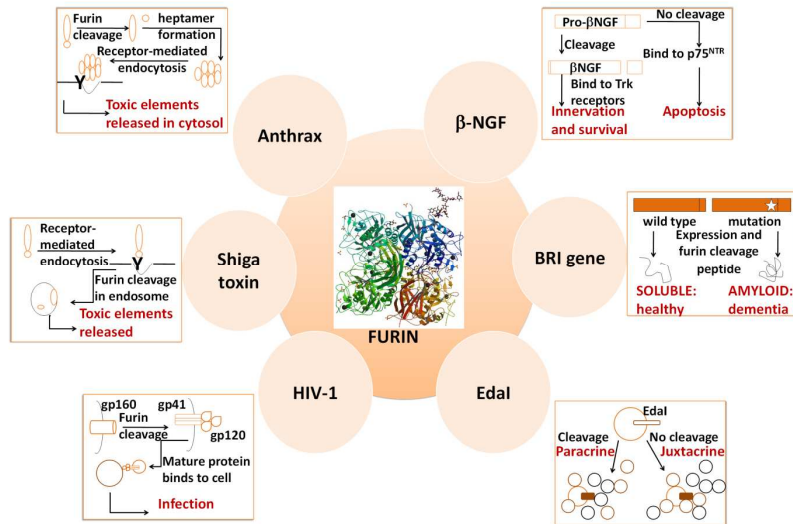
Figure 6. Furin substrates. The crystal structure of 53 kDa furin is shown in the center and various cell-encoded protein substrates (right side) are indicated as well as many foreign substrates to the cell (left side). Furin cleavage results in critical processing of these various substrates.

protein which is processed by furin in healthy individuals to release a 23 residue carboxy-terminal peptide [168]. However, two different mutations in the gene including a nucleotide substitution or decamer duplication cause a 34-residue amyloid peptide to be released upon furin cleavage, resulting in amyloid dementia.[169] Furin cleavage of the tumor necrosis factor protein ectodyplasin-A, Eda-1, allows paracrine signaling to control the formation of hair, sweat glands and teeth.[170] Absence of furin cleavage results in proximal juxtacrine signaling observed. Furin is also overexpressed in several types of cancers, likely caused due to its activation of several membrane-type matrix metalloproteinases (MT-MMPs) that play a role in developing and spreading of tumors [171]. As a result, furin-targeting to combat certain aggressive cancers may be a possible therapeutic option.

In addition to cell-encoded substrates, furin processes a diverse group of foreign proteinaceous substrates, including those from bacterial toxins such as Shiga toxins and anthrax. (Figure 6) Furin processes these foreign substrates in various areas of the cell.[172-174] Furin cleavage can activate translocation to the cytoplasm and subsequent infection of the cell. In addition to bacterial toxins, furin also activates many pathogenic viruses including HIV-1, measles, Ebola, and avian influenza.[175] Furin processing in many of these viruses allow the
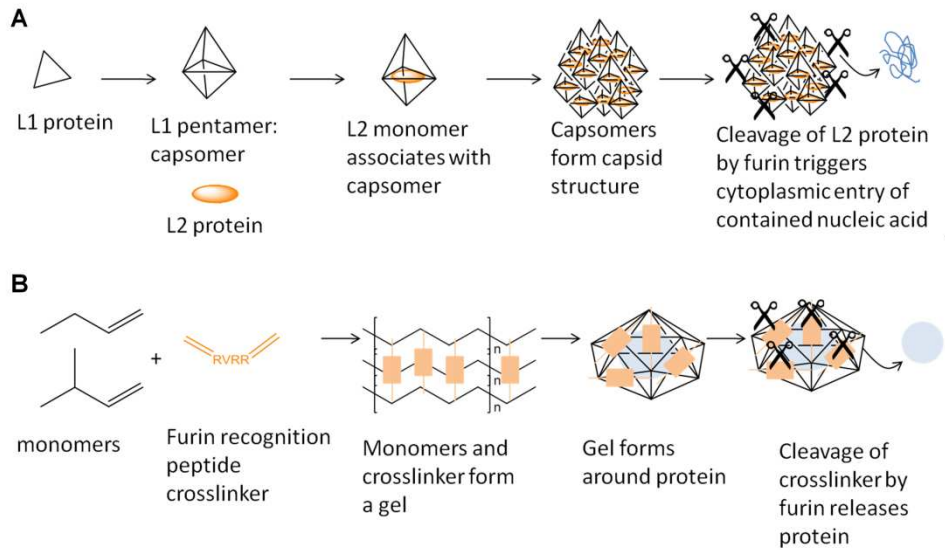
Figure 7. The mechanism of HPV infection, (A), is furin-mediated which can be emulated to create a biomimetic protein delivery vehicle as shown in (B) with the addition of monomers and crosslinkers to mimic the capsid structure of HPV.

mature envelope glycoprotein to become exposed. This mature envelope can expose fusogenic peptides which can fuse with the target-cell membrane. A previous study elucidated the significance of a furin-mediated cleavage of the papillomavirus (PV) minor capsid protein L2 for necessary dissociation of the capsid, release of viral DNA and subsequent transfections.[176] (Figure 7) We were motivated by these existing natural roles of furin, both in the maturation of cellular proteins and activation of foreign invaders. As such, we aimed to design a biomimetic protein delivery vehicle capable of delivering a wide variety of proteins in response to a general degradation trigger that relies on the activities of intracellular protease furin.

2.1.2. Physical Characterization of Protein NCs.

The biomimetic design of our NC was inspired from how natural foreign delivery vehicles, such as viruses, utilize furin to cleave their protective layers leading to release of invading cargo.[177] Furin-mediated processing of these viruses allows the mature viral envelope to become exposed or leads to disintegration of the capsid, thereby leading to successful transfections. Our strategy was to noncovalently encapsulate the target protein cargo in a thin, positively charged polymer layer, using two monomers and furin-cleavable peptides as

crosslinkers (CLs) (Figure 8A). The peptidyl CLs are analogous to various furin substrates, such as the PV L2 capsid protein. Upon entry into the cell, where furin activities are abundant at various intracellular locations, the crosslinkers are proteolyzed and the polymeric matrix degrades, leading to the

Figure 8. Schematics and physical characterization of degradable NCs. *(A) Structure of monomers, acrylamide, N-(3-aminopropyl) methacrylamide and synthesized furin-degradable crosslinker used to form NCs. (B) Monomers and furin-degradable crosslinkers are polymerized to create a degradable polymeric matrix around protein. NCs degrade intracellularly and protein releases upon proteolysis of the crosslinkers by furin. (C) TEM images of fresh NCs and (D) NCs after incubation with furin for 10 hrs. (E) eGFP release by 2.5 nmol NCs for 10 hrs. (●) Furin-degradable NCs; Furin-degradable NCs with 1 U (●) and 4 U (●) furin; (●) Furin-degradable NCs with 1 U furin and dec-RVKR-cmk; and (●) NCs with non-degradable crosslinkers. The data represents averages with error bars from three independent experiments.*

release of cargo in native form (Figure 8B).

We selected a highly favored furin substrate (RVRR) and synthesized a bisacrylated peptide crosslinker (Ahx-RVRRSK) as the NC crosslinker as shown in Scheme S1.[178, 179] Fmoc chemistry was used to synthesize a peptide with 6-aminohexanoic acid (Ahx) at the *N*-terminus and a methyltrityl (Mtt)-protected lysine residue at the *C*-terminus. After selective deprotection and cleavage of the Mtt protection group with 3% trifluoroacetic acid (TFA), the peptide was bisacrylated using acryolyl chloride. This strategy, which utilized differential acid-labile protection groups on the side chains of amino acids to synthesize the crosslinker, allowed acrylation of only the *N*-terminal and *C*-terminal free amine groups while preserving the arginine groups unmodified for furin recognition. Additionally, complete synthesis on amide resin resulted in high yield and purity of final peptide product. The crosslinker was purified with HPLC and characterized by LCMS analysis (*m/z*: $[M+2H]^{2+}=511$; $[M+3H]^{3+}=341$; expected molecular

weight: 1021). Upon incubation with 1 unit of furin, complete cleavage of 1 ng peptide was observed within 2 h (Figure S1 and Figure S3). To prepare the protein-containing NCs, monomers acrylamide (AAm) and positively charged *N*-(3-aminopropyl) methacrylamide (APMAAm), and crosslinkers (Figure 8A) were first physically adsorbed onto the surface of the target protein, which included enhanced green fluorescence protein (eGFP), caspase-3 (CP3), bovine serum albumin (BSA), or the transcription factor Klf4, in this study. This was followed by *in situ* free radical interfacial polymerization to form the polymeric shell and assemble the NC, which can disintegrate and release cargo upon furin cleavage.

The sizes of NCs were assessed to be between 10-15 nm by dynamic light scattering (DLS) (Table S1, Figure S4). The NCs displayed positive zeta potential of 7-9 mV (Table S1), which is desired for enhanced intracellular uptake.[180, 181] To evaluate the furin-degradable property of the synthesized NCs, we first examined NCs using transmission electron microscopy (TEM) and observed furin-degradable eGFP NCs to have a compact, spherical shape. In contrast, after 10 hrs incubation with furin (1 unit), the NCs appeared completely dissociated, less robust and were indistinguishable from native eGFP (Figure 8C,D). To confirm that the structural integrity of protein remained intact during NC synthesis and furin digestion, we performed circular dichroism (CD) to examine eGFP before and after NC degradation. CD spectra indicated that the secondary structure of eGFP remained unchanged during the entire NC assembly and disintegration process, and was identical to that of native eGFP in solution (Figure S5).

We then quantified the release of eGFP from NCs using enzyme-linked immunosorbant assay (ELISA) since only released native eGFP is able to bind to anti-GFP-antibody, while encapsulated eGFP is unable to be recognized by the antibody. In addition to furin-degradable NCs, we also examined protein release from non-degradable NCs that were crosslinked using *N,N'*-methylene bisacrylamide. In the absence of furin, degradable NCs did not display significant protein release over a period of 24 hrs (Figure 8E), which was comparable to that of

non-degradable NCs. This indicates that eGFP can remain encapsulated in the polymeric shell over an extended period of time and protein diffusion effects are negligible. In contrast, upon addition of 1 unit furin to furin-degradable NCs, a steady increase (~0.15 nmol eGFP/unit of furin-hr) in the amount of free eGFP was observed over 10 hrs, indicating gradual release of eGFP from the NCs. The slower-releasing phase observed before 6 hrs may be attributed to an initial period in which the peptide crosslinkers are being digested by furin. When an increased concentration of enzyme (4 units) was incubated with NCs, the release of protein occurred more rapidly and reached a similar plateau level corresponding to ~80% total eGFP encapsulated. When a competitive furin inhibitor, dec-RVKR-cmk[174], was added to the assay (10 μM), the release of eGFP was remarkably attenuated to the same level as the non-degradable and furin-free samples. To assess the stability of NCs we performed the eGFP release assay of furin-degradable NCs in conditions established for stability studies of nanoparticles, including the uses of an acidic pH 5.5 buffer and a high salt concentration of 500 mM NaCl.[182, 183] As shown in Figure S6, NCs did not show significant protein release in either of these conditions indicating the NC remains intact and is not subject to non-specific acid hydrolysis or destabilization due to shifts in ionic strength. These combined results confirmed that the release of native eGFP from the NCs was specifically dependent on the enzymatic activities of furin.

2.1.3. Intracellular Furin-mediated Native Protein Delivery in CHO cell lines.

Having established the furin-dependent degradability of the NCs, we then sought to demonstrate the ability of NCs to deliver native proteins to the nuclei of mammalian cells. The first target protein chosen was eGFP fused with the nuclear localization signal (NLS, sequence PKKKRKV) from the simian virus 40 large-T antigen (NLS-eGFP).[184] NLS-eGFP is chosen as a fluorescent marker for the following reasons: first, NC-mediated delivery into the cytosol of cells can be readily visualized. However, in the absence of NC degradation, the NLS tag will be concealed and thus confine the eGFP fluorescence in the cytosol. Subsequently following furin-mediated degradation of NCs, we expect NLS-eGFP to be released and lead to entry of eGFP

into the nucleus facilitated by the exposed NLS tag (Figure 9). The change in the localization of the eGFP signal will then be an indication of the release of protein cargo.

Figure 9. Schematic of nuclear localization signal (NLS) eGFP delivery to the cytosol of cells. If the polymeric nanocapsule degrades, the NLS will be exposed and the fluorescence will localize to the nuclei. If the nanocapsule remains intact, the NLS will remain hidden and fluorescence will be retained in the cytosol.

We first compared the extent of nuclear co-localization of delivered NLS-eGFP using different Chinese Hamster Ovary (CHO) cell lines with varied intracellular furin levels, including CHO-K1 that expresses furin at a normal level; FD11 that is furin-deficient; and FD11+furin which is the FD11 strain transfected with an overexpressed furin gene.[172] We incubated 200 nM furin-degradable NLS-eGFP NCs with CHO cell lines and examined intracellular delivery with confocal microscopy after 24 hours. Localization of eGFP signal to the nucleus was prominent with furin-degradable NCs in CHO-K1 and FD11+furin cells (Figure 10A). In contrast, eGFP fluorescence was only localized in the cytosol in FD11 cells and no nuclear entry was observed, indicating no capsule degradation in the absence of furin. Furthermore, when non-degradable NCs were used as delivery vehicles for NLS-eGFP, nearly all fluorescence was found only in the cytosol for all cell lines (Figure S5), confirming the inaccessibility of the encapsulated NLS-eGFP towards the nuclei.

To quantify the extent of nuclear delivery of NLS-eGFP, we isolated the nuclear fractions from these treated cells and measured the amount of eGFP using ELISA. As shown in Figure 10B, the levels of eGFP delivered to the nuclei by furin-degradable NCs was two to three times greater in furin-expressing cell lines compared to FD11. When these cells were co-cultured with furin degradable NCs and 25 μM dec-RVKR-cmk, the amount of eGFP in CHO-K1 decreased to

that of the FD11 levels. A smaller decrease was observed in FD11+furin cell lines treated with

furin inhibitor, which may be attributed to the higher expression levels of furin. As controls,

nearly no nuclear localization of eGFP was observed in 1) NLS-eGFP delivered by

nondegradable NCs; 2) untagged eGFP delivered by furin degradable NCs; and 3) NLS-eGFP

delivered by NCs crosslinked with Ahx-AAARSK (Figure S2), which is not recognized by furin

(Figure S7). The absence of nuclear eGFP delivery when NCs were crosslinked with a non-furin

specific peptide indicates that the peptide crosslinker is not subjected to hydrolysis by non-

specific proteases. Notably, NCs did not show significant cytotoxicity up to ~2 μM in cell-lines

treated with NLS-eGFP NCs for 24 hours (Figure 10C, Figure S8). Furthermore, FD11 and

FD11+furin cells treated with 400 nM furin-degradable NLS-eGFP NCs displayed identical cell

morphologies and no visible toxicity despite different intracellular eGFP localization, further

confirming the non-toxic nature of this delivery method (Figure 10D). Thus, proteolytically-

cleavable NCs can be constructed with specific peptide crossslinkers and the degradation to
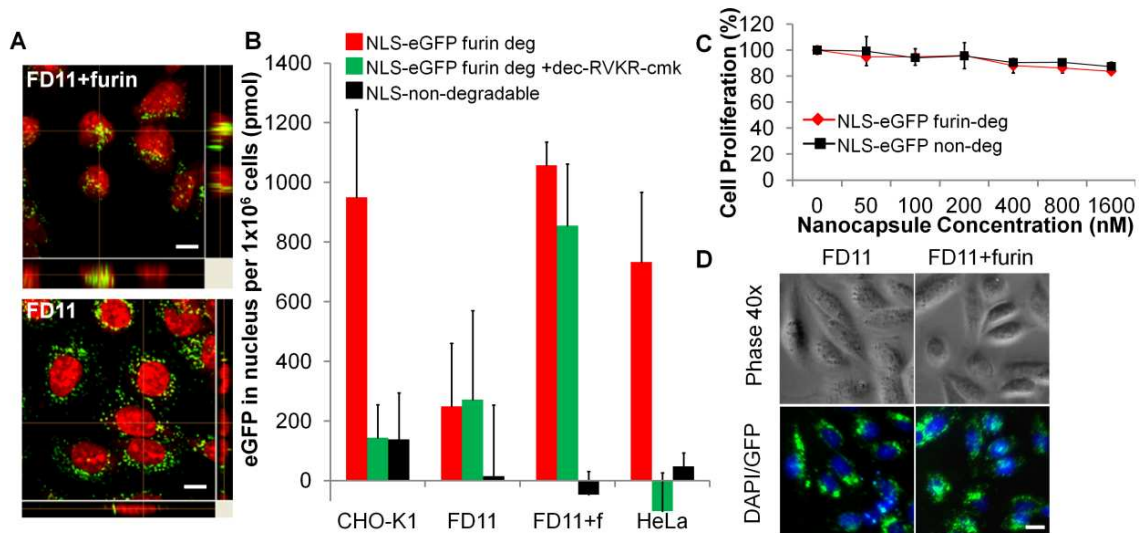
Figure 10. In vitro studies demonstrating furin-degradability of NCs. (A) Confocal images of 200 nM furin-degradable NLS-eGFP NCs delivered to FD11+furin cells and FD11 furin-deficient cells after 24 hrs treatment; red: nuclei, green: eGFP. The central panel shows a slice of the xy plane, the xz plane corresponding to the position of the crosshairs is shown on the right and the yz plane is shown at the bottom. The scale bars are 10 μm. **(B)** Quantification of eGFP in the nuclear fraction of NC-treated cells using ELISA. Cells were treated for 24 hrs before the nuclei were isolated. The data shown represents the average value with error bars from three independent experiments. **(C)** Cell proliferation profiles of NCs delivered to CHO-K1 cells for 24 hrs which were quantified by the MTS assay. **(D)** Representative phase and fluorescence images of CHO cell lines treated with NLS-eGFP degradable NCs. The scale bar is 100 μm.

release protein can be modulated by the activities of furin or other target endoproteases. Examination of furin-dependent nuclear delivery of eGFP utilizing 1) CHO cell lines with varying furin concentrations; 2) a competitive furin inhibitor dec-RVKR-cmk; and 3) nonspecific peptide crosslinkers (Ahx-AAARSK) collectively indicates that the presence of active intracellular furin and furin-degradable NCs are both required for successful delivery.

2.1.4. Internalization of Protein NCs in Human Cell Lines.

We then explored intracellular protein delivery to various human cell lines. We first studied the delivery of NCs to the HeLa cell line, which exhibits high levels of furin expression.[185] When furin-degradable NLS-eGFP NCs were delivered to HeLa cells, significant eGFP localization was observed within nuclei (Figure S5). Quantitative analysis of nuclear eGFP levels also confirmed the successful delivery of eGFP to HeLa cells using furin-degradable NCs (Figure 10B). We then explored the cellular trafficking of furin-degradable NLS-eGFP NCs in HeLa cells. We monitored eGFP fluorescence for 2 hrs following NC incubation with cells by staining early endosomal marker, EEA1 or the late endosomal marker, CI-MPR (Figure 11A). After 30 min incubation, eGFP NCs showed ~ 60% peak colocalization with EEA1 indicating that NCs are internalized by endocytosis (Figure 11B). The observation of eGFP fluorescence signals at later time points lacking colocalization with either endosomal marker indicates that several NCs or proteins are able to be delivered into the cytosol within 2 hours of cellular uptake (Figure 11A). The inefficient escape of protein from the endosome to the cytosol remains an obstacle in many current delivery approaches.[186, 187] Delivery methods that rely on cytosolic esterases or reducing environments to release protein may never reach the cytosol and become entrapped in endosomes, undergo lysosomal degradation and are eventually cleared from the system.

We also used HeLa cells to observe the effects of using various amounts of furin-degradable crosslinker (CL) to synthesize NCs. We varied the molar ratio of AAm:APMAAm:CL from 6:3.5:1 (A) to 6:3.5:0.5 (B) and synthesized furin-degradable NLS-eGFP NCs. Both NCs had similar size and charge (Table S1). As shown in Figure 11C, cells treated with NCs synthesized with more crosslinker (NC A) displayed higher colocalization with nuclei than those treated with NCs synthesized with less crosslinker (NC B), while the overall internalization of GFP and cell morphologies were comparable after 24 hrs. When the nuclear fractions were
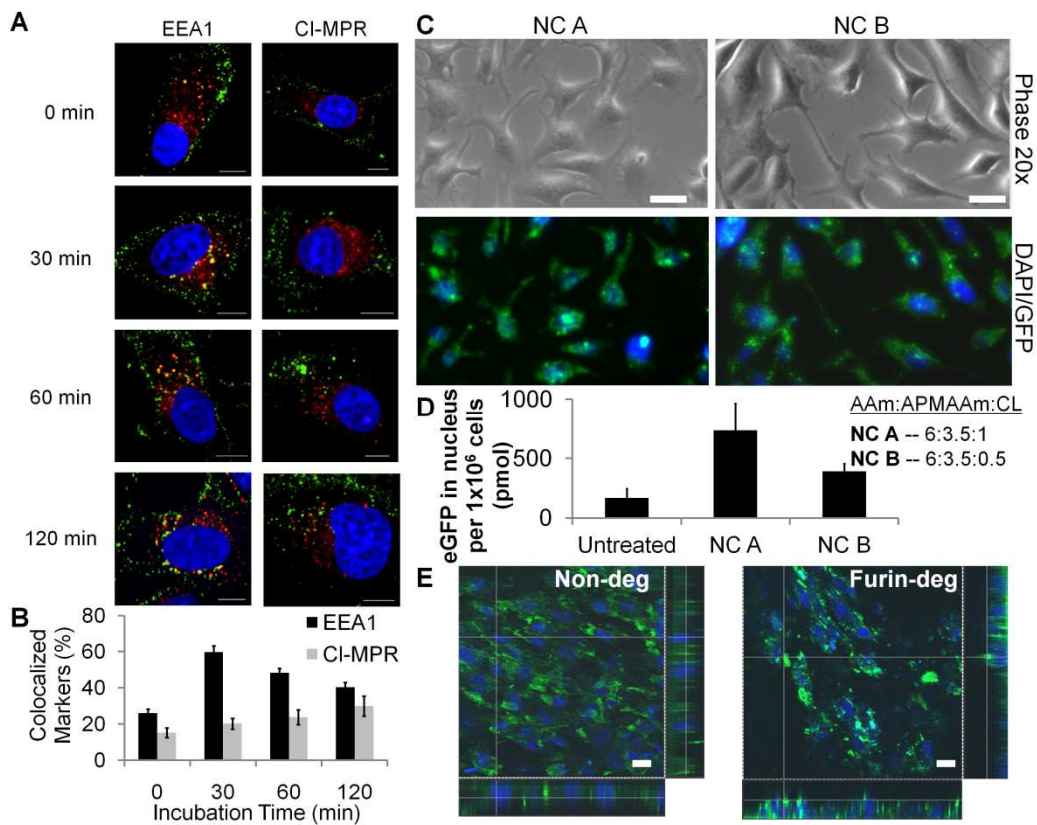
Figure 11. Cellular internalization of NCs in human cell lines. (A) The trafficking of NLS-eGFP NCs through endosomes. Early and late endosomes were detected by EEA1 antibody (left) and CI-MPR antibody (right), respectively which are stained in red. HeLa cells were incubated with 10 nM NLS-eGFP NCs at 37 °C for various time points, fixed and the overlap of eGFP with endosomal markers were observed by red and green colocalization resulting in a yellow color. The nuclei are stained with DAPI shown in blue. The scale bar is 10 μm. **(B)** Quantification of NLS-eGFP NCs colocalized with EEA1+ or CI-MPR+ endosomal markers at various incubation times. Colocalization coefficients were calculated using the Manders' overlap coefficient (>10 samples). **(C)** Phase and fluorescence images of HeLa cells treated with degradable NLS-eGFP NCs for 24 h with varying crosslinking density (blue: DAPI-stained nuclei; green: GFP). NC A was synthesized with twice the amount of furin-degradable crosslinker as NC B. The scale bars are 100 μm. **(D)** Quantification of eGFP using ELISA in extracted nuclei of HeLa cells treated with NC A and NC B with varying crosslinking densities of NCs. **(E)** Confocal images of AFDC cells treated with 200 nM non-degradable (left) and furin-degradable (right) NLS-eGFP NCs. blue: Hoescht stained nuclei, green: eGFP. The scale bars are 50 μm.

extracted and eGFP was quantified with ELISA, nuclear eGFP of NC A-treated cells was significantly higher than that of cells treated with NC B (Figure 11D). These results imply that the degradability and surface chemistry of NCs may play an important role in internalization and may facilitate cytosolic native protein delivery at various cellular entry points.

We then examined protein delivery into human amniotic fluid-derived cells (hAFDCs). hAFDCs have the potential to differentiate into all three germ layers[188] and act as somatic resources which can be efficiently induced into a pluripotent state.[189] Hence, controlled delivery of various factors to tune the functions of these cells has significant therapeutic potential. We delivered furin-degradable and non-degradable NLS-eGFP NCs to hAFDCs and examined the extent of nuclear delivery using confocal microscopy as shown in Figure 11E. hAFDCs treated with 200 nM furin-degradable NCs show a marked overlap between cell nuclei and protein, while fluorescence signals from non-degradable NCs were only detected in the cytosol. These results strongly indicate that furin-degradable NCs can be used to deliver proteins to the nuclei of a diverse array of mammalian cells.

2.1.5. Delivery of anticancer Caspase-3 to HeLa cells.

To further demonstrate the utility of furin-mediated release of functional protein cargo from the degradable NCs, we prepared NCs containing CP3. CP3 is a potent executioner when delivered in native form to cells as it acts as a signal peptidase in the cellular apoptotic pathway.[190, 191] Therefore, cell apoptosis is the physiological change observed upon successful delivery and release of native CP3 protein. We previously delivered CP3 to cells using self-degradable NCs crosslinked with CP3-cleavable peptides[160]; here we seek to generalize the degradability of that system by utilizing the activities of intracellular furin instead. CP3 NCs were prepared in similar fashion as the eGFP NCs starting from purified, recombinant CP3. Various control CP3 NCs were also synthesized to facilitate comparison to the furin degradable vehicle.   After confirmation of surface charges and sizes (Table S1), the CP3 NCs were added to HeLa cells. As shown in Figure 12A, cell death was only observed in HeLa cells treated with furin-

degradable CP3 NCs, with IC_{50} of ~400 nM. In contrast, cells treated with unencapsulated native CP3, non-degradable NCs, and furin-degradable BSA NCs all exhibited minimal apoptotic death within the concentrations of NCs used, confirming the furin-dependent release of CP3 and the relatively nontoxic nature of the polymeric capsule. This indicates that only furin-degradable CP3 NCs are able to both enter the cell and be degraded to release the executioner protein which can induce apoptosis. To confirm the cell death observed was indeed apoptosis, we performed the terminal deoxynucleotidyl transferase dUTP nick end labeling (TUNEL) assay which detects DNA fragmentation by labeling the terminal end of nucleic acids.[192] When cells were treated with 200 nM CP3 NCs or protein, trademark cell membrane blebbing and shrinkage characteristics of apoptotic cells were observed in cells treated with furin-degradable
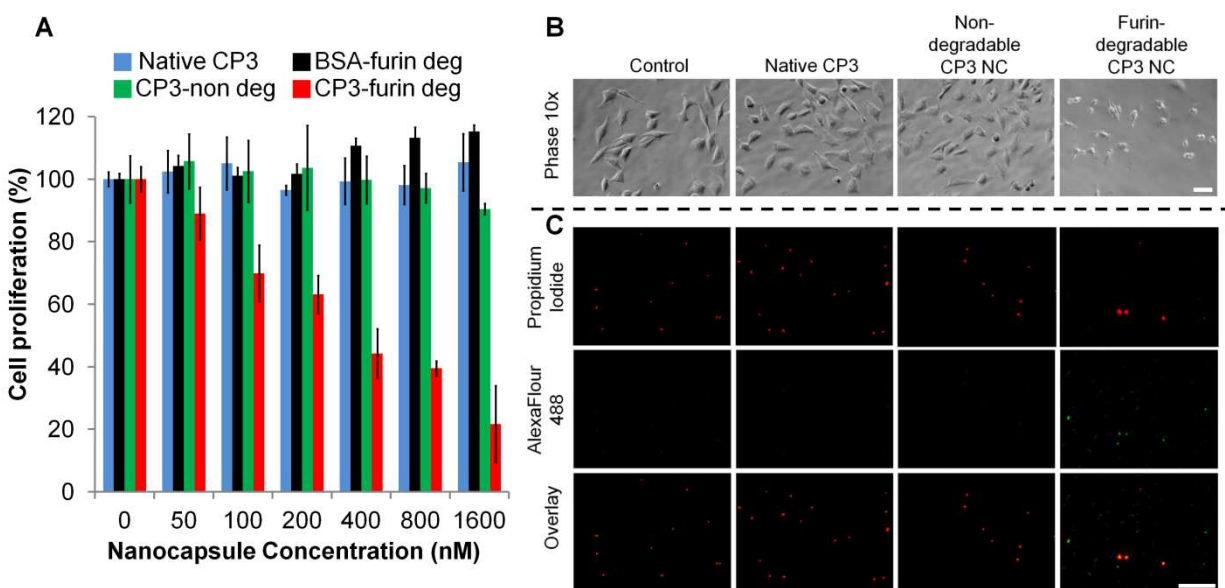
Figure 12. Cytosolic delivery of caspase-3 to HeLa cells. (A) Cell death profiles of HeLa cells treated with various crosslinked NCs/protein for 24 hours before performing the MTS assay for quantification of cell proliferation. (B) Cell phase images prior to the TUNEL assay of HeLa cells treated with NCs for 24 hours. The scale bar is 200 μm. (C) TUNEL assay results following detachment of NC-treated cells, permeabilization and staining. Propidium iodide (red) signifies the total DNA content while AlexaFluor 488-tagged antibody (green) corresponds to nick end DNA. The scale bar is 200 μm.

CP3 NCs (Figure 12B). After detachment of cells and performance of the TUNEL assay, detection of DNA nicks observed with AlexaFlour488-labeled antibody (green) were only detected in cells treated with furin-degradable CP3 NCs (Figure 12C). In contrast, native CP3-

treated cells or non-degradable CP3 NC-treated cells did not show signals of nicked DNA in the total DNA content visualized with propidium iodide (red). This indicates that furin-degradable NCs are able to deliver active CP3 to the cytosol and lead to apoptosis.

The successful delivery of CP3 also implicates the future potential of this system to deliver various cancer therapeutics which can interact with cellular machinery to activate the apoptotic pathway.[193] The amount of furin-degradable crosslinkers incorporated in the NC can be tuned to achieve cell-specific intracellular protein delivery, as furin is upregulated in breast, ovary, head and neck, and brain, as well as non–small cell lung carcinomas, in comparison to normal cells.[194-197] In this study, a positive surface charge on the NC was targeted to facilitate cellular entry by interaction with the negatively charged phospholipid bilayer membrane.[7] To achieve selective cellular uptake, targeting positive ligands could be attached to the surface of the NCs and the surface charge could be adjusted to neutral by using uncharged monomers.[198]

2.1.6. Delivery of a transcription factor to nuclei of MEF cells.

To demonstrate the delivery of biologically relevant nuclear protein cargos to cells, we prepared NCs encapsulating the transcription factor Klf4. Klf4 is critical in regulating expression levels of genes involved in maintaining the cell cycle as well as cellular structure, adhesion, metabolism and signaling.[199] Many studies implicate Klf4 as a tumor suppressor for colorectal and gastric cancers.[200] Particularly, Klf4 has been shown to be one of the essential factors needed to maintain a pluripotent state.[102] Recently, recombinant iPS transcription factor proteins were fused to protein transduction domains (PTDs) of multiple arginines (9R or 11R), transduced into mouse and human fibroblasts and reprogrammed to produce induced pluripotent stem (iPS) cells.[158, 159] 11R-tagged proteins have been delivered *in vitro* and *in vivo* to subcellular compartments such as nuclei and mitochondria in a variety of tissues and organs including the brain, heart, and lymphocytes, thereby asserting 11R tags as a useful delivery strategy for protein therapeutics.[201] We sought to compare intracellular delivery of 11R-tagged proteins and protein NCs using Klf4 as a model.

We synthesized NCs with Klf4-11R and verified the size of nanocapsules to be ~20 nm with TEM (Figure S9). We directly determined the extent of protein delivery by performing immunocytochemistry after culturing mouse embryonic fibroblast (MEF) cells with Klf4-11R or furin-degradable Klf4 NCs. As shown in Figure 13, Klf4 delivered via NC can be prominently detected in nuclei of cells which are counterstained with Hoescht and examined using confocal microscopy. Virtually every cell nucleus shows a strong signal of Klf4 staining. The degree of staining is comparable to the positive control, BJ-iPS cells, which are neonatal human foreskin fibroblasts which have been reprogrammed into iPS cells and have high expression levels of Klf4.[101] In contrast, Klf4-11R shows much weaker intensity and much less colocalization with nuclei indicating delivery of Klf4 was not as efficient. PTD-tagged cargo often becomes trapped in endosomal compartments with no mechanism of release into the cytosol and <1% of the
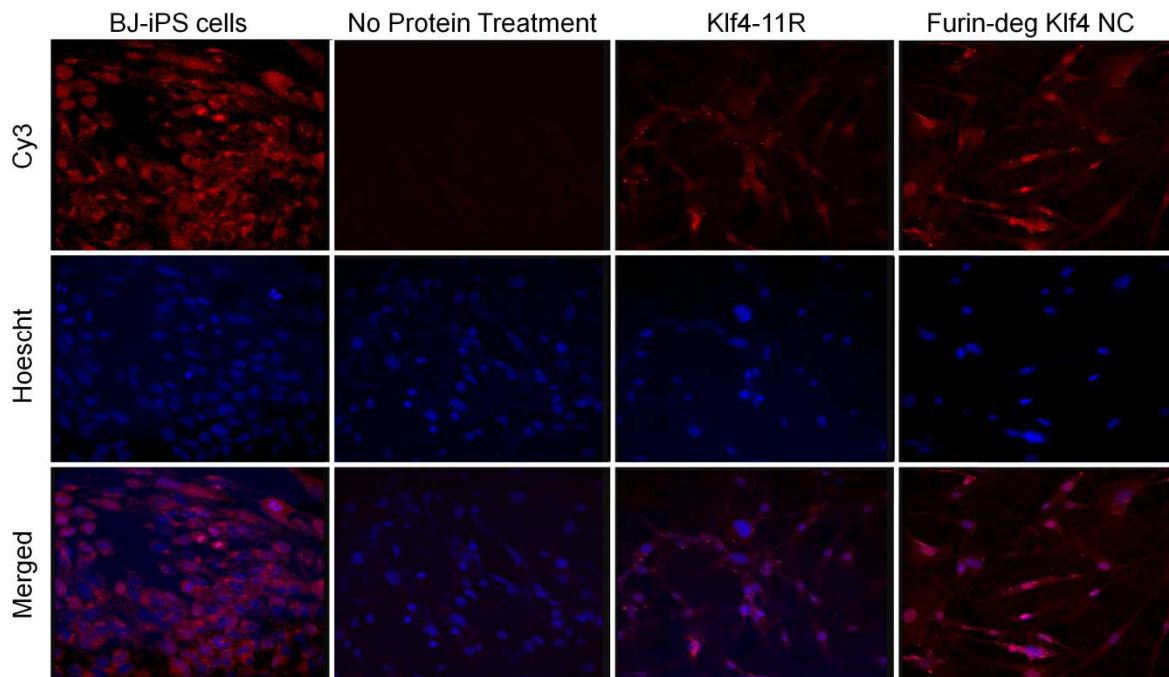
Figure 13. Intracellular delivery of Klf4 to MEF cells. Klf4 immunostaining in MEF cultures treated with Klf4-11R and furin degradable Klf4 NCs was examined using confocal imaging. BJ-iPSCs were also immunostained as a positive control and cells without any treatment were used as a negative control. The top panel shows Klf4 immunostaining with Cy3 conjugated antibody (red), middle panel shows nuclear staining using Hoescht dye (blue) and bottom panel shows overlap between both.

protein cargo may be released.[15, 202] The prominent staining of Klf4 in the nuclei of MEF cells suggests that NCs may offer more protection for preservation of protein structure and activity. PTD-tagged proteins and other proteins which are exposed to the acidic environment in the endosome often experience degradation and loss of activity. The cargo can also be degraded or subject to proteolysis during cellular entry. In contrast, the endoprotease-mediated delivery system has a protective polymer layer during cellular uptake until cleavage by furin and release of protein. Collectively, these findings demonstrate that degradable nanocapsules are suitable vehicles for nuclear delivery for transcription factors. The successful nuclear delivery of Klf4 using furin-degradable NCs is also particularly promising as a reprogramming tool. Direct delivery of transcription factors would allow patient-specific therapies which eliminate risks arising from genetic-based methods including unexpected modifications in target cell genomes.

2.1.7. Conclusions from Endoprotease-Degradable NCs.

Intracellular delivery of active proteins is an essential goal in various medical applications, including cancer therapy, imaging, vaccination, and treating loss of functioning genes in many diseases.[3] Protein-based therapeutic methods are safer alternatives to gene therapies because no random or permanent genetic changes are involved, and only transient actions of proteins are required for desired effects. However, most native proteins are unable to penetrate the cell membrane and often suffer from loss of function due to proteolysis or aggregation in serum. Consequently, a general intracellular protein delivery system is highly desirable for delivery of diverse targets which have different therapeutic uses. Particularly, using an enzymatic-based method would achieve a level of specificity and control which is challenging with current methods.

We successfully demonstrated both cytosolic and nuclear delivery of proteins using our engineered NC carrier which degrades in response to the ubiquitous endoprotease furin. Different cell lines were demonstrated to be amenable hosts for furin-mediated delivery including the immortalized HeLa, the highly regenerative hAFDC, and the essential structural

MEF. We also showed that protein cargos of different sizes and tertiary structures can be encapsulated and released reversibly without loss of bioactivity, including the 27 kDa β−barrel eGFP[203]; the 51 kDa Klf4 that has three zinc finger regions[204]; and the 64 kDa CP3 which is a heterotetramer[205]. In summary, through extensive imaging and quantitative analysis *in vitro,* we have shown the successful delivery of both cytosolic and nuclear proteins based on specific furin-mediated degradation and cargo release. This approach may also be applicable to the intracellular delivery of other therapeutics including small drugs, peptides, siRNA, and plasmid DNA.

2.2. Intracellular Protein Delivery Using Microemulsion Nanoparticles

Another method to synthesize polymeric carriers for encapsulation of proteins is to create nanoparticles (NPs) using inverse emulsion conditions. This system has been widely developed in previous studies and specifically has been used for protein vaccination applications.[66, 206] To synthesize NPs, an organic and an aqueous phase are prepared. The organic phase consists of hexane with a mixture of two surfactants, Tween 80 and Span 80, which are added beyond the critical micelle concentration to create inverse micelles. The aqueous phase which includes protein, monomers, crosslinkers and APS initiator is added to the organic phase. A probe sonicator is used to create an emulsion in which the aqueous phase forms droplets inside the micelles, TEMED is added to initiate polymerization inside the micelles. To recover the protein NPs, the reaction mixture is centrifuged and washed several times. The NP fabrication method relies on shear stress by the sonicator to create aqueous droplets inside the micelles. As a result, protein NP formation is driven by the strong shear forces and can be extended to various proteins, crosslinkers, and monomers. On the other hand, the emulsion-based fabrication method employs organic solvents and extensive shear stress which may deteriorate the activity of the protein during fabrication. We sought to determine if protein NPs could be formed using our engineered furin-degradable platform.

2.2.1. Physical Characterization of Protein Nanoparticles

We aimed to use inverse emulsion-based encapsulation to create protein NPs that incorporated furin-degradable or non-degradable crosslinkers. The major components for synthesis of NPs is shown in Figure 14A including the two surfactants, Tween 80 and Span 80 which create the inverse micelles where polymerization occurs. The polar heads orient inwards with the hydrophobic tails orient outwards in hexane. The aqueous phase consisted of acrylamide, N-(3-aminopropyl) methacrylamide and either the non-degradable *N,N'*-methylene bisacrylamide or furin-degradable crosslinkers. Several formulations were used to yield protein NPs encapsulating CP3 and eGFP proteins. (Table S2, Figure S10) As shown in Figure 14B,

47
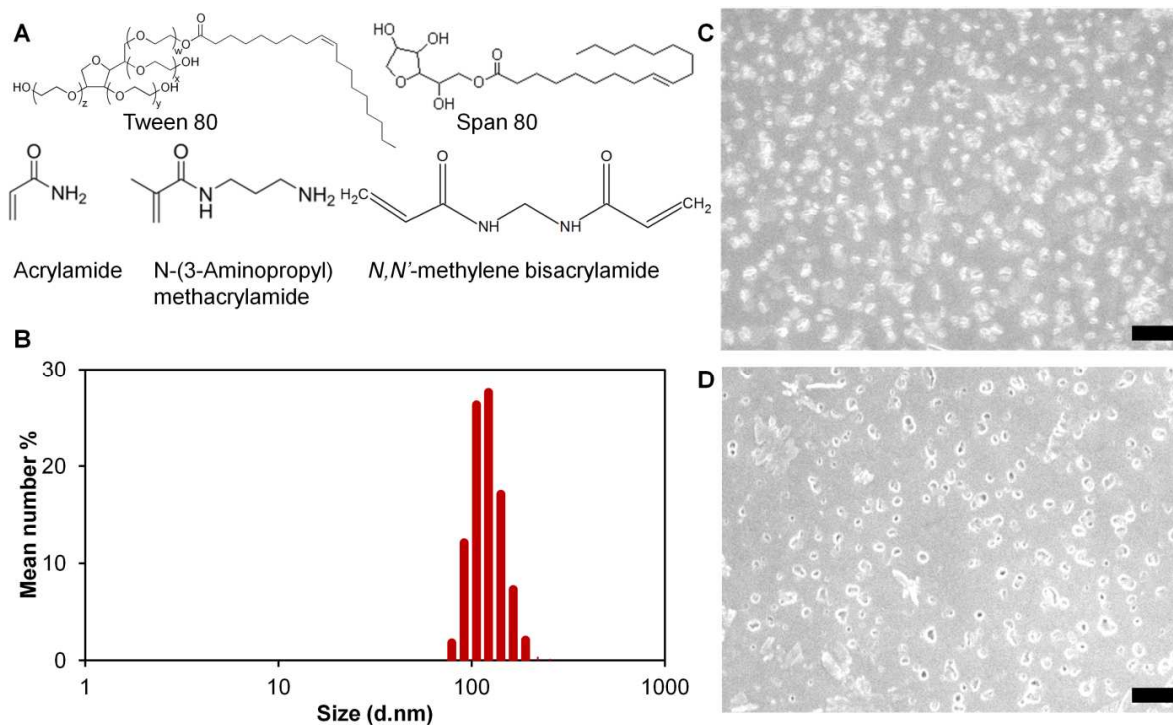
Figure 14. Protein nanoparticle synthesis and physical characterization. (A) Tween 80 and Span 80 were used to create inverse micelles in hexane. Subsequently the aqueous phase consisting of polymer, crosslinkers and APS were sonicated into the micelles and polymerization was initiated using TEMED. (B) Dynamic light scattering measurements for furin-degradable GFP NPs. Scanning electron microscopy images for (C) furin-degradable GFP NPs and (D) non-degradable GFP NPs. The scale bar corresponds to 1 μm.

emulsion-based NP synthesis encapsulating eGFP using furin-crosslinkers yielded particles around 120 nm in diameter. These size measurements were further confirmed using scanning electron microscopy to image both furin-degradable eGFP NPs and non-degradable eGFP NPs as shown in Figure 14C and D. Physical characterization of protein NPs suggested that the NPs were able to encapsulate protein in robust, spherical 60-100 nm polymeric carriers.

2.2.2. Intracellular Delivery of Protein Nanoparticles

In order to evaluate the ability of protein NPs to deliver cargo intracellularly, we encapsulated eGFP so that we could assess delivery using fluorescent microscopy. Furin-degradable and non-degradable eGFP NPs were incubated with HeLa cells and evaluated for their ability to deliver protein to the cytosol. The cells were imaged at 4 hours, 8 hours and 20 hours to evaluate differences in protein delivery. As shown in Figure 15, both non-degradable and furin-degradable NPs were able to deliver eGFP inside HeLa cells. In Figure 15A, the
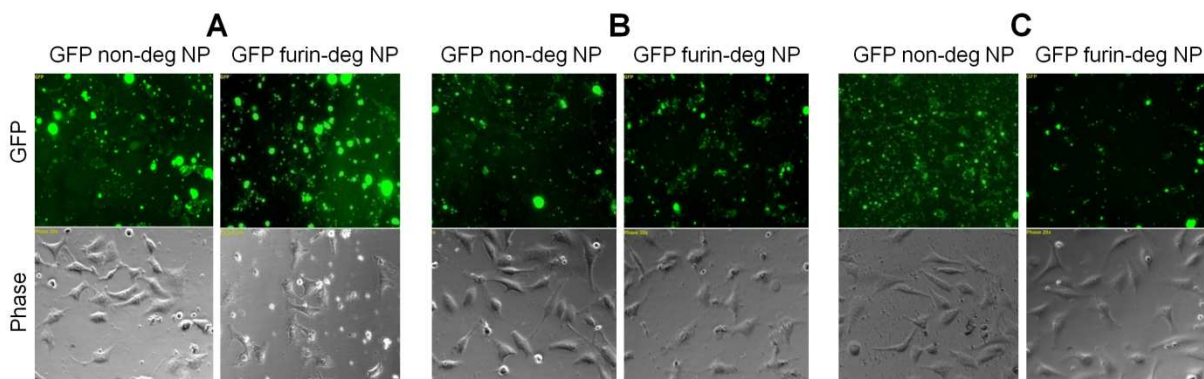
Figure 15. Intracellular delivery of GFP NPs to HeLa cells. Cells were treated with 200 nM GFP furin-degradable or non-degradable GFP NPs. Cells were imaged at (A) 4 hours, (B) 8 hours and (C) 20 hours post-incubation with cells.

appearance of large clustered eGFP NPs appears in both samples which diminishes over time as seen in Figure 15B and C. A noticeable difference is evidenced by the difference in GFP fluorescence intensity over time. Cells were imaged with the same exposure time at each time point in order to compare the intensity level over time. Cells treated with non-degradable GFP NPs maintain a similar intensity at all three time points. In contrast, furin-degradable NP-treated cells exhibit a less intense fluorescence at the 8 hour and 20 hour time points as compared to 4 hours. This phenomenon suggests that protein delivered by degradable NCs is degraded faster inside the cell than protein delivered through non-degradable NPs. As such, it is likely that furin-degradable NPs are able to be degraded intracellularly since wild-type GFP has a half-life of ~26 hours in mammalian cells.[207] These images demonstrate that furin-degradable NPs are able to deliver protein to the cytosol of HeLa cells in an efficient manner.

2.2.3. *In Vivo* Delivery of OVA Nanoparticles

The World Health Organization considers vaccination to be the most cost-effective strategy for controlling infectious diseases.[208] In fact when evaluating direct effects on public health, current vaccination therapies rank second only to the availability of clean water supply. Certainly, vaccination comprises an enormous role in modern medicine and has contributed a great deal to immunization against diseases such as smallpox, polio, measles, mumps, rubella, hepatitis B and Hemophilus type B.[209] These traditional vaccines are based on intact disease-

49

causing microbial agents and are comprised of live attenuated or inactivated organisms that do not cause infection but instead induce protective immunity. Despite widespread use, these traditional vaccines have many disadvantages. There are many infectious diseases including HIV/AIDS, turberculosis and malaria which are not controlled by vaccines and others which require complex immunization administration methods.[210] Cancer vaccines also remain elusive despite much concerted effort over the last decade.[211] A large area of concern for traditional vaccines includes the possibility of genetic variations in the antigen components of infectious agents which can cause development of new strains for which new vaccines must be developed. There are also safety risks associated with traditional vaccines in which a risk of reversion may occur during replication of a live virus or mutation to a more pathogenic strain and attenuated viruses may still provoke disease in immunocompromised individuals. Due to potential therapeutic implications in such insidious diseases as HIV, cancer and hepatitis C and much safer administration, protein subunit vaccines are an area of great interest. Furthermore, protein vaccinations offer low toxicity and enhanced targeted immune response.

The goal of vaccination is to activate the adaptive branches to induce protective memory responses. Specific cells called antigen presenting cells capture antigens and process them into small peptide fragments which are presented in two ways by Major Histocompatibility Complex (MHC) molecules.[212, 213] Class I presentation is recognized by CD8 T cells which activate into Cytotoxic T lymphocytes (CTLs) or memory T cells. Antigens presented by MHC class II molecules are recognized by CD4 T cells which later mature into helper T cells that secrete soluble signals that accelerate or suppress responses. Helper T cells produce memory B cells and plasma B cells which secrete antibodies specific to the antigen. Ovalbumin (OVA) protein is a widely used model protein antigen used to characterize novel vaccination methods to analyze antigen uptake, presentation and processing. OVA has well studied CTL (OVA$_{254-264}$: SIINFEKL) and CD4 (OVA$_{323-339}$: ISQAVHAAHAEINEAGR) epitopes that are recognized by OT1 and OT2 T

50

cell receptors (TCRs) respectively.[214] We aimed to determine if NPs encapsulating OVA were able to stimulate an immune response in mice.

OVA NPs were synthesized using inverse microemulsion procedures and physical properties were evaluated using dynamic light scattering. C57BL/6 (B6) mice were subcutaneously injected into the lower footpads with 140 μg of non-degradable and furin-degradable OVA NPs. The immunized mice were evaluated for immune responses after 14 days. Mice were sacrificed using CO_2 and were dissected to extract splenocytes which were analyzed by IFN-γ staining and ELISPOT assays for resulting antigen-specific responses.[215] As seen in, Figure 16A, a near 3.5 fold increase in costaining of IFN-γ and CD8 was observed from restimulated splenocytes from mice treated with OVA furin-degradable NPs compared to mice treated with non-degradable OVA NPs. The increase in IFN-γ/CD8 positive cells for mice treated with furin-degradable NPs indicates that upon injection of degradable OVA NPs, T-cell proliferation occurs thereby resulting in activated CTLs and memory T cells. We further performed the ELISPOT assay which allows the visualization of
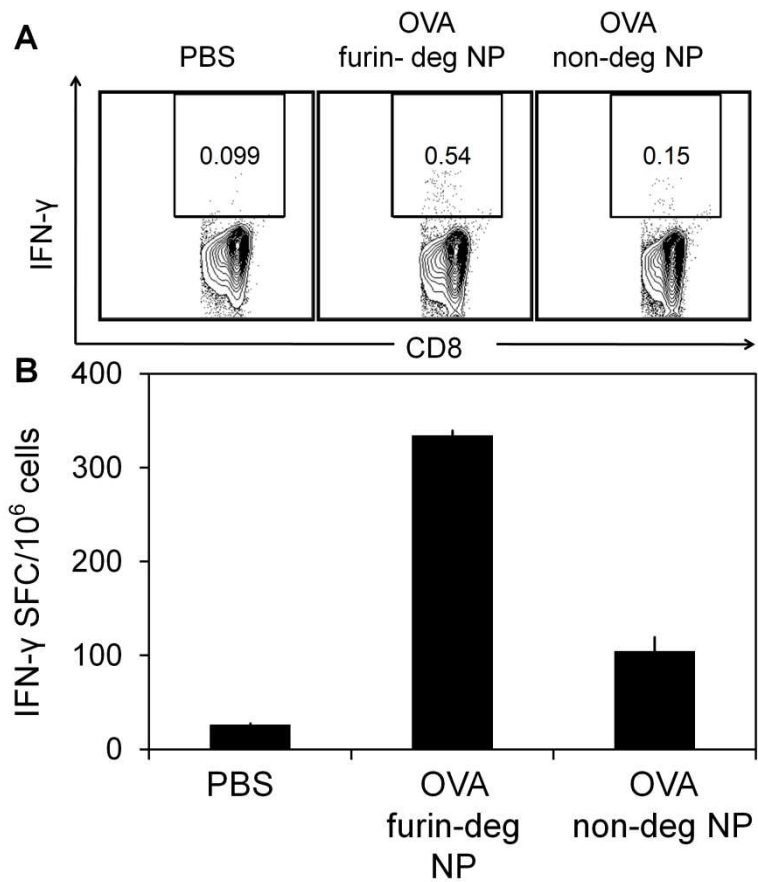
Figure 16. Splenocytes were assessed for activation of cytotoxic T lymphocytes after OVA NP injection in mice. (A) Splenocytes were co-cultured with OVA epitope peptides for 6 h and stained with IFN-γ and CD8 antibodies. Cell markers were assessed using FACS (B) ELISPOT assay in which splenocytes were co-cultured with OVA epitope peptides and screened for IFN-γ secretion. IFN-γ was quantified by counting the spot-forming cells per million cells.

secretory products of individual activated or responding cells (Figure 16B). When splenocytes were re-activated with OVA epitopes, IFN-γ was secreted by more than 3-fold higher by cells from mice treated with degradable NPs compared to mice treated with PBS or non-degradable NPs. These combined assays suggest that degradable NPs are able to deliver proteins to APCs for class I antigen presentation.

These *in vivo* studies demonstrate that protein NPs are able to deliver protein antigens to APCs. Furthermore, the engineered degradability of NPs using the furin-degradable crosslinker for synthesis allowed a 3-4 fold increase in effectiveness of antigen presentation compared to mice injected with non-degradable NPs. Further studies to assess B cell responses and MHC class I pathway would be helpful to determine the mode of antigen presentation. Furthermore, targeting studies to direct delivery to dendritic cells (DCs) could be useful for development of protein vaccinations. [213, 216] Dendritic cells are unique APCs in their ability to activate both memory and naïve T cells thus acting as a link between innate and adaptive immunity. DCs can capture and process protein antigens into peptides which are presented on MHCs and recognized by T cells. DCs can also migrate from the periphery to lymphoids with T-cell rich areas where they can interact to bring about clonal selection thereby controlling many T-cell responses. As a result, targeting DCs could represent the main objective in designing new delivery systems for subunit vaccine development.

3. ENGINEERED BIOCOMPATIBLE DEGRADABLE POLYMERIC NANOCAPSULES

Thus far, our group had developed polymeric protein nanocapsules (NCs) to facilitate intracellular delivery of diverse proteins.[57, 58, 217] These NCs have been engineered to encapsulate proteins without covalent modification and have crosslinkers that can degrade intracellularly. To achieve intracellular release of protein, the crosslinkers are designed to be degradable only when inside the cells. We used a peptidyl crosslinker containing a highly favored substrate (RVRR) of furin, a ubiquitous endoprotease in mammalian cells.[218] Upon entry into the cell, where furin activities are abundant, the crosslinkers are proteolyzed and the polymeric matrix is degraded, leading to the release of cargo in native form. Another degradation strategy is by using a redox-responsive, disulfide-containing crosslinker *N,N'*-bis(acryloyl)cystamine.[219] The polymer shell maintains its integrity under oxidative conditions outside the cell but undergoes degradation and cargo release after entry into the more reducing cytosol. We have successfully delivered recombinant proteins to human cell lines using both furin-degradable and redox-responsive NCs. However, our approach so far is based on the less desirable polyacrylamide polymer. Here we demonstrate the synthesis, optimization and application of poly(ethylene) glycol (PEG) based protein NCs in the nuclear delivery of proteins.

3.1. Synthesis of Polyethylene glycol-based Protein Nanocapsules

In order to develop an intracellular protein delivery system that is feasible for *in vivo* applications, a non-cytotoxic polymeric platform is desired. PEG is the most widely used polymer for drug delivery applications due to its biocompatibility and ability to reduce cargo aggregation and proteolysis while increasing circulation time.[220] We selected a short chain length PEG ($M_n \sim 480$) as a monomer for NC synthesis motivated by favorable properties of low molecular weight PEG including complete water solubility[221], formation of loosely packed particles[222] and easy excretion by humans[223]. A positively charged co-monomer, *N*-(3-aminopropyl) methacrylamide (M2), was also used in relatively lower quantities to provide a

slight positive charge on the surface of the NC needed for cellular entry.[74] A two-step procedure is applied to fabricate the protein NCs: first, a co-monomer mixture of M2 and PEG are deposited onto the surface of target protein by adsorption; next *in situ* polymerization is initiated in an aqueous solution, containing monomers and furin or redox-responsive crosslinkers which allow intracellular degradability of NCs (Figure 17A,B). The polymerization is allowed to proceed for 1 hour after which unreacted small molecules are removed by ultrafiltration.

We first used nuclear localization signal-tagged enhanced green fluorescent protein
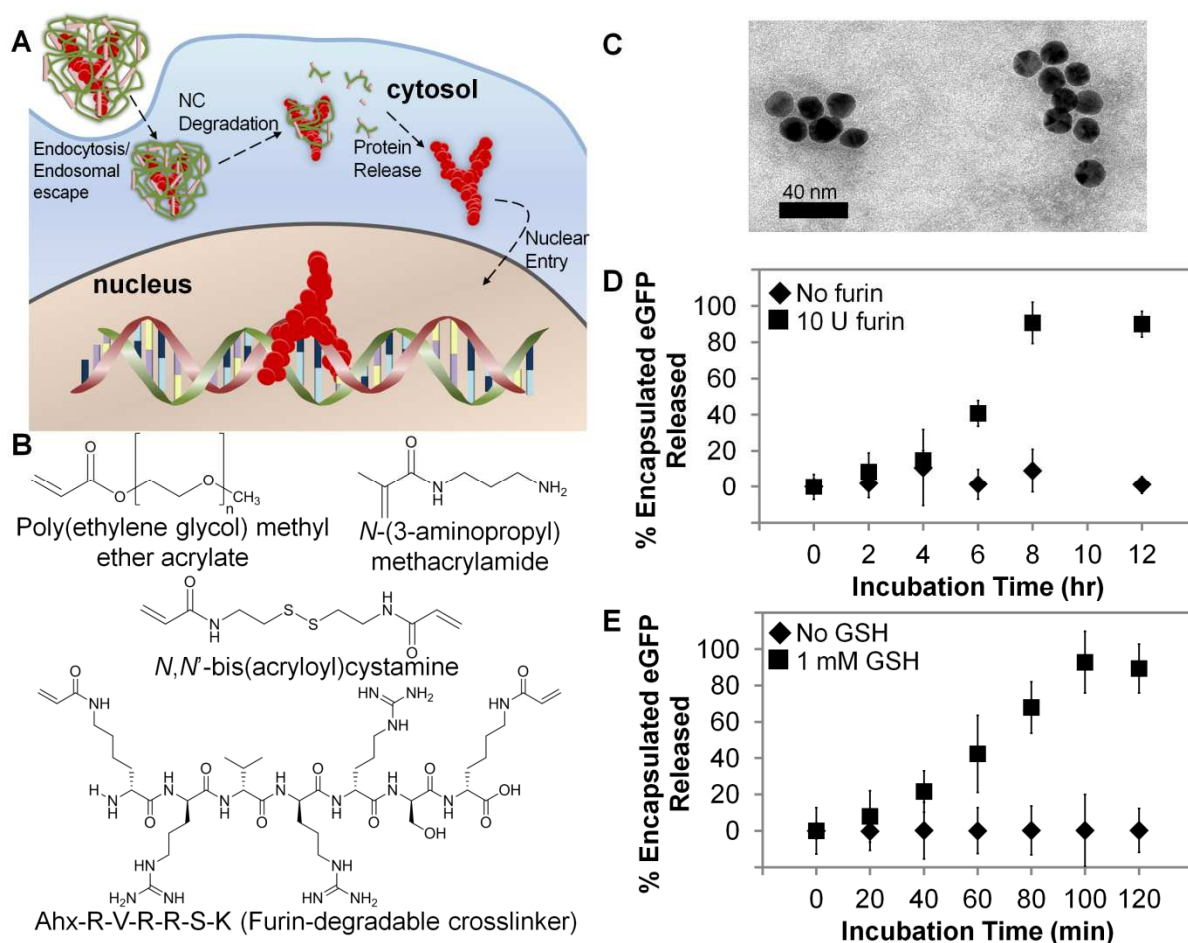
Figure 17. Furin-degradable and Redox-responsive PEG NCs can release encapsulated protein. *(A)* **Schematic of NC-mediated TF nuclear delivery. NCs are internalized into cells, the polymeric shell degrades due to furin proteolysis or reduction in the cytosol of the crosslinker (pink), the released TF in native form localizes to the nucleus to bind DNA and initiate transcription of genes.** *(B)* **Structures of monomers and crosslinkers used for NC synthesis.** *(C)* **TEM image of redox-responsive NLS-eGFP PEG NCs. The scale bar corresponds to 40 nm. NLS-eGFP release from** *(D)* **150 nmol furin-degradable NCs upon incubation with 10 U furin at 37°C and** *(E)* **10 µg NLS-eGFP redox-responsive NCs after incubation with 1 mM GSH at 37°C at various time points quantified by ELISA. Data shown represents average values with standard deviation from three independent experiments.**

(NLS-eGFP) as protein cargo to examine NC synthesis, and to establish the capability of PEG NCs to carry protein across the membrane, degrade in response to cellular cues and release protein destined for the nuclei of cells. As shown in Figure 17C, under preparation conditions, NLS-eGFP PEG NCs are uniform and spherical in size (10-20 nm) as evidenced by transmission electron microscopy (TEM) and dynamic light scattering (DLS) (Figure S11). We further quantified the release of encapsulated protein from degradable NCs using ELISA for both furin-degradable (Figure 17D) and redox-responsive (Figure 17E) NCs. Upon incubation with 10 units furin or 1 mM glutathione (GSH), degradable PEG NCs released ~90% of the encapsulated NLS-eGFP protein. In contrast, NCs released <5% of NLS-eGFP without degradation stimuli indicating that the polymeric layer can maintain structural integrity when subject to incubation at 37℃ and no outward diffu sion of the encapsulated cargo takes place.

We next sought to optimize the NC formulation to achieve the maximum relative content of PEG monomer while retaining cellular internalization. NLS-eGFP NCs were synthesized with varying PEG:M2 molar ratios using a non-degradable (ND) crosslinker (*N,N'*-methylene bisacrylamide). The NCs were physically characterized by DLS to determine the size and ζ−potential while uptake efficiency was measured by incubation with HeLa cells followed by visualization with fluorescent microscopy (Figure S11, Figure S12). As shown in Figure S11, a maximum PEG:M2 molar ratio of 3.3 was determined above which the eGFP fluorescence was undetectable inside cells, presumably due to the low ζ−potential of the NCs [224]. Additionally, NC diameters and ζ−potentials were measured along with cellular uptake efficiency to establish the optimal total amount of monomers for NC formation (total moles monomers:moles protein=21:1) (Figure S11, Figure S12). We selected a PEG:M2 molar ratio of 2.6 which afforded NCs with the most desired properties, including an average diameter of ~10 nm, lower positive ζ−potential between 0-3 mV and the resulting intracellular eGFP signal as measured by fluorescent microscopy.

3.2. Optimization of PEG NCs

We next optimized the cytosolic release properties of the NCs through tuning of the crosslinking ratio (moles crosslinker: total moles monomers) (Figure 18). The crosslinking density of NCs is a critical synthesis parameter that directly impacts intracellular degradability; a low crosslinking ratio can result in a loose polymeric matrix which "leaks" protein to the outside environment before the desired destination, whereas a high crosslinking ratio can result in a denser NC that is unable to be degraded inside the cell in a timely fashion. Using intracellular NLS-eGFP fluorescence distribution as a reporter, we can evaluate the extent of crosslinker degradation
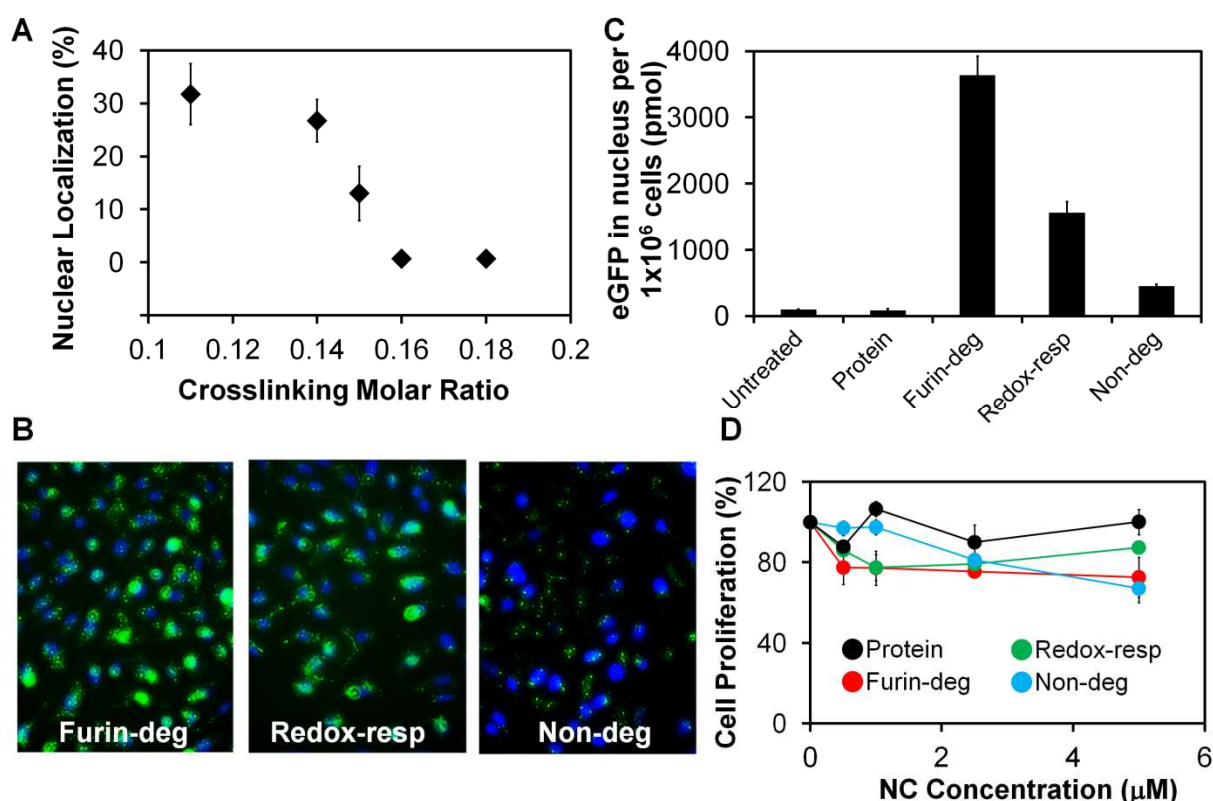
Figure 18. Biocompatible degradable PEG NCs can be engineered to deliver proteins to the nucleus. *(A)* **Localization of eGFP with nuclei when HeLa cells were treated with 400 nM NLS-eGFP non-degradable NCs with various crosslinking ratios for 24 h before imaging. Data represents average values and standard deviation of 10 images.** *(B)* **Representative images of HeLa cells treated with NLS-eGFP NCs prepared with the same molar ratio of PEG:M2 and the same crosslinking ratio with either furin degradable (furin-deg), redox responsive (redox-resp) or non-degradable (non-deg) crosslinkers. Cells were treated for 24 h with 400 nM NCs before being fixed and stained. (green: eGFP; blue: DAPI-stained nuclei)** *(C)* **Quantification of eGFP in the nuclear fraction of HFF cells using ELISA. Cells were treated with 400 nM NLS-eGFP NCs prepared with various crosslinkers for 24 h before the nuclei were isolated. The data represent the average and standard deviation of three treatments.** *(D)* **Cell proliferation profiles of various concentrations of NLS-eGFP NCs delivered to HFF cells for 24 h and quantified by the MTS assay.**

and protein release from the NCs. If the NC is unable to degrade intracellularly, fluorescence from NLS-eGFP will be retained in the cytosol due to inaccessibility of the NLS tag. However, upon disassembly of the NC polymeric layer and release of NLS-eGFP in the cytosol, the exposed NLS will guide the entry of the protein into the nuclei where green fluorescence can be visualized. To determine the minimal crosslinker density that can completely return protein cargo in the absence of degradation, NLS-eGFP NCs were prepared with a PEG:M2 ratio of 2.6 with varying crosslinking ratios using ND crosslinkers and delivered to HeLa cells. As shown in Figure 18A, NLS-eGFP delivered to HeLa cells with ND NCs synthesized from a crosslinking ratio <0.16 displayed nuclear localization, likely due to the more porous polymeric matrix that enabled outward diffusion of NLS-eGFP without degradation. Near zero nuclear localization of NLS-eGFP was found when the crosslinker ratio is >0.16 when preparing ND NCs.

Using optimized PEG:M2 (2.6) and crosslinking ratio (0.16), NLS-eGFP PEG NCs synthesized with furin or redox-responsive crosslinkers were prepared. Compared to the ND NCs described above, the three different crosslinkers afforded NCs with similar physical properties (Table S3). When delivered to HeLa cells, degradable NCs afforded significant colocalization of green fluorescence in the nuclei (Figure 18B). Optimized NLS-eGFP NCs were also delivered to human foreskin fibroblast (HFF) cells and nuclear fractions were isolated for quantification of eGFP using ELISA (Figure 18C). Nuclear eGFP concentrations were more than 1000 fold enhanced in HFF cells treated with degradable NCs compared to cells treated with native NLS-eGFP protein which is unable to enter cells. Importantly, none of the NCs displayed significant cytotoxicity in HFF or HeLa cells up to concentrations of 5 μM, promoting the biocompatibility of optimized PEG-based NCs (Figure 18D, Figure S13).

4. NUCLEAR DELIVERY OF TRANSCRIPTION FACTORS USING DEGRADABLE POLYMERIC NANOCAPSULES

4.1. Functional Delivery of a Differentiation Transcription Factor, MyoD

After establishing the capability of the new PEG-based NCs as nanocarriers for nuclear protein delivery, we targeted the delivery of a recombinant TF that can drive the differentiation of specific cells. MyoD is a TF belonging to the basic helix-loop-helix (bHLH) TF family, which contains a structural motif of two α-helices connected by a loop.[225] MyoD is a master regulatory TF capable of activating muscle-specific genes and stimulating the complete myogenesis process when introduced into a large variety of cell types.[226] MyoD function is characterized to be intimately correlated with its structural integrity which has been elucidated in many previous studies; the basic DNA-binding region and α-helices must remain intact for promoter binding and dimer formation, respectively.[227]

4.1.1. Expression, Purification and Nanocapsule Synthesis of MyoD

Mouse full-length MyoD protein (45 kDa) was expressed in *E.coli* BL21(DE3) cells with a polyhistidine tag, purified from inclusion bodies using affinity chromatography and refolded through extensive dialysis. Circular dichroism (CD) was performed to confirm that refolded MyoD regained the correct secondary structure content[228] (Figure S14). We subsequently synthesized MyoD NCs using the optimized PEG formulation with non-degradable and degradable crosslinkers and obtained NCs with sizes and ζ-potentials similar to each other (Figure 19A). MyoD NCs exhibited slightly positive ζ-potentials after synthesis as desired for cellular uptake; in contrast, native MyoD displayed a negative ζ-potential before encapsulation. Interestingly, we observed decreases in sizes and size variances of MyoD NCs (~10 nm) following encapsulation when compared to native MyoD protein (~14 nm) (Figure S15). The basic region of bHLH TFs is known to be unstructured in the absence of DNA but undergoes a conformational change into α-helices when bound to cognate DNA sequences.[229] As a result,
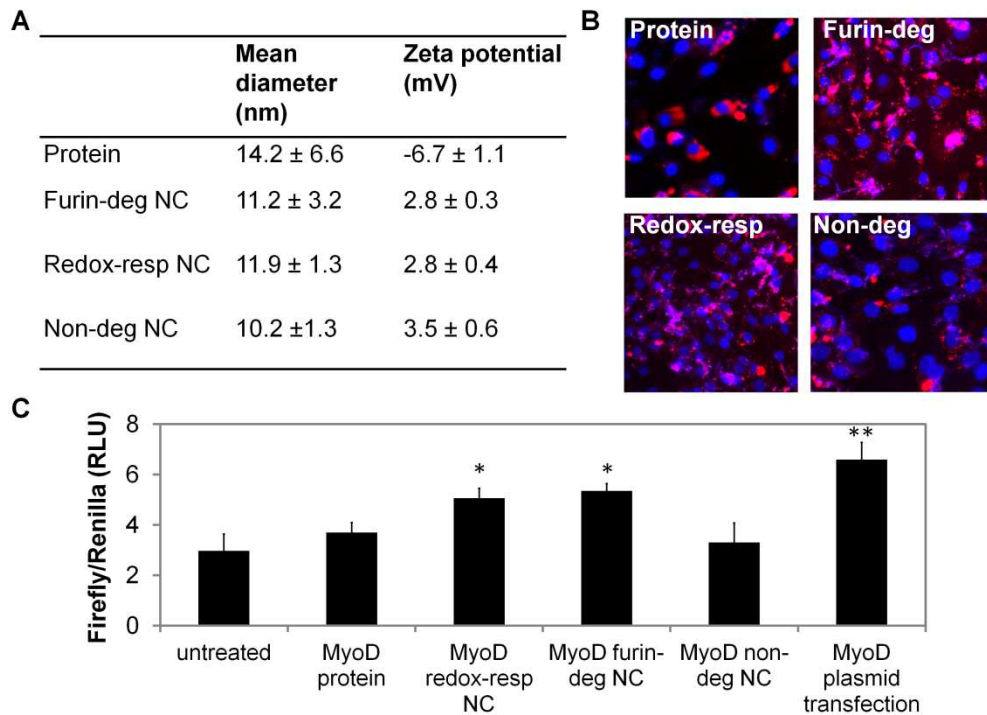
Figure 19. MyoD protein can be encapsulated in degradable PEG NCs and delivered in active form to cells. *(A)* **Mean hydrodynamic size and ζ–potential of MyoD protein and NCs prepared with various crosslinkers. (n=6).** *(B)* **Z-stack imaging of C2C12 myoblasts which were treated with 2 doses of 400 nM rhodamine-tagged MyoD protein/NCs for 48 h before being fixed and stained. (red: rhodamine-tagged MyoD; blue: DAPI-stained nuclei; purple: nuclear colocalization)** *(C)* **Dual-luciferase assay in C2C12 cells which were transfected with a MyoD-responsive firefly luciferase construct (*MyoD-luc*) and subsequently treated with 2 doses of 400 nM MyoD protein/NCs for 48 h before cells were harvested and assayed for luciferase activity. (n=4) Data is the average and standard deviation. Unpaired student *t*-test; $^{*}P<0.05$; $^{**}P<0.01$.**

the unstructured domains of MyoD may contribute to the larger hydrodynamic radius obtained from DLS measurements. Polymerization of an encapsulating layer around MyoD may therefore serve to decrease the size of MyoD in solution by constraining motion of the unstructured regions into a more compact shape.

To examine intracellular localization of delivered MyoD in C2C12 mouse myoblast cells[230], MyoD was first conjugated to a fluorescent rhodamine dye to yield MyoD-rho prior to encapsulation. As observed by confocal microscopy (Figure 19B), enhanced nuclear localization of MyoD-rho delivered *via* degradable NCs is observed in C2C12 cells in comparison to native MyoD-rho. As expected, MyoD-rho encapsulated in a ND NC exhibited little to no nuclear colocalization, further confirming the complete encapsulation of MyoD. These observations are consistent with previous findings indicating that native MyoD protein is able to penetrate cell

membranes due to an internal PTD sequence, however nuclear localization is highly inefficient compared to those delivered by degradable NCs, likely due to protein entrapment in endosomal vesicles and degradation during cellular entry.[231]

To demonstrate that MyoD delivered to nuclei by NCs was in active form, we constructed a luciferase reporter plasmid (*MyoD-luc*) containing 4 copies of the E-box sequence (CACCTG) upstream of the firefly luciferase gene. bHLH TFs are known to recognize and bind the E-box sequence to enhance transcription of downstream genes.[232] C2C12 cells were cotransfected with *MyoD-luc* and an internal control *Renilla* luciferase plasmid using Lipofectamine© and treated with 2 doses of 400 nM MyoD protein/NCs for 48 h. As shown in Figure 19C, the levels of Firefly/Renilla luciferase expression were increased for cells treated with degradable MyoD NCs or transfected with *MyoD* DNA. The lower level of increased luciferase expression may occur because the E-box sequence is not specific for MyoD and is recognized by other bHLH TFs, thereby contributing to background luciferase levels in untreated cells. Both furin-degradable and redox-responsive MyoD NC treated cells demonstrated significant increases in firefly luciferase expression (~1.5 fold). In contrast, cells treated with native MyoD and ND MyoD NC did not show significant increase in luciferase signals compared to untreated cells.

4.1.2. Differentiation of Myoblast Cells using Degradable NCs

C2C12 myoblast cells are embryonic progenitor cells which have the potential to develop into all three muscle types: skeletal, cardiac or smooth muscle.[227] When introduced into cells from the mesoderm layer, MyoD commits cells to the skeletal lineage and further regulates the process by increasing its own expression as well as enhancing expression of other myogenic TFs and differentiated muscle proteins in a feed-forward mechanism. These cellular actions lead to myogenic differentiation and a phenotypic change from proliferating myoblasts to contractile multinucleated muscle fibers made of myotubes. Having established that degradable PEG NCs can deliver recombinant MyoD in active form to the nuclei of C2C12 cells, we devised
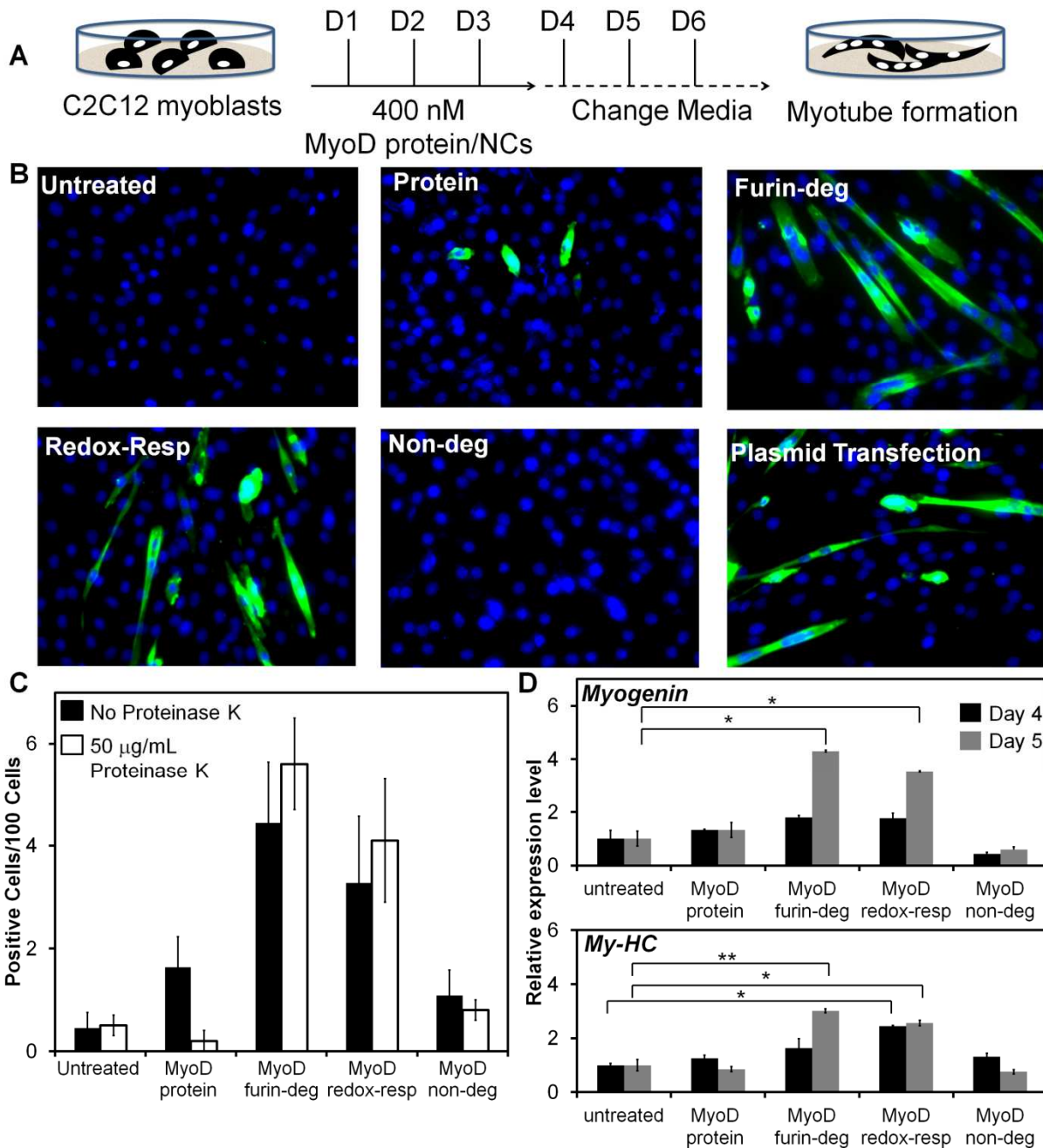
Figure 20. C2C12 myoblasts can be differentiated into myotubes using degradable MyoD NCs. *(A)* Schematic of treatment of C2C12 myoblasts with MyoD protein/NCs to induce differentiation to multinucleated, elongated myotubes. *(B)* Fluorescent images of C2C12 cells after MyoD protein/NC treatment. Cells were immunostained with a myosin heavy chain (My-HC) antibody conjugated with an Alexa-Fluor 488 antibody (green). Nuclei were counterstained with DAPI (blue). *(C)* Quantification of positively-stained cells for each treatment group with and without 50 µg/mL proteinase K for 1 h at 37℃. Data is the average and standard deviation of 10 images. *(D)* Real-time PCR analysis of the relative expression of muscle-specific genes of myogenin and My-HC in treated C2C12 cells at day 4 and day 5 of treatment. (n=2). Unpaired student *t*-test; [*]P<0.05; [**]P<0.01.

a treatment protocol for myoblasts in which cells were treated for 3 days with 400 nM of either

native MyoD protein or MyoD NCs (Figure 20A). Subsequently, the media was changed each

day until day 7 when cells were analyzed for differentiation. To test the extent of differentiation of myoblast cells into mature myotubes, we performed immunostaining using a myosin-heavy chain (My-HC) antibody. My-HC is the major muscle protein of the contractile apparatus of mature muscle fibers and its increased expression is correlated with increased expression of MyoD.[233, 234] As evidenced by fluorescent imaging and quantification (Figure 20B and C), an increased number of cells exhibited My-HC expression when treated with degradable MyoD NCs as compared to cells treated with ND NCs or native MyoD protein. More excitingly, cells treated with degradable NCs also displayed elongation and multinucleation which are hallmark morphological properties of differentiated myotubes.[235] In contrast, untreated and ND MyoD NC-treated cells did not show positive staining for My-HC or morphological changes. Native MyoD protein-treated cells displayed low levels of positive staining for My-HC but did not exhibit elongated multinucleated myotubes as observed in cells treated with degradable MyoD NCs, possibly due to incomplete differentiation as a result of inefficient delivery. Notably, cells treated with degradable MyoD NCs displayed similar differentiation patterns and efficiencies to cells transfected with *MyoD* plasmid using Lipofectamine[©].

We further characterized the differentiation of myoblast cells by analyzing gene expression of myogenic markers My-HC and myogenin using quantitative real time PCR at various time points during the treatment (Figure 20D, Figure S16, Table S4). Myogenin is an essential bHLH TF acting downstream of MyoD that coordinates skeletal muscle development into early myotubes.[236] As shown in Figure 20D, degradable MyoD NC-treated cells showed a gradual increase in myogenin and My-HC expression and exhibited a significant increase in myogenic gene expression compared to untreated cells within 5 days after treatment. In contrast, cells treated with native MyoD and ND MyoD NCs did not exhibit significant increases in myogenin or My-HC expression within day 5. The late-stage increased expression of myogenin in MyoD protein-treated cells may be attributed to partial differentiation of myoblasts which is further supported by low expression of the later myogenic differentiation marker, My-

HC observed from immunostaining and real-time PCR (Figure S16). The enhanced gene expression at earlier time points in degradable MyoD NC-treated cells may correlate to a greater quantity of functional MyoD being present in the nuclei, thereby providing the foundation to drive differentiation through cooperative association with MyoD or other related proteins to bind DNA and initiate transcription of myogenic proteins. The myogenic differentiation initiated by MyoD degradable NCs indicates that structural motifs of MyoD are preserved throughout the entire delivery and release steps. In addition to the requirement for the basic DNA-binding region of MyoD to be intact for E-box promoter binding and subsequent transcription [237-239], the α-helices of MyoD must also form homodimers or interact with the E47 co-activator to form heterodimers to activate differentiation marker expression.[240-242] Moreover, MyoD adopts different conformations in response to particular co-activators, further establishing the importance of maintaining intact MyoD structure for eventual myogenic differentiation.

4.1.3. Protease Treatment of MyoD NCs

A desired property of nanocarriers for intracellular delivery is the ability to protect encapsulated biological components from potential degradation encountered before and during cellular entry. The unstructured regions of MyoD are targets of cellular proteases and can be inactivated upon proteolysis. To test the ability of degradable NCs to withstand external proteolysis, we incubated MyoD protein or MyoD NCs with proteinase K (PK), a broad spectrum serine protease [243]. MyoD protein or MyoD NCs were incubated with 50 μg/mL PK at 37°C for 1 h and subsequently incubated with C2C12 cells using the differentiation treatment protocol (Figure 20A). As shown in Figure 20C and Figure S17, degradable NC-treated cells persisted in forming elongated and multinucleated mature myotubes as evidenced by immunostaining and subsequent quantification. In contrast, native MyoD protein-treated cells completely lost the ability to drive the differentiation of myoblasts into myotubes, reflected in the same number of positively stained cells as background levels (Figure 20C). These combined results confirm the ability of

polymeric NCs to shield proteins from external degradation factors such as proteolysis and retain the activity of encapsulated protein.

4.1.4. Conclusions from MyoD Delivery using NCs

Intracellular delivery of recombinant TFs has extensive therapeutic impact by directing cell fate without introducing foreign genetic material into cells. The various structural components of TFs required for interacting with a plethora of macromolecular partners/targets necessitate the proteins to remain unmodified during the internalization and delivery process. In this study, we demonstrated the design, synthesis and optimization of PEG-based degradable protein NCs. Notably, PEG NCs did not display cytotoxicity in concentrations up to 5 μM, supporting the future development of degradable NCs for *in vivo* applications. We established that the *in situ* polymerization strategy can package the TF MyoD into robust, spherical and sub-20 nm nanocapsules. The degradable NCs can subsequently deliver MyoD to the cytosol of myoblast cells, release functional MyoD to enter the nuclei and initiate myogenic differentiation. Importantly, PEG NCs are validated as a platform which retains encapsulated protein structure and activity as evidenced by the ability of MyoD to perform complex downstream processes and regulate myogenesis.

4.2. Functional Delivery of a Transdifferentiation Transcription Factor, Pdx1

Diabetes is a chronic disease resulting from high blood sugar that affects more than 171 million people worldwide and is projected to rise to 366 million in 2030.[244] Type I diabetes results primarily from a T-cell-mediated autoimmune response against β-cells in the pancreas which are responsible for producing insulin.[245] Consequently, glucose cannot be effectively transported into cells resulting in plasma glucose concentrations exceeding 200 mg/dL.[246] Type I diabetes patients suffer from polyuria, polydispia, polyphagia and weight loss and have increased risks for cardiovascular diseases, neuropathy, nephropathy, osteoporosis, pregnancy complications, hearing problems and eye damage. [247-249] Untreated type 1 diabetes commonly leads to diabetic ketoacidosis, a life-threatening condition in which the liver begins to convert fatty acids into acidic ketone bodies in response to insulin shortage.[250] Currently, addition of exogenous insulin remains the primary treatment option for type I diabetic patients and can be administered through subcutaneous injection or insulin pumps.[251] Due to the lifelong need to monitor glucose level and invasive insulin treatments, alternative therapeutic methods for type 1 diabetes that improve the quality of life are desired.

Replacement with healthy pancreatic β-cells could free diabetic patients from constant glucose testing, dietary restrictions, insulin injections and maintain continuous normoglycemia.[252] However pancreas or islet implantations suffer from strong immune responses and restriction of donors.[253] An alternative is regenerative medicine which aims to replace damaged tissues by replacing affected cells with functional cells of the same type.[84] Since differentiated β-cells cannot be expanded *in vitro*, alternative means for generation *in vivo* have been explored.[141] An example is the production of pancreatic β-islet cells by inducing transdifferentiation of liver cells or exocrine pancreatic cells through forced expression of specific transcription factors (TFs).[142, 148] Liver and pancreatic progenitor cells develop from the endoderm layer and continue to have evolutionary-conserved signals and transcription factors

during maturation. Some organisms display a composite liver-pancreas organ displaying the intimate biological composition between both cells.[254] 20% of mice livers express insulin at low levels serving as additional evidence for the propensity of liver cells to transdifferentiate into pancreatic β-cells.[146, 255] Exocrine cells are also suitable candidates for transdifferentiation to an endocrine cell line since they also derive from the endoderm layer.[256] Furthermore, when exocrine cells are cultured *in vitro* and are dissociated, activation of endocrine genes is observed.[257, 258] Several groups have reprogrammed exocrine cells into endocrine β-cells using expression of TFs.[142, 259, 260]

A master TF involved in pancreatic development is pancreatic and duodenal homeobox gene 1 or Pdx1. Pdx1 is a homeodomain TF belonging to the ParaHox family and consists of the trademark helix-turn-helix structure in which three α-helices are connected by short loop regions.[261] The C-terminal helix associates directly with DNA to form a complex in an induced-fit model which depends on DNA conformation in response to binding of other TFs.[262] Homozygous PDX1 knockout mice form pancreatic buds but do not develop the pancreas.[263] In addition to pancreatic development, Pdx1 regulates insulin production and other essential genes for islet β-cell development.[264] Heterozygous mutations of Pdx1 in humans causes early onset of diabetes.[265] Due to these crucial transcriptional regulatory roles, genetic reprogramming of liver cells into pancreatic β-cells has been demonstrated by delivery of Pdx1 by introducing recombinant adenoviruses[266-268], lentiviruses[269] and transgenic DNA[270]. The transdifferentiation shifts are confirmed by activated expression of insulin and other pancreatic genes coupled with the ability to lower blood glucose levels in diabetic mice. To enhance intracellular delivery of Pdx1 protein, a TAT PTD can be fused to the protein.[271, 272] Notably, other TFs can enhance the transdifferentiation abilities of Pdx1 such as Neurogenin3 or Ngn3, Mafa or NeuroD.[142] Ngn3 is expressed in pancreatic endocrine progenitor cells and is critical for endocrine pancreatic cell fate specification.[273] In the pancreas, Mafa is exclusively expressed in β-cells and serves as a

strong transactivator for insulin expression and secretion as well as β-cell survival.[274] NeuroD is a bHLH TF which forms a dimer with E47 and binds around E14 to specify the endocrine lineage.[275] These critical TFs involved in various stages of pancreatic development can work synergistically to reprogram non-β cells into pancreatic β-cells.

For sufficient insulin production and secretion to control diabetic blood glucose levels, only ~1% of liver cells need to transdifferentiate into β-islet cells.[141, 276] Despite numerous studies, this feasible therapeutic target remains largely experimental due to the lack of safe delivery methods. Adenoviral vectors are attractive due to lack of insertional mutagenesis but exhibit extreme immune responses in clinical trials which can lead to death.[277] Kojima *et al.* observed fulminant hepatitis in mice and massive death upon tail-vein injection of helper-dependent adenovirus-Pdx1.[278] Direct delivery of protein is safer than viral methods but is difficult due to instability of native, unprotected proteins.[23] For this reason, although Pdx1 contains an internal Antennapedia-like protein transduction domain (PTD) to promote cellular entry through macropinocytosis[279, 280], its direct delivery *in vivo* for liver cell transdifferentiation has been met with difficulties. Koya and coworkers delivered TAT-Pdx1 to diabetic mice intraperitoneally, presumably to avoid proteolysis and aggregation of Pdx1 in the bloodstream.[272] Therefore, an effective protein delivery method that can transport native proteins and circumvent protein instability in serum can be a valuable tool in not only liver-pancreas transdifferentiation, but for *in vivo* cellular reprogramming in general.[281] As such, degradable polymeric NCs for efficient delivery of master TFs such as Pdx1/Ngn3/Mafa/NeuroD to liver cells may drive the transdifferentiation of a subpopulation into pancreatic beta-like cells that express insulin *in vivo* and could represent a new therapeutic option for treating this debilitating disease. We also aimed to establish the ability of degradable protein NCs to deliver TFs to induce transdifferentiation of one differentiated cell lineage into another lineage for therapeutic implications.

4.2.1. Pdx1 Purification and Nanocapsule Synthesis

Full-length rat Pdx1 protein (~45 kDa) was expressed in *E.coli* BL21 cells with a C-terminal polyhistidine tag and purified using nickel resin chromatography (Figure 21A). The purification process was optimized by adjusting the incubation time with nickel resin as well as by incorporating a protease inhibitor to avoid degraded products (Figure S18). We subsequently tagged Pdx1 with rhodamine and synthesized Pdx1 NCs using the PEG formulation with non-degradable and degradable crosslinkers and obtained NCs with sizes and ζ-potentials similar to each other (Figure 21B). Similar to observations in MyoD experiments, Pdx1 protein exhibited a larger hydrodynamic diameter and variance prior to encapsulation indicating that the NC may constrain the loose motion of TF side chains into a compact form. We further analyzed the ability of NCs to deliver protein into liver cells by incubating 400 nM Pdx1 protein/NCs with

	Size (nm)	Zeta potential (mV)
Pdx1-rho	12.2 ± 5.3	-7.6 ± 1.5
Pdx1-rho redox-resp NC	6.3 ± 1.6	2.8 ± 1.0
Pdx1-rho furin-deg NC	7.5 ± 1.5	3.3 ± 0.1
Pdx1-rho non-deg NC	7.7 ± 1.1	5.2 ± 0.8
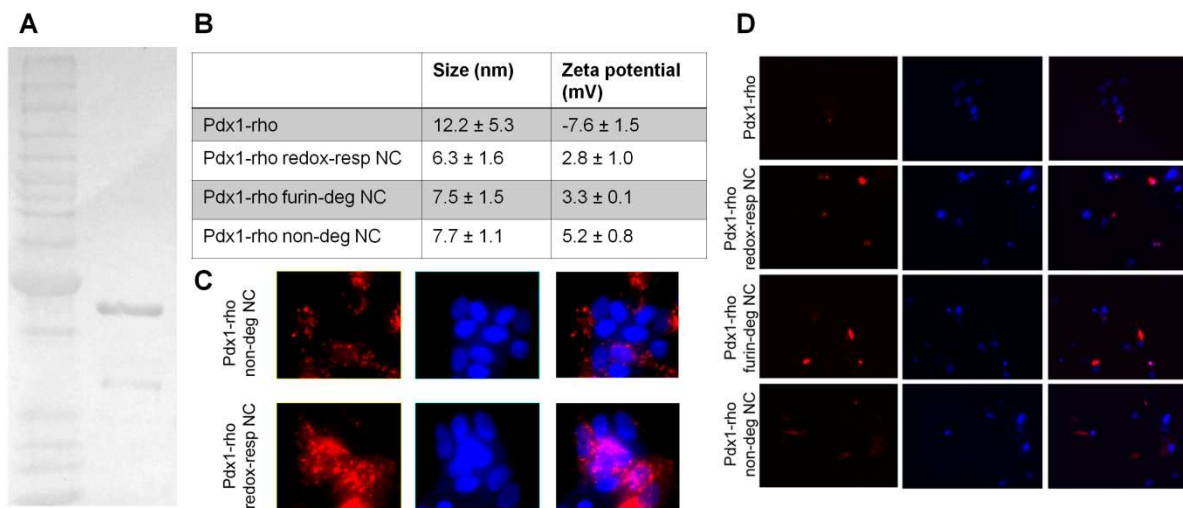
Figure 21. Purification of Pdx1 protein, NC formation and uptake in liver cells. (A) SDS-PAGE gel of purified Pdx1 protein (~45kDa). The ladder is Benchmark protein ladder. (B) Hydrodynamic size and zeta potential of rhodamine-tagged Pdx1 protein and NCs. (C) Uptake of Pdx1-rho in HepG2 liver carcinoma cells and (D) Fetal liver cells. Cells were treated once with 400 nM protein/NCs and imaged 24 hours later. Red: Pdx1; Blue: DAPI-stained nuclei.

HepG2 and fetal liver cells (Figure 21C,D). The HepG2 cell line is a hepatocellular carcinoma cell line which is often used for liver metabolism and targeting studies.[282] Optimization of NCs using HepG2 cells may help provide information of desirable formulation and delivery parameters of Pdx1 for liver transdifferentiation. Human fetal liver cells were also used to

assess Pdx1 delivery via NCs. As seen in Figure 21C and D, a marked overlap of Pdx1 and cell nuclei is observed when degradable NCs are used for Pdx1 delivery. In contrast, Pdx1 remains constrained to the cytosol when non-degradable NCs are delivered. Interestingly, native Pdx1 protein did not show significant uptake in liver cells despite its internal PTD sequence. Insufficient delivery of native Pdx1 due to proteolysis or degradation may explain the addition of extra PTD tags on the surface of Pdx1 used by other research groups to induce efficient transdifferentiation.

Figure 22. Biological assays to determine activity of delivered Pdx1. (A) Dual-luciferase assay performed on HepG2 cells which were treated once with either 400 nM or 1600 nM Pdx1 redox responsive NCs with differing crosslinking ratios. Firefly/Renilla ratios are normalized with 1 being the ratio for untreated cells. (B) MTS assay assessing the biocompatibility of degradable Pdx1 NCs. NCs were incubated with HepG2 cells for 48 h before the cells were assessed for cytotoxicity (C) qPCR on fetal liver cells treated with 400 nM protein/NCs after 5 days to determine gene expression of human Pdx1, Insulin and IAPP. Expression was normalized to GADPH.

4.2.2. Biological Activity of Pdx1 Delivered to Liver cells

We sought to further characterize the ability of degradable NCs to deliver Pdx1 in active form to the nuclei of liver cells. To directly optimize the formulation of NCs to yield the desired phenotype, we performed a dual luciferase assay using RIP2-luc which encodes the rat insulin II promoter upstream of the reporter luciferase gene.[283] As shown in Figure 22A, optimal crosslinking densities for redox-responsive NCs were identified which yielded increasing Firefly luciferase expression in HepG2 cells. According to these results, the

most favorable formulations to induce an increase in firefly luciferase expression were NC 5, 8, 11 and 12 which used crosslinking ratios of 0.11, 0.13, 0.15 and 0.19, respectively. Interestingly, increasing the concentration of delivered Pdx1 NCs did not significantly increase the luciferase expression for specific NC formulations. As shown in Figure 22B, degradable NCs showed similar non-cytotoxic profiles to cells as Pdx1 native protein up to concentrations ~1.6 μM, suggesting the NCs exhibited biocompatible properties towards liver cells. We further desired to assess the ability of degradable Pdx1 NCs to induce β-cell specific gene expression. (Table S5) Fetal liver cells were treated 3 times with 400 nM protein/NCs and cells were harvested after 5 days to assess the gene expression of Pdx1, Islet Amyloid Polypeptide or IAPP, and Insulin. IAPP is a peptide hormone co-secreted with insulin in β-cells in a ratio of ~100:1.[284] As shown in Figure 22C, a slight increase in Pdx1, insulin and IAPP expression was observed in fetal liver cells treated with degradable Pdx1 NCs compared to cells treated with native protein or non-degradable NCs. The enhanced expression of genes associated with the β-cell genotype does suggest a slight activation induced by Pdx1 protein delivered through redox-responsive NCs. The greatest difference was a two-fold increase in insulin expression in cells treated with redox-responsive Pdx1 NCs. However, this increase in insulin expression remains far below threshold values in literature which are necessary for transdifferentiation of liver cells to pancreatic cells.

The addition of other TFs along with Pdx1 may enhance the transdifferentiation profile of liver cells due to the synergistic effects of several factors working together. A potential candidate TF to work alongside Pdx1 is NeuroD, a TF expressed in pancreatic and intestinal endocrine cells and neural tissue.[285] NeuroD plays an important role in early stages of pancreatic islet morphogenesis and maintains adult β-cell function by positively regulating insulin expression.[286] NeuroD is expressed in the developing and adult pancreas and is expressed in all endocrine cells of mature islets. Mice which do not express NeuroD do not have islets, have fewer β-cells and develop diabetes while mice overexpressing NeuroD have an increasing number of

endocrine cells in the pancreas.[287] Several research groups have used NeuroD for transdifferentiation or reprogramming of various cell types into β-cells, either alone or with other TFs or growth factors.[288-291] NeuroD protein injection into the caudal vein of diabetic mice was found to reverse hyperglycemia within one week.[292] It has been found that insulin-enhancer elements E-box and A-box strongly contribute in regulating cell-specific expression of insulin; specifically, Pdx1's binding to the A-box along with NeuroD's binding to the E-box are imperative for insulin gene transcription.[293, 294] Studies have suggested that Pdx1 and NeuroD physically interact to form a nucleoprotein complex on the insulin gene that mediates the formation of a short DNA loop.[295] For these reasons, the delivery of Pdx1 and NeuroD together could lead to surrogate insulin-producing cells which could replace defective β-cells.[296]

Figure 23. Effect of transfected NeuroD on Pdx1 protein delivery. Dual-luciferase assay was performed on HepG2 cells which were first transfected with NeuroD plasmid and then treated once with either (A) 400 nM or (B) 800 nM Pdx1 NCs with differing crosslinking ratios. Firefly/Renilla ratios are normalized with 1 being the ratio for untreated cells.

To this end, we transfected HepG2 cells with NeuroD and repeated previously used treatment protocols with Pdx1 degradable NCs to determine if the addition of NeuroD could help transdifferentiation properties. After transfecting HepG2 cells with NeuroD and RIP2-luc, cells were treated with Pdx1 NCs, lysed and evaluated for firefly luciferase expression. As shown in Figure 23, an enhanced Firefly/Renilla luciferase signal was observed for several cell groups treated with NeuroD and Pdx1 NCs compared to cells only treated with Pdx1 NCs. There also seemed to be a dependence of luciferase expression on crosslinking ratio used for NCs which

was similar to observations from Figure 22A. With 400 nM Pdx1 NCs, the transfection of NeuroD resulted in a near two-fold increase in firefly luciferase expression (Figure 23A). Treatment with 800 nM Pdx1 NCs, did not result in increased expression for specific formulations as seen in Figure 23B. These findings suggest that NeuroD could be useful in increasing the effect of delivered Pdx1. However, the enhancement level remains below appreciable levels for transdifferentiation of liver cells to pancreatic β-cells. In order to induce insulin expression and other downstream factors necessary for cell reprogramming, a stronger induction of insulin expression will be necessary. This may be accomplished by addition of other growth factors, TFs or genetic delivery to assist NC-mediated protein delivery.

4.3.3. Biological Assays to Probe Activity of Delivered Pdx1 to Exocrine Pancreatic Cells

To enhance the effect of transdifferentiation by Pdx1 NCs into β-cells, several other cell lines may have increased propensity for reprogramming compared to liver cells. For example, several groups have used embryonic stem cells and added Pdx1 exogenously to induce β-cell formation or insulin-producing cells.[297-299] The plasticity of embryonic stem cells and ability to differentiate into all three germ layers make them suitable candidates for β-cell precursors. However, several studies have found that while insulin-producing cells can be induced from embryonic stem cells, often the gene expression, metabolism, growth potential and secretory function can be different from β-cells.[300] Efficient and complete transdifferentiation may be achieved using cells which are more similar in lineage to endocrine pancreatic β-cells.[301] Furthermore, *in vitro* differentiation followed by expansion *ex vivo* could provide a suitable path for implantation of β-cells.[141] Despite varied functional roles and morphological characteristics, endocrine and exocrine cells share the same embryological origin of the gut endoderm.[302] The combinatorial activities of a small number of TFs leads to pancreatic stem cell populations and eventual pancreatic cell fate specification.[303] As such, exocrine and endocrine cells share an intimate interrelation among endoderm cell types. Several groups have utilized exocrine cell

lines to create endocrine cells due to their similar developmental mechanisms and biosimilarity.[142, 257, 258, 304-306]

AR42J cells are exocrine rat cells which were originally derived from an azaserine-induced pancreatic tumor.[307] AR42J-B13 are a subclone of AR42J cells which exhibit enhanced capability to differentiate into insulin-secreting cells[308] as well as the ability to differentiate into hepatocytes[309]. AR42J-B13 cells are characterized by being easily cultured and have a stable phenotype which can be challenging for primary pancreatic exocrine cells which can undergo de-differentiation in suspension culture[310] or ductal transformation in adherent culture[311]. Furthermore, analysis of AR42J-B13 cells is limited to one cell type compared to samples of pancreatic tissue from animals which can be contaminated with connective tissue cells and blood vessels in addition to the epithelium. AR42J-B13 cells have been converted to insulin-producing cells after culture on Matrigel[312] and specific growth factor treatment[313] but in this study, none of these methods were used.

To assess if Pdx1 protein could be delivered using degradable NCs to AR42J-B13 cells, we encapsulated rhodamine-tagged Pdx1 in NCs and incubated them with AR42J-B13 cells for
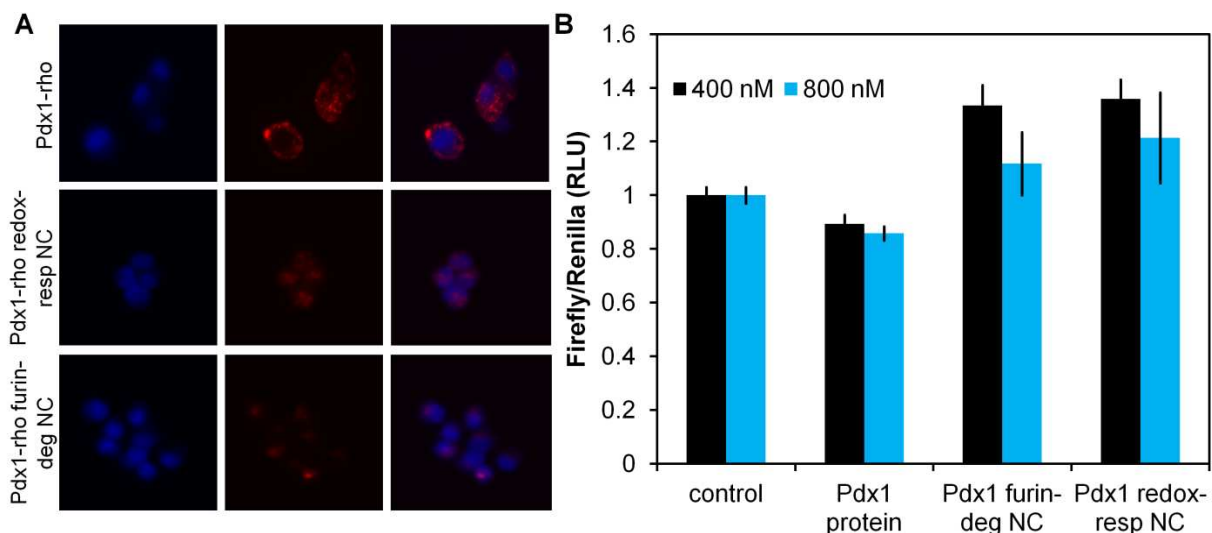
Figure 24. Pdx1 delivery to AR42J-B13 cells. (A) AR42J-B13 cells were treated once with 400 nM protein/NCs and imaged 24 hours later. Red: Pdx1; Blue: DAPI-stained nuclei. (B) Dual-luciferase assay performed on AR42J-B13 cells which were treated once with either 400 nM or 800 nM Pdx1 redox responsive NCs with differing crosslinking ratios. Firefly/Renilla ratios are normalized with 1 being the ratio for untreated cells. Data shown are the mean and standard deviation, n=4

24 hours. As shown in Figure 24A, an enhanced nuclear localization of Pdx1 protein was observed when delivery was achieved using degradable NCs with redox-responsive or furin-degradable crosslinkers compared to Pdx1 native protein. Native protein was constricted to the cytosol of cells. Interestingly, a higher degree of delivery was achieved for native protein in AR42J-B13 cells as compared to HepG2 and fetal liver cells as shown in Figure 21C and D. We also delivered Pdx1 protein/NCs to AR42J-B13 cells while transfecting RIP2-luc to assess the ability of delivered Pdx1 to activate the insulin promoter. As seen in Figure 24B, a slight increase in firefly luciferase expression (~1.5 fold) was observed for cells treated with 400 nM redox-responsive or furin-degradable Pdx1 NCs. In contrast, the level of luciferase expression in cells treated with Pdx1 protein remained similar to that of untreated cells. We further shifted our focus to the ability of degradable NCs to induce gene expression of endocrine markers.

To assess the ability of delivered Pdx1 to activate the downstream genes for β-cell formation, we treated AR42J-B13 cells with 4 treatments of 400 nM protein/NCs over 7 days. AR42J-B13 cells were first evaluated for morphological changes upon Pdx1 treatment. As shown in Figure 25A, untreated cells remained round-shaped and clustered together, a hallmark morphological property of AR42J-B13 cells.[308] In contrast, cells which were treated with Pdx1 degradable NCs showed fewer round-shaped cells and an emergence of spindle-shaped cells, a characteristic property of cells differentiating to an endocrine phenotype.[314-316] Furthermore, the cells are more dispersed and flattened which is similar to observations in previous studies.[317] AR42J-B13 cells treated with Pdx1 protein exhibited modest emergence of spindle-like cells but remained tightly clustered and with a round morphology indicating that the delivery of Pdx1 was not as efficient as with degradable NCs.

We further assessed the ability of delivered Pdx1 to activate gene expression by harvesting AR42J-B13 cells and performing quantitative real-time PCR on genes relevant to β-cell differentiation.[318] (Table S5) As shown in Figure 25B, AR42J-B13 cells treated with
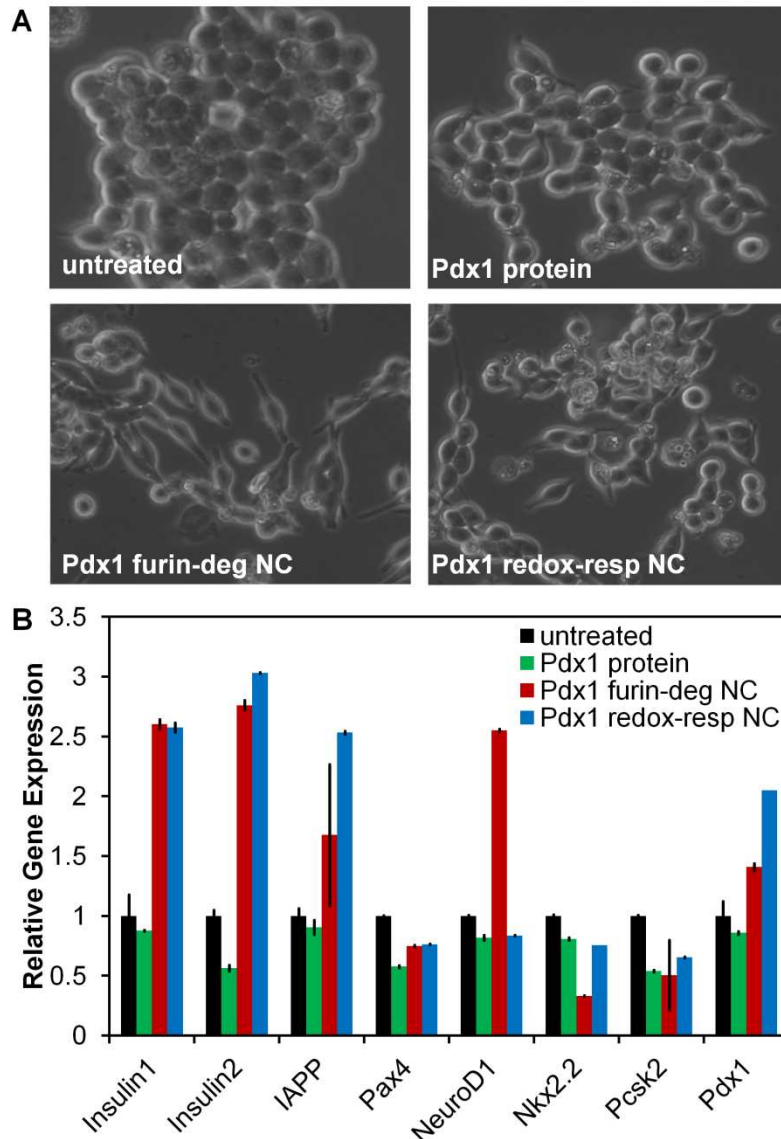
Figure 25. AR42J-B13 cells assessed for phenotype and genotype changes. Cells were treated with 400 nM Pdx1 protein/NCs for 4 treatments over 7 days and evaluated for morphology and gene expression. (A) Morphological changes shown in phase images of AR42J-B13 cells post-treatment. (B) Cells were harvested and evaluated for b-cell gene expression. Expression was normalized to rat GADPH. n=2.

degradable Pdx1 NCs began to express the *Insulin1 and Insulin2* genes as evidenced by the near ~3 fold increase in gene expression. Expression of IAPP which is not typically expressed in AR42J-B13 cells was also enhanced in cells treated with degradable NCs by a 1.5-2 fold increase. We also assessed gene expression levels of genes encoding β-cell transcription factors such as NeuroD1 and Nkx2.2. Cells treated with furin-degradable Pdx1 NCs exhibited a ~2.5 fold increase in NeuroD1 expression, which is expressed in the late differentiation process for β-cell commitment.

Expression of later TF Pax4, which is critical for islet development, and Pcsk2 which is a pro-insulin process enzyme were not enhanced in treated cells. The expression of endogenous Pdx1 was modestly increased. Pdx1 protein-treated AR42J-B13 cells did not show enhancement of any downstream genes. These findings indicate that degradable Pdx1 NCs were able to deliver Pdx1 to enhance the gene expression of several key TFs and proteins

downstream in the β-cell differentiation process. For a greater enhancement of gene expression required for transdifferentiation, the addition of other transcription factors and growth factors may enhance the ability to direct cell fate. Furthermore, chromatin remodeling factors or other DNA-based protein delivery may prime the cell towards a transdifferentiating state which is difficult to achieve with exogenous delivery of recombinant protein.

4.3. Delivery of a Combination of Transcription Factors for Formation of iPS Cells

Stem cell biology has grown dramatically after the groundbreaking discovery that somatic cells can be reprogrammed to induced pluripotent stem (iPS) cells from both mouse embryonic and adult fibroblasts upon the expression of a defined set of transcription factors, Oct4, Sox2, Klf4 and c-Myc (OSKM), which were delivered retrovirally.[95, 100] These cells are able to self-renew, maintain pluripotency *in vitro* and *in vivo* and differentiate into cell types of all three germ layers. These findings suggested the possibility of disease and patient-specific regenerative medicine therapies as well as a powerful means to create disease models in culture and to screen the efficacy and safety of drugs. However, retroviral or lentiviral delivery methods raise safety concerns because viral integration within endogenous genomes can result in harmful gene activation.[108] To combat the safety concerns of viral integration and move towards potential clinical applications, iPS cells have also been generated using episomal vectors,[319] adenoviruses,[151] plasmids[152, 153] and transposons followed by transgene removal using Cre-mediated excision[154]. However the safety concerns of delivering these transcription factors using any genetic method remain widespread because of the potential for unexpected genetic modifications by the exogenous sequences in target cells. Furthermore, these DNA-based methods require extensive validation of the vector-free status of iPS cells through Southern hybridization and DNA sequencing.

Several groups have succeeded in using permeable recombinant proteins Oct4, Sox2, Klf4, and c-Myc to make mouse and human iPS cells. One approach for intracellular delivery is to tag recombinant proteins with a cell-penetrating peptide such as HIV glycoprotein fragment Tat and poly-arginine (R) peptide.[12, 15] Such a technology has recently been used to transduce cell reprogramming factors Oct4, Sox2, Klf4, and c-Myc into mouse and human fibroblasts to make induced pluripotent stem cells.[158, 159] However, there are major limitations in the use of eleven-arginine (11R)-tagged Yamanaka factors in cell reprogramming. First, these recombinant factors are not stable in cell culture, thus a majority of Oct4-11R, Sox2-11R, Klf4-11R, and c-

Myc-11R proteins are degraded in cell culture medium. Similarly, for those residual factors that are transduced through endocytosis, a majority of those proteins are also degraded by proteolysis intracellularly. Therefore, the efficiency of using current intracellular delivery methods for cell reprogramming is extremely low and is currently beyond any practical use. Kim *et al.* reported iPS reprogramming in 1 out of 100,000 human fibroblasts by applying cell extract expressing the four factors tagged with a nonarginine (9R) PTD. Zhou *et al.* purified the four factors genetically fused to a C-terminal 11R PTD from *E.coli* inclusion bodies to reprogram 6 out of 100,000 MEF cells. The efficiency of PTD-based methods are 10 fold less than viral methods and thus, beyond any practical use.

4.3.1. Physical Characterization of OSKM Nanocapsules

The synthesis of OSKM NCs was optimized using physical adsorption of monomers and crosslinkers to the surface of protein and subsequently by initiating polymerization using free radical initiators. As shown in Figure 26A, NCs synthesized with this formulation utilizing *in situ* polymerization yields
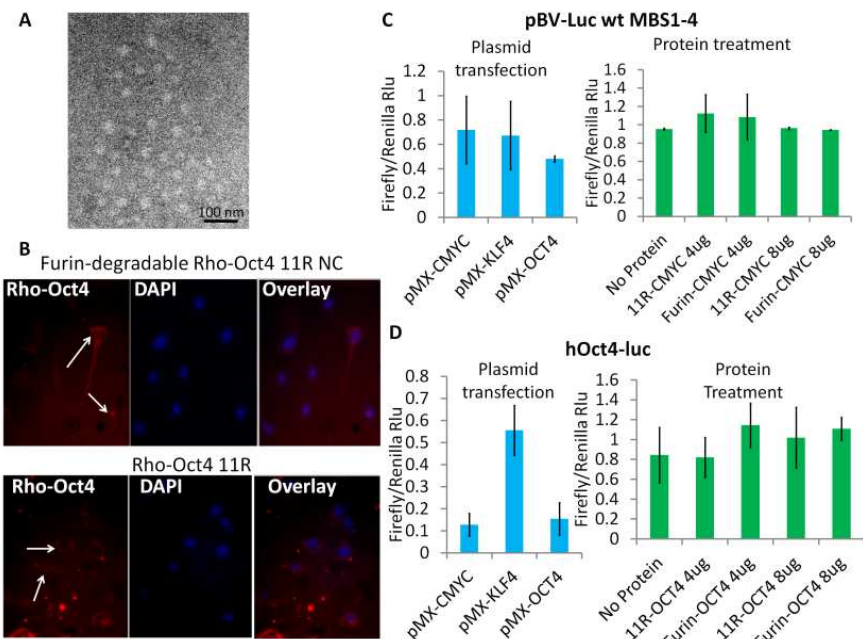
Figure 26. Characterization of protein NCs. *(A)* TEM image of Oct4-11R NCs. *(B)* Fluorescence images of rhodamine-tagged Oct4 protein delivered to HFF cells *via* 11R-tag and furin-degradable NCs. Red: rho-Oct4; Blue: DAPI-stained nuclei. *(C)* Dual-luciferase assay for 293T cells treated with the cMyc reporter plasmid pBV-Luc MBS1-4 and *(D)* the Oct4 reporter plasmid hOct4-luc.

robust, spherical particles ~20 nm, as assessed by transmission electron microscopy (TEM). To directly visualize the ability of the positively-charged NCs to permeate the cell membrane of human cells, we conjugated NHS-rhodamine to the surface free amine groups on Oct4-11R

protein. We then cultured human foreskin fibroblast (HFF) cells and treated them with either Rho-Oct4-11R or Rho-Oct4-11R NCs. As shown in Figure 26B, furin-degradable NCs encapsulating tagged Oct4 showed a larger overlap with nuclei compared to Oct4-11R which showed some areas of distinct lack of overlap with nuclei (arrows). This may result from entrapment of protein in endosomes or degradation during cellular uptake.

4.3.2. Biological Assays Assessing Activity of Delivered OSKM Proteins

We also sought to assess the ability of NCs to activate specific promoter-driven luciferase reporter constructs as we described in our proposal. Specific luciferase constructs were obtained for c-Myc, pBV-Luc wt MBS1-4, and Oct4, hOct4-luc. As shown in Figure 26C and D, a level of specificity was not achieved with these constructs for delivered OSKM proteins. To improve the specificity and sensitivity of the assay, we developed luciferase constructs including 3x minimal binding sites[320] for each OSKM protein upstream of an enhancer promoter region in pGL3-promoter vector (Figure 27A). We created these constructs denoted pGL3-OS (Oct4/Sox2 responsive, pGL3-K (Klf4-responsive) and pGL3-M (c-Myc-responsive). The transient transfection luciferase assay was used to verify the sensitivity of
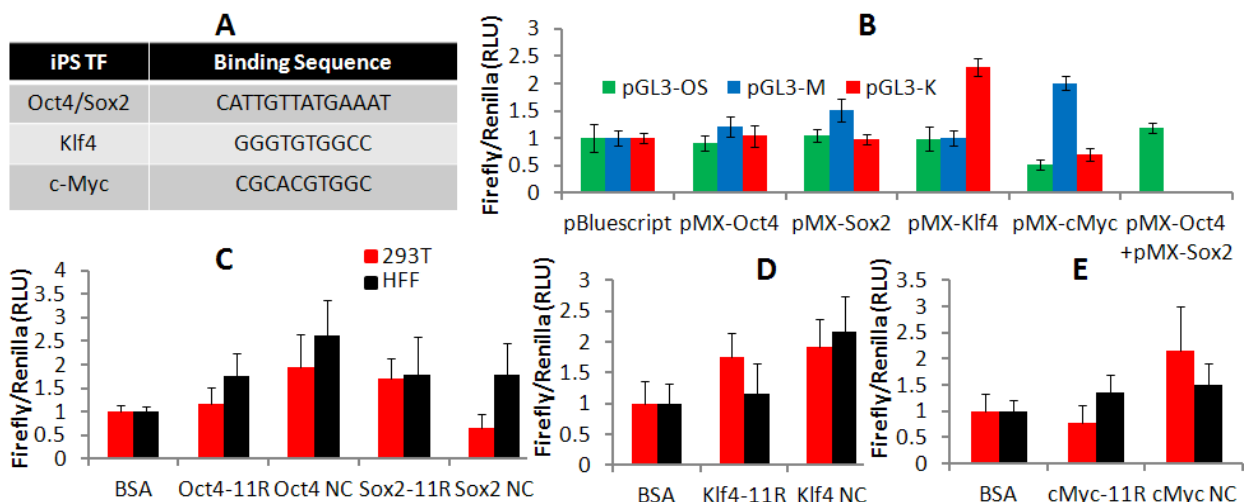
Figure 27. Dual-luciferase assay design and results. *(A)* Binding sequences of OSKM proteins which were cloned upstream of a luciferase promoter. *(B)* Verification of reporter activity with pMX expression plasmids. *(C)* Dual-luciferase assay after 48 h for 293T (red) and HFF (black) cells treated with 400 nM protein/NCs and reporter plasmids pGL3-OS, *(D)* pGL3-K and *(E)* pGL3-M

each construct using expression plasmids of each OSKM transcription factor (Figure 27B). Subsequently, increased luciferase expression was

Figure 28. Immunocytochemistry for delivered proteins via furin-degradable NCs (Oct4 or Sox2) or 11R tags in MEF cells. Control cells were untreated. Red: protein; Blue: Hoescht-stained nuclei
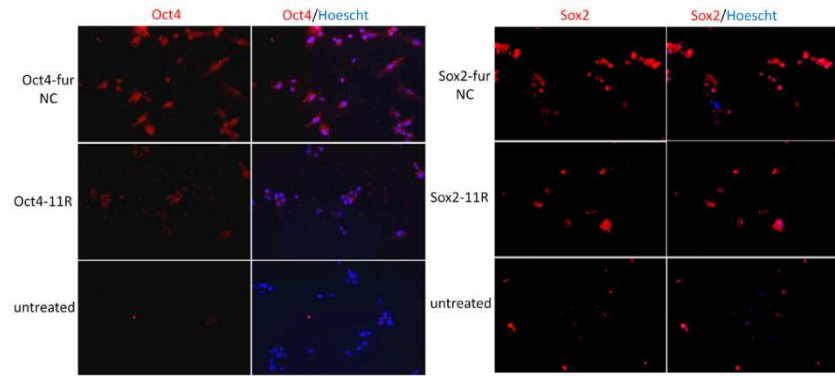
demonstrated in both 293T and HFF cells treated with furin-degradable NCs compared to 11R protein (Figure 27C, D and E) indicating that the protein was delivered in active form to the cell. We also assessed the ability of proteins to be delivered to the nuclei of different cells lines using immunocytochemistry as we previously showed with Klf4. As shown in Figure 28, enhanced nuclear delivery was observed in MEF cells treated with Oct4 and Sox2 NCs compared to 11R protein counterparts.

4.3.3. Delivery of OSKM proteins to induce pluripotency

After establishing the ability of OSKM NCs to deliver proteins to the nuclei of a variety of cell lines, we aimed to deliver NCs to induce pluripotency to cells. The candidate cell line selected were neural stem cells (NSCs). NSCs endogenously express *Sox2* which is known to maintain the multipotency and stemness of NSCs.[321, 322] In comparison to ESCs, NSCs express *Sox2* twofold higher, *c-Myc* tenfold higher and *Klf4* eightfold lower.[103] As a result, the addition of exogenous Oct4 and Klf4 have been sufficient to reprogram NSCs into iPS cells suggesting that somatic cells that endogenously express pluripotent markers can be reprogrammed using a reduced number of exogenous factors. Due to the relative ease of reprogramming, NSCs seemed like a viable cell line option for subsequent reprogramming experiments.

NSCs were seeded in 6 well plates at a density of 5×10^4 cells per well and were treated with 400 nM of each furin-degradable OSKM NC every alternate day for a total of 4 treatments. As shown in Figure 29, dense, compact colonies developed in NSCs treated with furin-

degradable OSKM NCs within 21 days. After 30 days, the cells were transferred to a MEF feeder layer and cultured in ESC medium. However, the colonies observed before transferring to the MEF cells did not reappear. The colonies may have appeared due to enhanced proliferation rather than iPS cell formation which could be initiated by c-Myc overexpression which can enhance gene amplification and cell growth.[323] As a result, the appeared iPS flat edged colonies could be merely enhanced NSC proliferations.

Figure 29. Phase image of NSCs treated on days 2, 4, 6 and 8 with 400 nM OSKM furin-degradable NCs. Colonies emerged by day 21 in NC-treated cells (top) as compared to untreated cells (bottom). Treated NSCs were subsequently transferred to MEF feeder cells

For enhanced effectiveness for reprogramming, several small molecules which have helped induce pluripotency could be added to the protocol. For example, the histone deacetylase inhibitor valproic acid (VPA) has been shown to boost reprogramming rates for iPS and somatic cell nuclear transfer by modulating chromatin remodeling which results in epigenetic effects.[155] The histone methyltransferase inhibitor BIX-1294 can also improve iPS reprogramming efforts by facilitating a shift of the epigenetic balance from a silenced state of pluripotency genes to an active transcription state for cell reprogramming.[324] Other transcription factors have also been shown to enhance the efficiency of iPS cell production.[102] For example, Nanog is a 35 kDa transcription factor involved in ES cell proliferation and self renewal and has been found to co-occupy promoters of several hundred genes in ES cells along with Oct4 and Sox2, implying they work in coordination or as a complex in promoting pluripotency.[325] Lin28 is an mRNA binding protein expressed in embryonic stem cells and may play a central role in blocking miRNA-mediated differentiation in stem cells.[326] The addition of these factors and small

molecules may boost reprogramming efficiency using nanocapsules and provide a favorable epigenetic shift for the NSCs.

5. DELIVERY OF mRNA TO THE CYTOSOL OF CELLS USING DEGRADABLE POLYMERIC NANOCAPSULES

An alternative to protein delivery to the nuclei of cells can be delivery of the encoding mRNA to the cytosol of cells.[327] In comparison to DNA or TF protein delivery which must be delivered to the nuclei of target cells, the cytosolic target of mRNA delivery eliminates the need for delivery through the additional nuclear barrier.[328] In comparison to DNA delivery, mRNA delivery is useful to treat cells where DNA-based delivery is low because of the absence of cell cycle-dependent breakdown of the nuclear envelope, as is the case with most non-dividing cells.[329, 330] Furthermore, the transient nature of mRNA delivery allows near negligible possibility of genomic integration[331] and the subsequent degradation of mRNA by ubiquitous RNases eliminates risks of long-term effects[332]. Furthermore, the protein expression resulting from mRNA delivery can be adjustable and controlled due to optimization of transient delivery.[333, 334] As such, mRNA delivery is practical for applications in which a short or intermittent expression of protein product is expected to have a valuable consequence.[335] As such, mRNA delivery has been demonstrated for reprogramming using transcription factors for induced pluripotent stem cell generation and differentiation[157], expression of nucleases for site-specific chromosomal modification[336] and recombinase expression for genome modification[337].

To date, mRNA delivery has been achieved by several methods. Direct injection of mRNA into mouse skeletal muscle has yielded strong expression of several proteins in active form[338] and injection of naked model antigen $\beta-$gal mRNA elicited a specific cytotoxic T lymphocyte (CTL) response[339]. Liposomes or lipoplexes have also been used to incorporate mRNA including synthetic cationic lipid, N-[1-(2,3-dioleyloxy)propyl]-N,N,N-trimethylammonium chloride (DOTMA), incorporated into a liposome[340] or N-[1-(2,3-Dioleoyloxy)propyl]-N,N,N-trimethylammonium chloride (DOTAP) carbonate apatite-cationic conjugates for luciferase expression[341]. Cholesterol-phosphatidylcholine-phosphatidylserine liposomes have been demonstrated to show CTL response to influenza virus nucleoprotein[342] Polyplexes based on

low molecular weight PEI and PLL achieved strong expression of reporter genes in HUVEC cells[343] while polyhistidine and polylysine conjugate polyplexes demonstrated delivery of mRNA in PC3 cells[344]. Gene gun delivery or gold microparticle-mediated delivery have also been utilized for delivery of mRNA to yield functional protein expression for immunization applications.[345, 346] Electroporation of mRNA has also been extensively explored for immunization or gene expression applications.[347-349]

A challenge for mRNA delivery is the elicited innate immune response which occurs post-delivery of synthetic mRNA which can greatly impact the efficacy of delivery. Both double stranded and single stranded RNA interact with pattern recognition receptors (PRRs) including Toll-like receptors (TLRs) which behave as the primary defense against microbial invasion.[350] It is well-known that uncapped triphosphates can trigger ssRNA immunogenic responses detected by the ssRNA sensor RIG-1 which can activate PKR, a global repressor of protein translation.[351-353] As such, the synthesis of *in vitro* transcription mRNA with a phosphatase can result in reductions in cytotoxicity after mRNA transfection in target cells.[157] Additionally, eukaryotic mRNA undergoes nucleotide modifications *in vivo* which reduce signaling by RIG-1 and PKR as well as ssRNA sensors TLR7 and TLR8.[354, 355] Synthesis of mRNA using modified ribonucleoside bases 5-methylcytidine for cytidine or pseudouridine for uridine during *in vitro* transcription can significantly attenuate interferon signaling.[157] With these considerations in mind, we sought to determine if degradable polymeric NCs could be capable of delivering mRNA to the cytosol of cells for subsequent protein expression.

5.1.1. Synthesis of mRNA and Encapsulation using Degradable NCs

To assess whether NCs are able to encapsulate mRNA, we first synthesized mRNA encoding Venus using *in vitro* transcription. Venus is a variant of yellow fluorescent protein (YFP) which has increased brightness, reduced chloride sensitivity and faster maturation.[356] The components of the transcription reaction contained linearized DNA encoding Venus under the
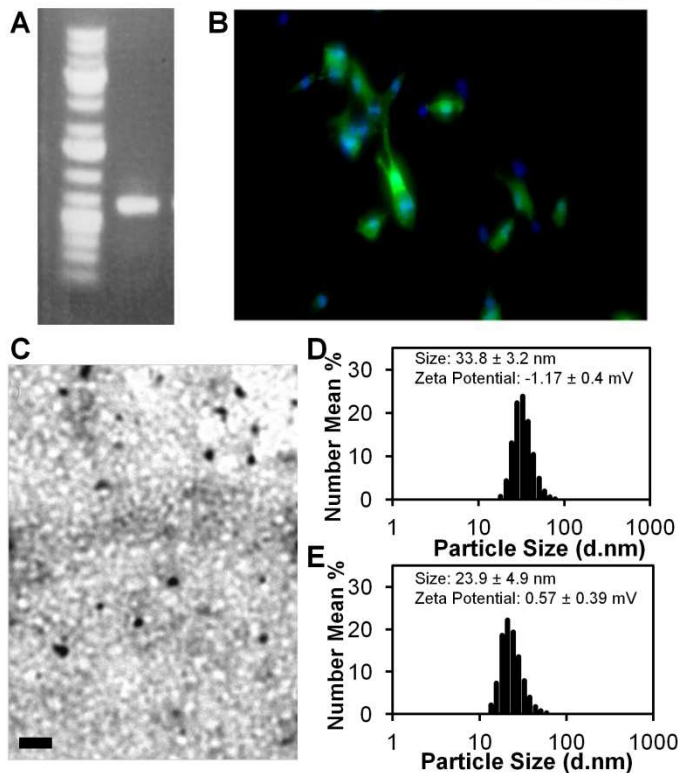
Figure 30. Venus mRNA synthesis and NC formation. (A) mRNA synthesis using *in vitro* transcription. (B) Verification of mRNA purity, stability and utility. Neural stem cells were transfected with Venus mRNA using Lipofectamine 2000. Cells were fixed and stained with an anti-YFP antibody and DAPI. Green: YFP antibody; Blue: DAPI-stained nuclei. (C) TEM image of mRNA NCs. The scale bar corresponds to 100 nm. Dynamic light scattering measurements for (D) native mRNA and (E) mRNA disulfide NCs.

control of the Sp6 promoter, 25 mM NTPs (ATP, GTP, 5-methylcytidine and pseudouridine) and 32 mM 5' guanine cap. The 5' cap is found on the 5' end of an mRNA molecule and is characterized by a guanine nucleotide connected to the mRNA via an unusual 5′ to 5′ triphosphate linkage. The cap signifies mature mRNA and helps maintain mRNA stability during subsequent translation.[357] The reaction was initiated using Sp6 enzyme; after the mRNA synthesis was complete, DNase was used to degrade the DNA template and alkaline phosphatase was used to reduce cytotoxicity of the

synthesized mRNA. As shown in Figure 30A, a clear band was observed indicating successful Venus mRNA synthesis. To assess the purity, stability and utility of the modified mRNA, Lipofectamine 2000 was used to transfect mRNA into neural stem cells. As shown in Figure 30B, transfected Venus mRNA resulted in a high level of expression in several neural stem cells, indicating that the *in vitro* transcription yielded a stable and functional mRNA product. We subsequently synthesized mRNA NCs using the acrylamide-based platform using similar protocols as protein NCs. As shown in Figure 30C, TEM images of mRNA redox-responsive NCs display compact spherical particles around 20 nm in diameter. Dyanamic light scattering was performed on native mRNA and mRNA NCs to assess the physical properties of mRNA NCs. As shown in Figure 30D and E, mRNA is negatively charged and exhibits a ~30 nm cluster

size in solution. After polymerization and formation of NC, charged monomers complex the mRNA into smaller NCs around 20 nm with a slight positive charge.

5.1.2. Stability Studies of mRNA NCs

After confirming synthesis of NCs encapsulating mRNA, we sought to determine the stability characteristics of mRNA NCs in comparison to the naked mRNA. Since the mRNA was synthesized using modified bases, it already displayed enhanced stability compared to unmodified mRNA as evidenced in previous studies.[157, 358] As such, we performed a set of
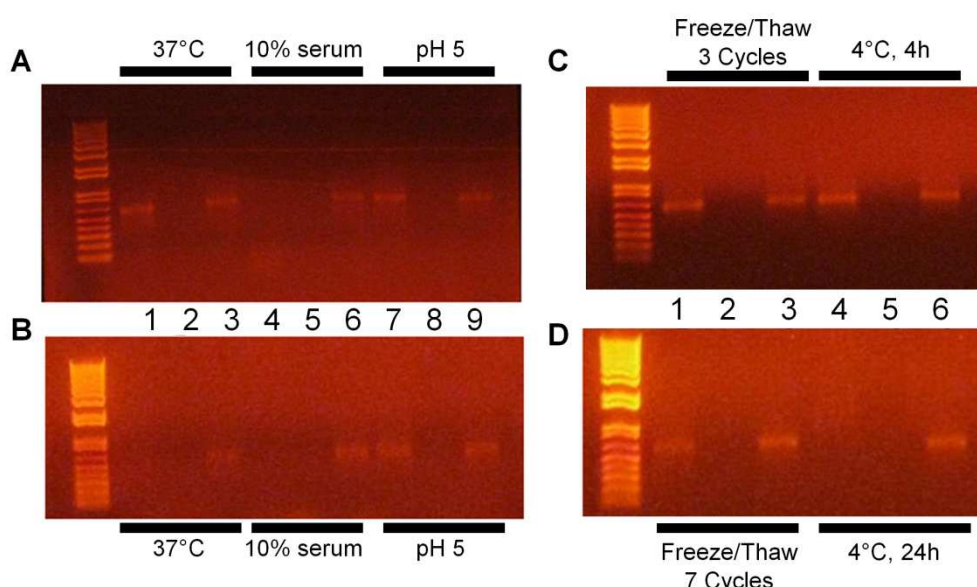
Figure 31. Stability assays to assess mRNA NCs. Naked mRNA and mRNA NCs were subjected to physiological conditions of 37℃, 10% serum and pH 5 for (A) 4 hours or (B) 24 hours. Lanes are numbered in the following manner for (A) and (B): 1. mRNA at 37℃, 2. NC at 37℃, 3. NC at 37℃, degraded, 4. mRNA in 10% serum, 5. NC in 10% serum, 6. NC in 10% serum, degraded, 7. mRNA in pH 5, 8. NC in pH 5, 9. NC in pH 5, degraded. Naked mRNA and mRNA NCs were also tested for stability in various storage/handling conditions in (C) using 3 or (D) 7 freeze/thaw cycles and storage at 4℃ for (C) 4 or (D) 24 hours. La nes are numbered in the following manner: 1. mRNA Freeze Thaw, 2. NC Freeze Thaw, 3.NC Freeze Thaw, degraded, 4. mRNA at 4℃, 5. NC at 4℃ and 6. NC at 4℃, degr aded.

stability assays to characterize Venus mRNA redox-responsive NCs.

As shown in Figure 31, we subjected both mRNA NC and naked mRNA to various conditions for 4 or 24 hours and assessed the stability of mRNA by running the sample on an agarose gel. For mRNA NCs, we degraded the polymeric matrix after the treatment using glutathione and ran the exposed RNA on the gel. Several observations are key from Figure 31. Firstly, no RNA band is observed in NC samples post-treatment indicating that the polymeric NC

remains intact at all conditions tested. Even though the modified mRNA is more stable than unmodified mRNA, naked mRNA remained especially sensitive to certain treatments including 10% serum for both 4 and 24 h (Figure 31A and B, lane 4) , 37°C for 24 h (Figure 31B, lane 1) and 4°C for 24 h (Figure 31D, lane 4) as shown by the smearing or absence of RNA band. In comparison, encapsulated RNA stays intact and exhibits a non-degraded band. These stability studies indicate that NCs can help mRNA remain stable at physiological conditions such as 37°C, in the presence of serum and at acidic conditions of the endosome (pH~5). Furthermore, NCs can enhance mRNA stability during storage/handling conditions such as at 4°C and through multiple freeze/thaw cycles.

5.1.3. Intracellular Delivery of mRNA using Degradable NCs.

We then wanted to assess the ability of NCs to deliver mRNA in active form to the cytosol for subsequent translation into functional protein. To assess both delivery of mRNA and protein translation, we synthesized Venus mRNA using small amounts of Alexa-Fluor-UTP
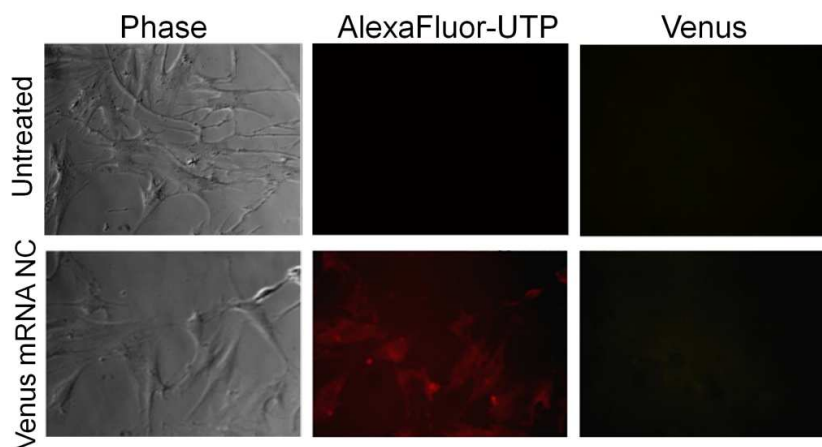
Figure 32. Venus mRNA was delivered using NCs (2 μg) to HFF cells. Images shown are the phase images, AlexaFluor 594-UTP-incorporated Venus mRNA and YFP expression. Cells were treated for 24 hours before live imaging.

nucleosides. As such, the synthesized mRNA displayed a red fluorescent tag while the protein product would display a yellow/green product which could be differentiated by fluorescent microscopy.

87

As shown in Figure 32, HFF cells were treated with Venus mRNA NCs for 24 hours and subsequently imaged. mRNA NC-treated cells clearly showed uptake of mRNA as shown by the middle panel in comparison to control untreated cells. However, expression of Venus was not observed in NC-treated HFF cells. When the treatments were repeated using increased amount of mRNA NCs and by extending the incubation time with cells, Venus expression was still not observed. These results may indicate that the NC formation can alter the mRNA structure in such a way that prevents translation once the mRNA is delivered to the cytosol. The mRNA phosphate backbone or RNA bases may be affected by the free radical polymerization process during NC synthesis which render the nucleic acid modified and inactive for downstream translations. Another possibility is that the mRNA is entrapped in the endosomes during the uptake process and is eventually cleared or degraded by cellular enzymes.

6. CONCLUDING REMARKS

As outlined in this dissertation, intracellular protein delivery is an important therapeutic goal for treatment of loss-of-function diseases, cancer therapies, vaccination, regenerative medicine and imaging applications. Furthermore, intracellular delivery of recombinant proteins can also enable direct investigation of the functions of proteins on cellular processes for research applications. Delivery of proteins is hindered by intrinsic properties of proteins such as large size, uneven charge distribution and structural fragility. Material-based nanocarriers can assist the intracellular delivery of proteins by utilizing materials which can shield proteins from degradation and pentrate cellular barriers. Various polymeric nanocarriers have been described in recent years which have used the diversity of polymers to synthesize protein nanocarriers for targeting, stability, biocompatibility, transduction ability and stimuli response applications. Several synthesis strategies and protein loading techniques have been developed and several insights into delivery efficiency, cellular uptake and protein release mechanisms have been elucidated.

Despite several advances, intracellular protein delivery remains in early stages and continued efforts must be made to develop delivery systems. Several obstacles remain for effective and efficient delivery. For example, covalent modifications to protein surfaces may cause irreversible changes to protein structure and subsequent loss-of-function. Non-covalent are often weakly stable in serum and lead to leakage of the protein from nanocarrier. Efficient cytosolic delivery of proteins remains challenging since many nanocarriers lack the ability to be released from the endosome to the cytosol, resulting in lysosomal degradation. The controlled release of protein from nanocarriers is another challenging obstacle. Several nanocarriers have been synthesized with stimuli-responsive components such as pH, redox, enzymatic, temperature, magnetic or light-sensitive moeities. However, the desired timing of protein release remains elusive depending on the preferred biological effects. The targeting of proteins to specific cells or organs for disease-specific therapies is another bottleneck to advancement in

clinical applications. Under *in vivo* conditions, protein nanocarriers will encounter several barriers during the delivery process. It is imperative to design delivery vehicles which will accumulate in the desired cells or organs either by the enhanced permeability and retention effect mediated-passive targeting or by active targeting through conjugating targeting moeities including antibodies, receptor ligands and aptamers. Efficiency of protein delivery remains well below levels comparable to gene delivery which must be enhanced for biomedical applications. Exogenous protein often does not induce the same cellular pathways as endogenously produced protein, thereby reducing observed biological functions. The need for recombinant purification of proteins prior to nanocarrier synthesis also limits the scalability of nanocarriers since purification processes can be costly and several complex proteins cannot be expressed and purified solubly. In the next few years, several new generations of protein nanocarriers will be synthesized as interdisciplinary research leads to new approaches of tailored biomaterials for intracellular delivery.

TFs are key specialized proteins with the remarkable ability to change cell fate. The last decade has observed increasing studies based on reprogramming of differentiated cells to yield pluripotent cells or transdifferentiation of cells of one lineage into another lineage. These remarkable studies open the path towards patient-specific therapies and the formation of disease models and drug screenings. Patient-derived cells which are reprogrammed or transdifferentiated would produce cells with the same genetic information as the patient. These cells could be introduced into the patient with reduced immunological responses for therapies or could be used in toxicology or disease models for testing of drugs. Transdifferentiation and reprogramming both have several advantages and disadvantages. One key observation is that the stress placed on cells during the reprogramming process can result in mutations of regulatory stress genes leading to increased tumor formation. In this regard, transdifferentiation may allow step-wise stages of cell lineage switch which is a more natural process. Delivery of

TFs to cells could provide limitless applications for regenerative medicine therapies. So far, TF delivery is restricted to DNA-based methods including the integrative retrovirus or lentivirus strategies which have induced several insertional mutagenesis deleterious effects. Several studies have stressed the importance of safer methods for cell reprogramming and transdifferentiation.

The furin-degradable NCs described represent a robust platform for encapsulation of several diverse proteins. By exploration of two different polymerization techniques including *in situ* and microemulsion synthesis, the endoprotease-degradability design of NCs were confirmed. The biological activity of ovalbumin and caspase-3 demonstrated the utility of NCs in delivering protein to the cytosol of cells for immunization or anti-cancer actions, respectively. Nuclear delivery of eGFP by furin-degradable NCs served as an inspiration for delivery of functional nuclear transcription factors. Myogenesis induced by the delivery of MyoD by NCs validated that PEG NCs retained activity of encapsulated protein so that it could perform complex downstream actions once released inside the cell. Pdx1 delivery by NCs demonstrated delivery to liver and exocrine cells and modest increase in β-cell gene expression levels. Reprogramming efforts of neural stem cells to induced pluripotent stem cells did not result in colony formation but activated reporter gene expression was increased.

Protein NCs were able to induce differentiation of myoblasts into myotube cells but less success was observed towards transdifferentiation and reprogramming applications. The one-factor myogenesis process has increased propensity to occur since cells are migrating towards a mature cell type from an immature cell type. Several factors which are needed to induce the myogenesis differentiation process are expressed at low levels in myoblast cells. As such, modest amounts of delivered protein may be able to induce an intracellular change which can drive the muscle differentiation process forward. In contrast, liver cells do not express similar genes to pancreatic $\beta-$cells which may cause the threshold level of delivered protein to be much

higher. Several studies have also elucidated the specific chromatin modifications in cells necessary for cell lineage switches. As such, complexed DNA of one cell type may be inaccessible to exogenous TFs aiming to transdifferentiate or reprogram the cell into another. Furthermore, cells are thought to have epigenetic memory of their original state which proves to be a challenge when attempting to change very different lineages by a "long jump". Additionally, exogenous protein delivery may not induce downstream or coactivator gene expression which are required for cellular processes. It may be required to supplement the exogenous protein with other sequential transcription factors, growth factors, microRNAs and chromatin remodeling factors. Though protein TF delivery remains challenging, the safe, transient properties of delivery should encourage increased strategies for stimulating cellular processes using delivery of active proteins. Increased elucidation of TF mechanisms coupled with additional optimization of polymeric nanocarriers will contribute to effective methods for TF delivery to cells.

7. SUPPLEMENTARY INFORMATION

7.1. Supplementary Information from Endoprotease-Mediated Intracellular Protein Delivery

Materials and Methods

Complete materials and methods can be found in the Supplementary Information.

Synthesis of furin-degradable peptide. Peptides were synthesized using an automatic peptide synthesizer. Standard solid-phase peptide synthesis protocols for Fmoc chemistry were used. Peptides were assembled in the C-terminal amide form using Rink Amide MBHA resins (Anaspec, Inc). Coupling of amino acids to the resin backbone was accomplished by a 0.9 equivalent of HBTU activation and 2 equivalents of DIEA. The Fmoc group was removed by 20% piperidine in DMF. Peptides were constructed with Fmoc-6-Ahx-OH at the N-terminal and Fmoc-Lys(Mtt)-OH at the C-terminal (Ahx-RVRRSK). The non-specific peptide (Ahx-AAARSK) was constructed in the same manner.

Resin bearing peptides were swollen in DCM and then the Mtt group was selectively removed with 3% TFA in DCM. The exposed primary amine groups were acrylolated using a 20 fold excess of acryloyl chloride and 20 fold excess of DIEA in DMF for one hour on ice, and then one hour at room temperature. The progress of acrylolation was monitored with the p-chloranil test. When a negative p-chloranil test was achieved, the resin was washed, dried under vacuum, and cleaved using TFA:water:TIPS in a 95:2.5:2.5 ratio. After cleavage, the peptide was drained into cold ether and washed and centrifuged 4 times. The crude peptide was dissolved in water and lyophilized. The non-specific peptide was constructed in the same manner.

Preparation of Protein NCs. 1 mg protein was diluted to 1 mL with 5 mM pH 9 $NaHCO_3$ buffer after which acrylamide (AAm) was added with stirring for 10 min at 4 ^{o}C. Next, *N*-(3-aminopropyl) methacrylamide (APMAAm) was added. Afterwards, the peptide crosslinker or

nondegradable crosslinker *N,N'*-methylene bisacrylamide was added. The molar ratio of AAm/APMAAm/crosslinker was 6/3.5/1. The polymerization was immediately initiated by adding 3 mg of ammonium persulfate and 3 μL of *N,N,N',N'*-tetramethylethylenediamine. The polymerization was allowed to proceed for 90 min at 4 ℃. Finally, buffer exchange with 100 mM HEPES, 1 mM $CaCl_2$, pH 7.5 was performed to remove unreacted monomers and initiators.

Cell free furin cleavage of peptide and NCs. 50 ng of furin crosslinker peptide or 2.5 nmol of furin-degradable protein NCs were added to 100 mM HEPES, 1 mM $CaCl_2$, pH 7.5 buffer into a total volume of 40 μL. 1 unit of furin enzyme was added to the reaction mixture and incubated at 37˚C for various times. 1 unit of enzyme is defined by Sigma as the amount of enzyme needed to release 1 pmole from flourogenic peptide Boc-RVRR-AMC in 1 min at 30 ℃. When furin inhibitor dec-RVKR-cmk (EMD Chemicals, Inc., Gibbstown, NJ) was used, it was added to the reaction mixture at a final concentration of 25 μM.

Enzyme-linked Immunosorbant Assay (ELISA). To quantify native eGFP protein released, a GFP ELISA kit was purchased from Cell Biolabs, Inc., San Diego, CA. We constructed a standard curve using known eGFP amounts with the kit's standard eGFP sample and by performing the assay. Briefly, samples were centrifuged for 10 min at 7000 rpm with a 30 kDa MWCO filter to isolate native eGFP protein. Then, the samples were loaded into anti-GFP rabbit antibody coated wells and incubated at 4℃ overnigh t. After careful washing, a detection antibody (anti-GFP mouse antibody) was added to each well and incubated at room temperature for 2 hours. Next, an anti IgG mouse-HRP conjugate antibody was added. After one hour, TMB substrate was added and incubated for 30 minutes. After the addition of stop solution to each well, absorbance at 450 nm was measured.

Cell Culture. HeLa, MEF, (ATCC, Manassas, VA) and CHO cells (a generous gift from Stephan Leppla, National Institutes of Health) were cultured in Dulbecco's Modified Eagle's Medium (Invitrogen) or DMEM supplemented with 10% bovine growth serum (Hyclone, Logan, UT) or

BGS, 1.5 g/L sodium bicarbonate, 100 □g/mL streptomycin and 100 U/mL penicillin. AFDC cells were cultured in Minimum Essential Medium (α-MEM; Invitrogen) supplemented with 10% fetal bovine serum (FBS). The cells were cultured at 37 oC, in 98% humidity and 5% CO2. Cells were regularly subcultured using Trypsin-EDTA.

Cellular Internalization Trafficking. NLS-eGFP NCs (10 nM) were added to HeLa cells at 4ºC for 30 min. The cells were shifted to 37 ºC for various incubation periods, fixed with 4% formaldehyde, permeabilized with 0.1% Triton X-100 and separately immunostained with antibodies against early endosomes (mouse anti-EEA1 Ab) and late endosomes (rabbit anti-CI-MPR Ab). Texas red goat anti-mouse IgG and Alexa Fluor647 goat anti-rabbit IgG were used as secondary antibodies. The nuclei of treated cells were stained with DAPI. To quantify the extent of colocalization between eGFP and endosomes, colocalization coefficients were calculated using the Manders' overlap coefficient by viewing more than 10 cells at each time point using the Nikon NIS-Elements software.

Nuclear and Cytoplasmic Fractionation. Cells were seeded into 6-well plates at a density of 1×10^5 cells per well and cultivated in 1.5 mL of DMEM with 10% BGS. The plates were incubated in 5% CO2 and at 37 ℃ for 12 h before be ing treated with 200 nM of appropriate NCs. dec-RVKR-cmk was used at a concentration of 25 μM. Cells were collected by trypsin-EDTA and collected by centrifugation after 24 hours. A Nuclear/Cytosol Fractionation Kit (BioVision, Inc., Mountain View, CA) was used to separate cytoplasmic and nuclear extracts from NC-treated cells. Fractions were obtained per the manufacturer's instructions. All procedures were performed at 4 ℃. Extracts were st ored at -80 ℃ until the GFP-ELISA assay was performed (Cell Biolabs, Inc., San Diego, CA) For nuclear staining and subsequent Z-stack imaging, nuclei were counterstained with TO-PRO-3 (Invitrogen).

TUNEL assay. Apoptosis was detected in isolated HeLa cells using a commercially available APO-BrdU Terminal Deoxynucleotidyl Transferase dUTP Nick End Labeling (TUNEL) assay kit from Invitrogen. Briefly, cells were seeded into 6-well plates at a density of 100,000 cells per

well and cultivated in 2 mL of Dulbecco's Modified Eagle's Medium (DMEM) with 10 % bovine growth serum (BGS). The plates were then incubated in 5% CO_2 and at 37 ^{o}C for 12 h to reach 70-80% confluency before addition of protein/nanocapsules. After 24 h incubation, cells were first fixed with 1% paraformaldehyde in phosphate-buffered saline, pH 7.4, followed by treatment with 70% ethanol on ice to permeabilize the membrane. The cells were then loaded with DNA labeling solution containing terminal deoxynucleotidyl transferase and bromodeoxyuridine (BrdUrd). Cells were then stained with Alexa Fluor® 488 dye-labeled anti-BrdUrd antibody for nick-end labeling. The cells were finally stained with propidium iodide (PI) solution containing RNase A for total DNA content and visualized under fluorescence microscope (Zeiss, Observer Z1) using appropriate filters for Alexa Fluor 488 and PI.

Immunostaining. Mouse embryonic fibroblast (MEF) cells were plated in 8-well chamber slides at a density of 10,000 cells/well. Cells were treated with 8 μg/mL of Klf4-11R or furin-degradable Klf4 for 6 hours and subsequently cultured in fresh media overnight. As a control, BJ-iPS cells were also cultured. Cells were then washed with PBS and fixed by 4% paraformaldehyde in PBS. Immunostaining was performed with rabbit anti-KLF antibody (1:1000, Santa Cruz Biotechnology) and Cy3 conjugated secondary Ab. Hoechst was used for nuclear counterstaining.

Materials

All materials were purchased from Sigma Aldrich unless noted otherwise. *N*-(3-aminopropyl) methacrylamide hydrochloride was purchased from Polymer Science, Inc. CellTiter 96® AQ$_{ueous}$ One Solution Cell Proliferation Assay (MTS) reagent was purchased from Promega Corporation. Deionized water was prepared using a Millipore NanoPure purification system. Klf4-11R was purchased from Stemgent, Inc.

Instruments

Absorbances for Bradford assay were measured on a Thermo Scientific GENESYS 20

spectrometer. TEM images of nanoparticles were obtained on a Philips EM-120 TEM instrument. Zeta potential and particle size distribution were measured on the Malvern particle sizer Nano-ZS. Peptides were synthesized on a C S Bio Co. CS336X solid phase peptide synthesizer. LCMS was conducted with a Shimadzu 2010 EV Liquid Chromatography Mass Spectrometer using positive electrospray ionization and a Phenomenex Luna 5u 2.0 X100 mm C18 reverse-phase column. Samples were separated over a linear gradient of 5% to 95% CH_3CN (vol/vol) for 30 min and 95% CH_3CN (vol/vol) for an additional 30 min in H_2O supplemented with 0.1 % (vol/vol) trifluoroacetic acid at a flow rate of 0.1 mL/min at room temperature. Fluorescent images of cells were obtained with either a Zeiss Axio Observer Z1 Inverted Microscope or a Yokogawa spinning-disk confocal microscope (Solamere Technology Group, Salt Lake City, UT) on a Nikon eclipse Ti-E Microscope equipped with a 60×1.49 Apo TIRF oil objective and a Cascade II: 512 EMCCD camera (Photometrics).

Construction of pET23a-NLS-eGFP

The NLS-eGFP gene was PCR amplified from the pET28a-eGFP plasmid template using the specific primers I (5'-AATA<u>CAT</u><i>ATG</i>**CCAAAGAAGAAGCGTAAGGTT**GTGAGCAAGGGCGAGGAGCT-3' with an NdeI site shown by underlining, start codon shown in italics, and nuclear localization signal shown in bold), and II (5'- AAT<u>GAATTC</u>ATCTCGTACAGCTCGTCCATGC-3' with an EcoRI site shown by underlining). This fragment was amplified and inserted between the *NdeI* and *EcoRI* sites of pET23a, thus resulting in pET23a-NLSeGFP with an in frame C-terminal His-tag. After sequence confirmation, the plasmid was transformed into *E.coli* BAP1 cells by electroporation. The resultant product was incubated at 37 ℃ for 30 minutes after which it was plated on Luria-Bertani (LB) plate containing 100 μg/mL ampicillin.

Protein Expression and Purification

Transformed cells were inoculated overnight at 37℃ with shaking in Luria-Bertani medium containing 100 μg/mL ampicillin. Overnight cultures were diluted 1:200 and grown in Fernbach

flasks containing 1 liter of LB medium with 100 μg/mL ampicillin at 37 ^{o}C with shaking at 270 rpm. When the cultures reached an absorbance A600 ~1.2, isopropyl β-D-thiogalactopyranoside was added to a final concentration of 0.1 mM to induce protein expression, and the cells were incubated at 16 ^{o}C overnight. The cells were harvested by centrifugation (3500g, 4 ^{o}C, 15 min), resuspended in 30 mL Buffer A (50 mM Tris–HCl, pH 8.0, 2 mM DTT, 2 mM EDTA), and lysed by sonication. Cell debris and insoluble proteins were removed by centrifugation (17,000g, 4 ^{o}C, 30 min). After centrifugation, the cleared cell lysate was incubated with 2 mL of Ni-NTA resin (Qiagen) for 3 hours at 4 ^{o}C. The protein was then purified using a step gradient of Buffer A with increasing concentrations of imidazole (10, 20, and 250 mM). NLS-eGFP was eluted with 5 mL Buffer A containing 250 mM imidazole. The protein concentration was qualitatively assessed by SDS-PAGE and quantitatively determined by the Bradford protein assay using bovine serum albumin (BSA) as the standard. The same procedures were used to express and purify CP3 from *E.coli* BAP1 cells using the wild-type CP3 expression plasmid pHC332 which was a generous gift from Dr. A. Clay Clark (North Carolina State University).

Cytotoxicity Study Using 3-(4,5-dimethylthiazol-2-yl)-5-(3-carboxymethoxyphenyl)-2-(4-sulfophenyl)-2H-tetrazolium)(MTS) Assay

Cells were seeded into 96-well plates at a density of 5,000 cells per well and cultivated in 100 µL of DMEM with 10 % BGS. The plates were then incubated in 5% CO_2 and at 37 ^{o}C for 12 h to reach 70-80% confluency before addition of protein/NCs. After 24 h or 48 h incubation with protein NCs, the cells were washed with PBS solution and incubated with 100 µL fresh DMEM and 20µL MTS solution (CellTiter 96$^®$ AQueous One Solution Cell Proliferation Assay, Invitrogen). The plates were incubated for an additional 3 h. The absorbance of the plates was read at 550 nm and a reference wavelength of 690 nm using a microplate reader (PowerWave X, Bio-tek Instruments, USA).

Scheme S1. Solid phase peptide synthesis approach for construction of a furin-degradable peptide crosslinker. Lysine-derivative 6-aminohexanoic acid (Ahx) was used at the N-terminal. The highly labile methyltrityl (Mtt) group was used to protect the C-terminal lysine. Selective deprotection of the Mtt group was achieved using 3% TFA in DCM. Acryolation reactions of the N and C terminal amine groups were subsequently performed using acryolyl chloride while the peptide remained attached to the resin. X denotes protecting groups on amino acid side chains (pentamethyldihydrobenzofuran-5-sulfonyl or Pbf for arginines and *O-tert*-butyl or tBu for serine).
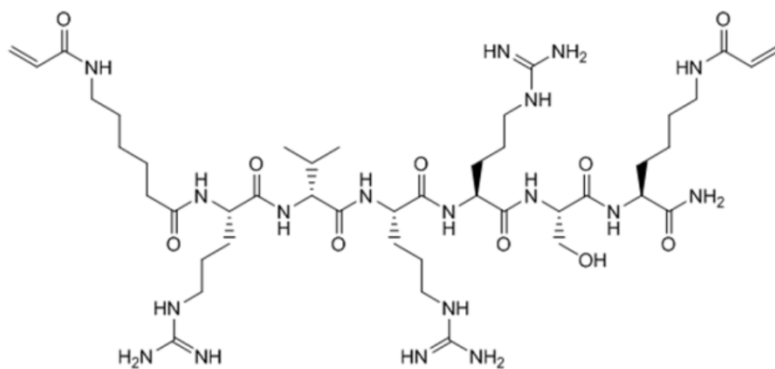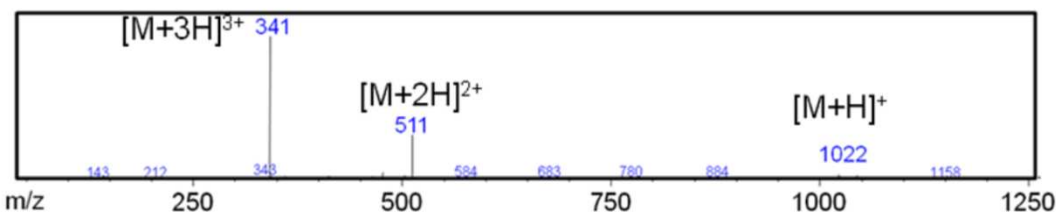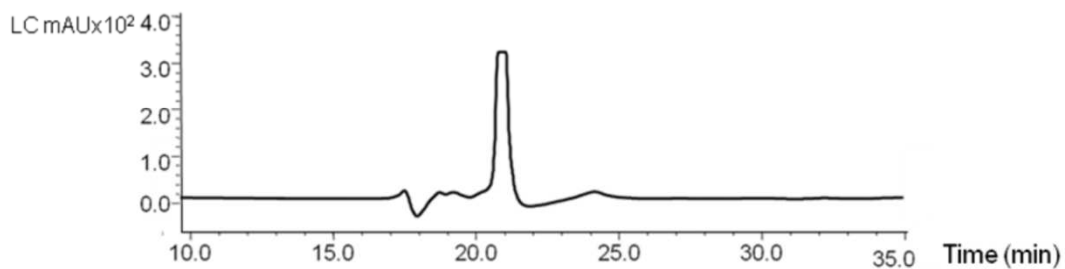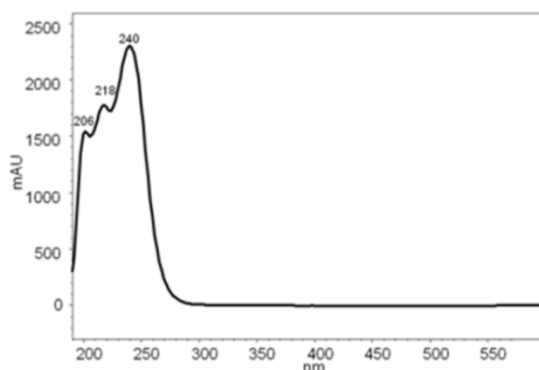
Figure S1 Chemical structure, UV, and LC-MS analysis of furin-degradable peptide crosslinker: Ahx-RVRRSK. LC-MS was conducted using positive electrospray ionization and a 5u 2.0 X100 mm C18 reverse-phase column. Samples were separated over a linear gradient of 5% to 95% CH_3CN (vol/vol) for 30 min and 95% CH_3CN (vol/vol) for an additional 30 min in H_2O supplemented with 0.1 % (vol/vol) trifluoroacetic acid at a flow rate of 0.1 mL/min at room temperature. As shown, the synthesis of the crosslinker was confirmed by identification of mass signals ($[M+2H]^{2+}=(1020+2)/2=511$; $[M+3H]^{3+}=(1020+3)/3=341$)).
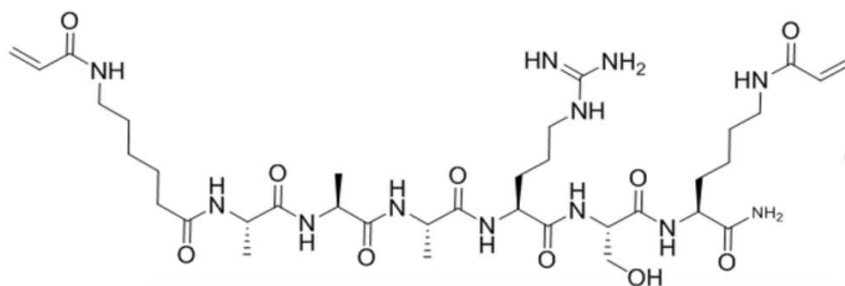
Chemical Formula:
$C_{36}H_{62}N_{12}O_{10}$
Exact Mass:
822.47
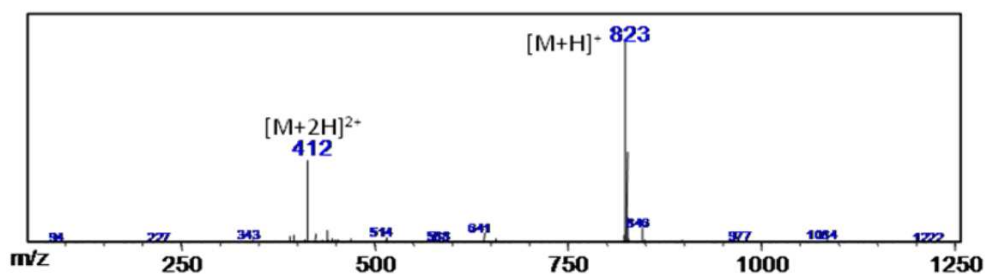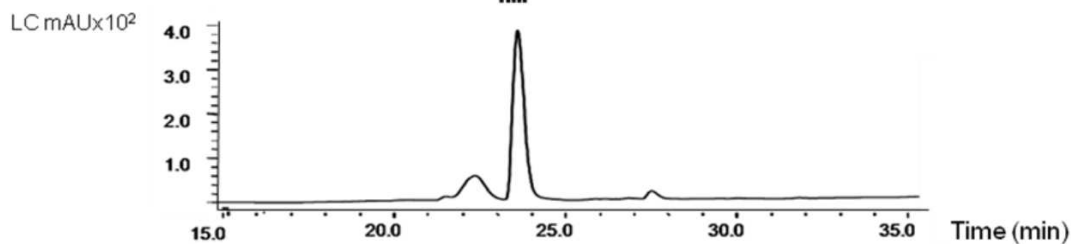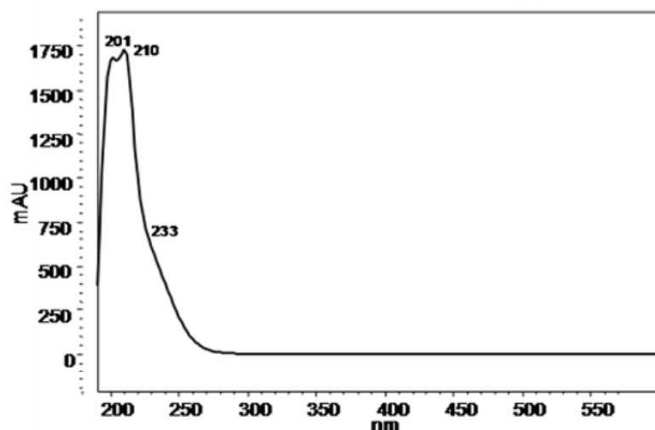
Figure S2 Chemical structure, UV, and LC-MS analysis of non-specific crosslinker: Ahx-AAARSK. LC-MS was conducted using positive electrospray ionization and a 5u 2.0 X100 mm C18 reverse-phase column. Samples were separated over a linear gradient of 5% to 95% CH3CN (vol/vol) for 30 min and 95% CH3CN (vol/vol) for an additional 30 min in H2O supplemented with 0.1 % (vol/vol) trifluoroacetic acid at a flow rate of 0.1 mL/min at room temperature. As shown, the synthesis of the crosslinker was confirmed by identification of mass signals ([M+H]+=(822+1)/1=823; [M+2H]2+=(822+2)/2=412)).
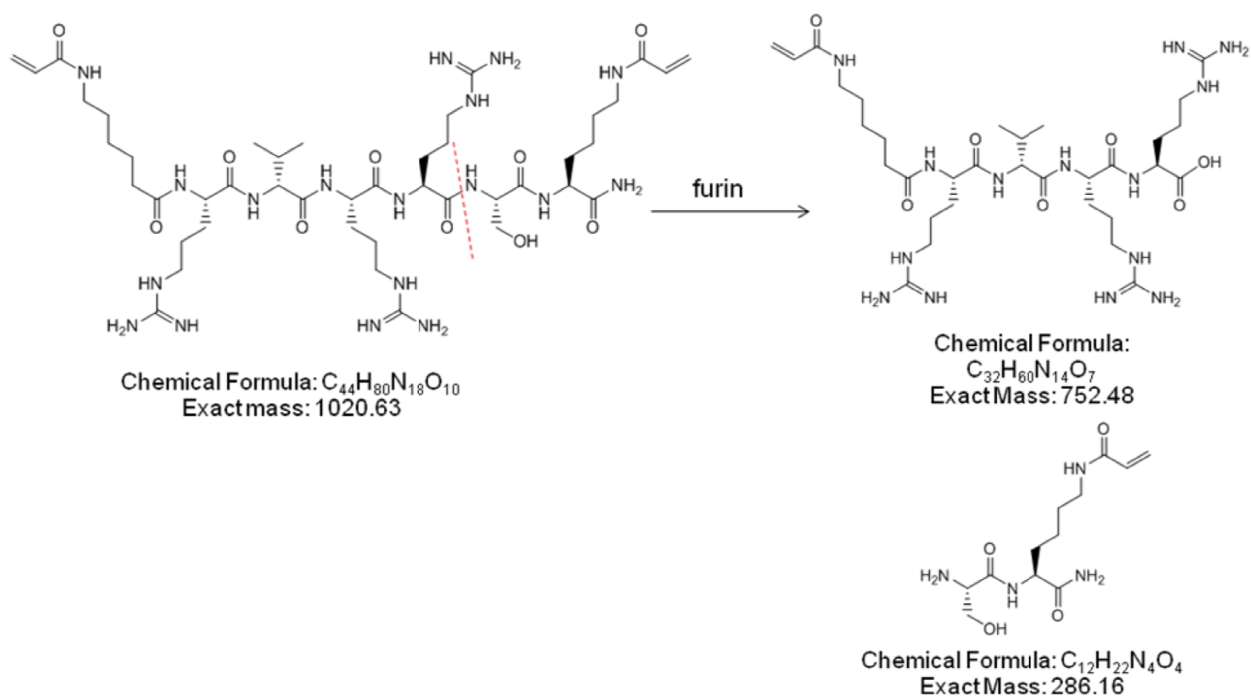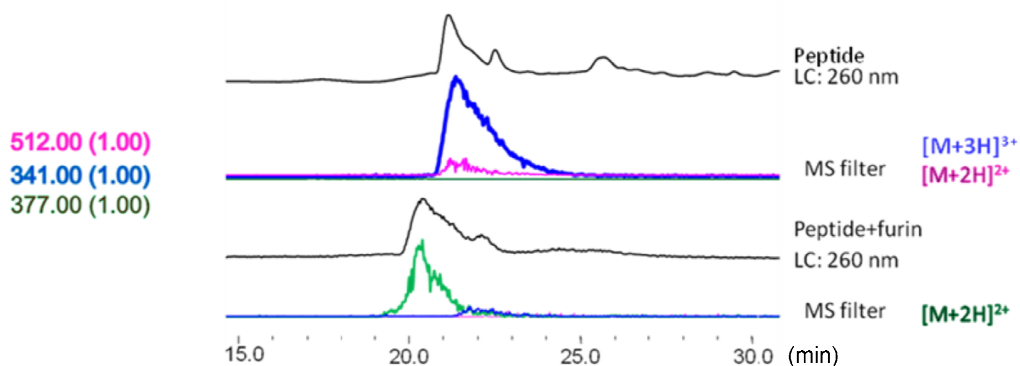
Figure S3. Digestion of 1 ng furin-degradable peptide with 1 unit furin enzyme for 2 hours. Top: Mass filter of the peptide after degradation with furin did not detect original crosslinker mass peaks of ([M+2H]2+=512; [M+3H]3+==341)) and instead detected a mass peak corresponding to the larger peptide fragment obtained by furin-mediated cleavage ([M+2H]2+=(752+2)/2=377). Bottom: Site-specific furin cleavage of the peptide crosslinker is indicated by the red dotted line to yield two peptide fragments. The larger fragment was detected by LC-MS analysis.

Table S1. Hydrodynamic size of proteins and NCs measured by dynamic light scattering and zeta potential by the Malvern Nano-ZS. Samples were diluted to 0.5 mg/mL with deionized water and 400 μL were used in a disposable folded capillary cell to measure size and zeta potential. Each sample was measured 3 times with 10 measurements each at 25℃. The mean value for ea ch sample is shown above.

PROTEIN	CROSSLINKER	SIZE (nm)	ZETA POTENTIAL (mV)
eGFP	None	5.4	-7.2
eGFP	Furin-degradable (Ahx-RVRRSK)	10.7	7.5
eGFP	Non-degradable (*N,N'*-Methylene bisacrylamide)	9.2	6.1
NLS-eGFP	None	5.4	-6.7
NLS-eGFP	Furin-degradable (AAm:APMAAm:CL=6:3.5:1) (Ahx-RVRRSK)	12.2	8.1
NLS-eGFP	Furin-degradable (AAm:APMAAm:CL=6:3.5:0.5) (Ahx-RVRRSK)	10.7	7.2
NLS-eGFP	Non-degradable (*N,N'*-Methylene bisacrylamide)	15.1	7.7
NLS-eGFP	Non-specific peptide (Ahx-AAARSK)	10.5	6.2
CP3	None	5.4	-4.1
CP3	Furin-degradable (Ahx-RVRRSK)	7.2	5.6
CP3	Non-degradable (*N,N'*-Methylene bisacrylamide)	10.4	7.8
BSA	None	5.6	-6.6
BSA	Furin-degradable (Ahx-RVRRSK)	9.7	6.7
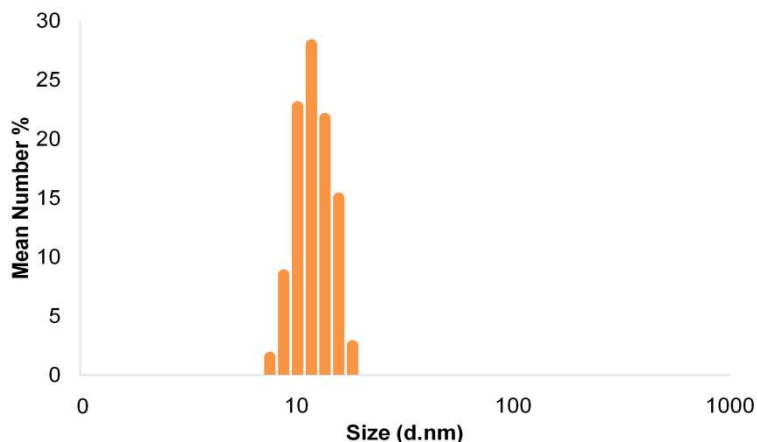
Figure S4. The hydrodynamic size of furin-degradable NLS-eGFP NCs as measured by dynamic light scattering in a 100 mM HEPES, 1 mM CaCl2, pH 7.5 buffer. NCs prepared with different proteins and/or crosslinkers displayed similar DLS profiles and are listed in Table S1.
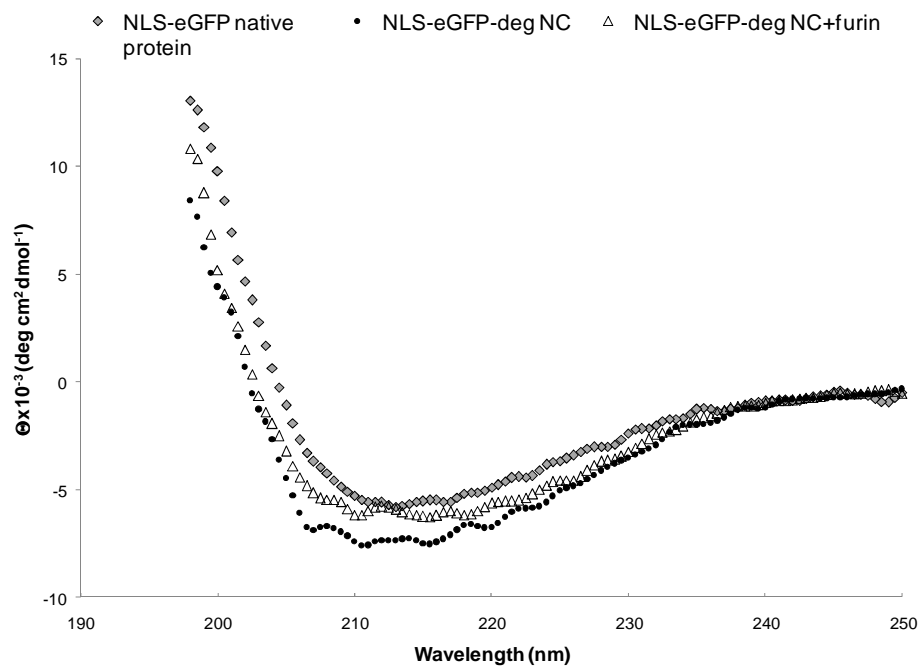
Figure S5. Far-UV circular dichroism spectra of native NLS-eGFP protein, NLS-eGFP furin-degradable NC, and NLS-eGFP furin-degradable NCs after furin degradation. The samples were placed in a quartz cuvette with a 1 cm path length and ellipticity was monitored in a Peltier-controlled cell at a rate of 10 nm per min at 25℃ in a Jasco spectropolarimeter (Jasco Inc., Eas ton, MD). 2.5 nmol native protein and protein NC were used. The degraded NC sample consisted of 2.5 nmol NC incubated with 1 unit furin at 37℃ for 10 hours before measurements were taken.
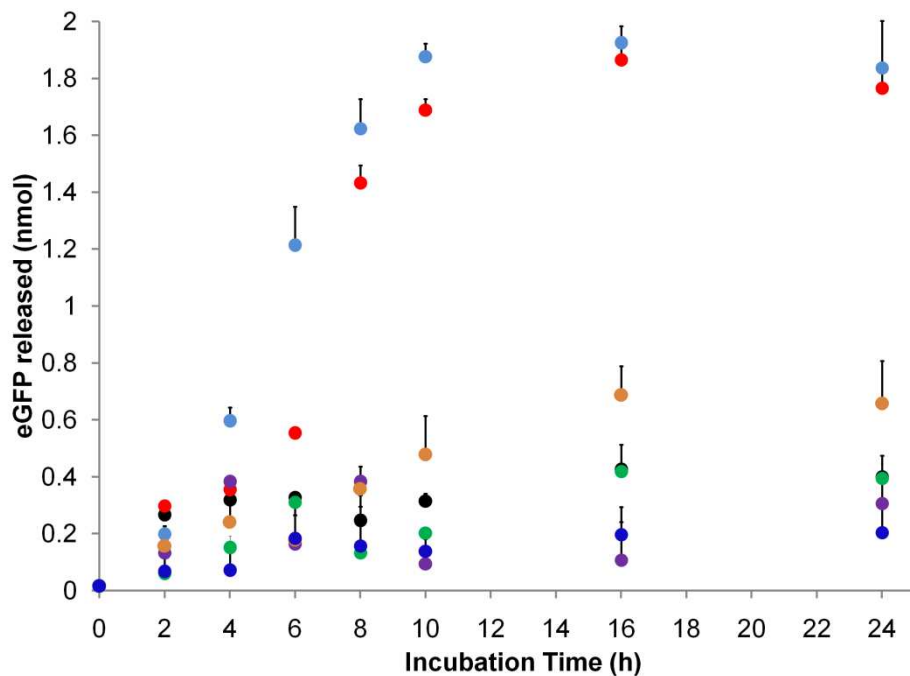
Figure S6. eGFP release by 2.5 nmol NCs for 24 hrs quantified using ELISA. (●) Furin-degradable NCs; Furin-degradable NCs with 1 U (●) and 4 U (●) furin; (●) Furin-degradable NCs with 1 U furin and dec-RVKR-cmk; (●) NCs with non-degradable crosslinkers. The stability studies of NCs were examined by quantifying release of eGFP in (●) acidic conditions: 100 mM HEPES, 1 mM CaCl$_2$, pH 5.5 buffer and in (●) high salt concentrations: 500 mM NaCl. The data represents averages with error bars from three independent experiments performed in triplicate.
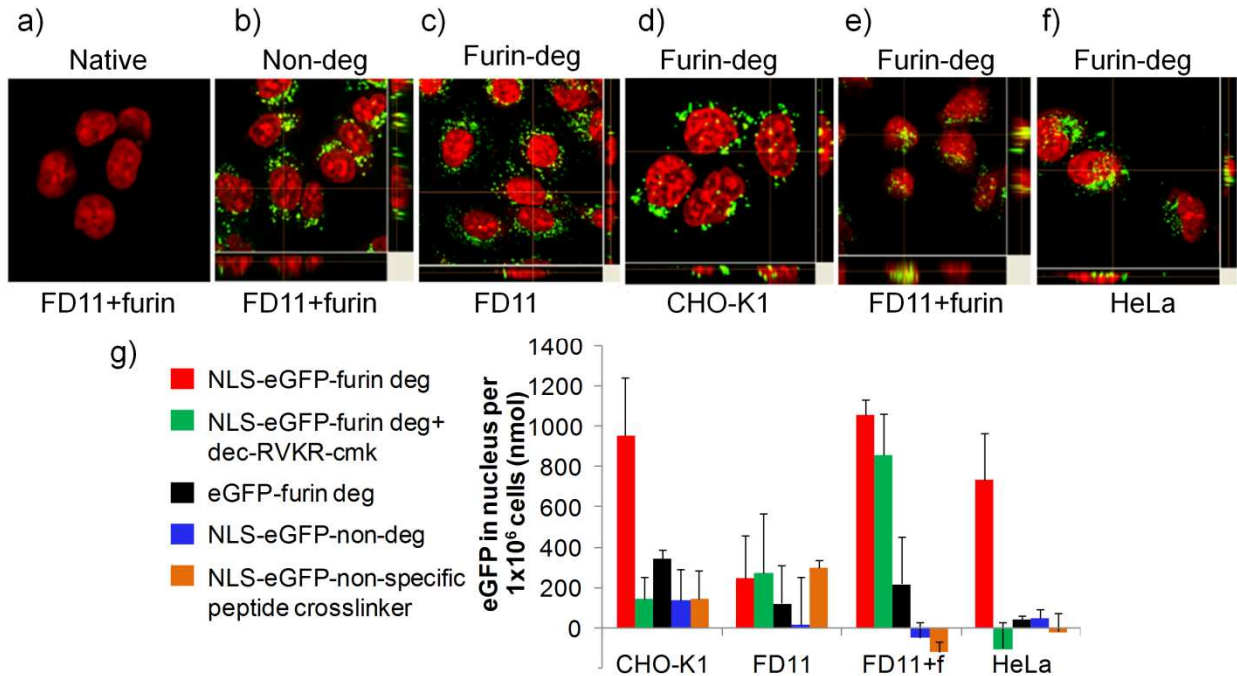
Figure S7. Confocal images of NLS-eGFP NC delivery show no cellular uptake of native protein (a) and no nuclear delivery for non-degradable protein NCs or degradable NCs to FD11 furin-deficient cells (b,c). Delivery of furin-degradable NCs to furin-expressing cell lines shows enhanced nuclear delivery (d-f). Red: nuclei; Green: eGFP. (g) Quantified eGFP levels using ELISA in the nuclear fractions of various crosslinked NCs which were obtained from the BioVision Nuclear/Cytoplasmic Fractionation Kit. All samples were incubated with cells at a concentration of 200 nM for 24 hours before confocal imaging or nuclear extraction.
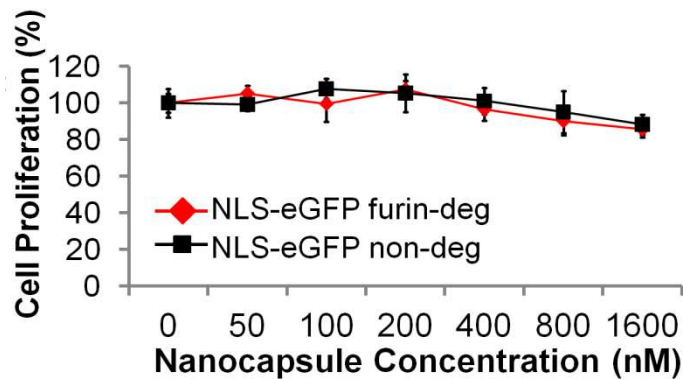
Figure S8. Cellular proliferation profile for HeLa cells treated with furin-degradable and non-degradable NCs for 24 h before the MTS assay was performed. There was no significant cytotoxicity up to 1.6 μM.
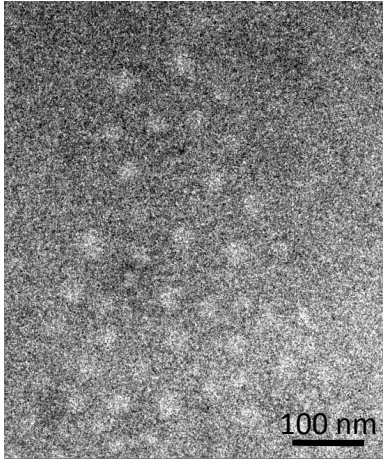
Figure S9. TEM image of Klf4-11R NCs constructed with furin degradable crosslinkers. The size of NCs were determined to be ~20 nm.

7.2. Supplementary Information from Intracellular Protein Delivery Using Microemulsion Microparticles

Synthesis of Microparticles

Both degradable and non-degradable nanoparticles were prepared using inverse emulsion polymerization. The organic phase was prepared using 3 mL hexane with a 90 mg surfactant mixture containing a 3:1 weight ratio of Span 80(sorbitan monooleate): Tween 80(polyethyleneglycol-sorbitan monooleate). The aqueous phase was prepared by mixing 2 mg protein with 0.25 mL of 300 mM sodium phosphate buffer pH 8.0 and incubating for 5 minutes on ice. Next, 41.6 mg of acrylamide was added and incubated on ice. After 10 minutes, 41.6 mg of N-(3-aminopropyl) methacrylamide was added to the aqueous mixture and incubated for 5 minutes. Then 4.5 mg non-degradable crosslinker (N,N'-methylene bisacrylamide) or 0. 5 mg furin degradable crosslinker was added to the mixture along with 3 mg ammonium persulfate. The aqueous phase was then added to the organic phase and sonicated using a flat tip probe on ice for 30 s with a Branson sonicator 450 using an output setting of 2 and a duty cycle of 40%. After the inverse emulsion was made, 3 μL of N,N,N',N'-tetramethylethylene diamine was added with stirring to initiate polymerization. The polymerization was done at room temperature for 10 min. Next the mixture was centrifuged for 10 min at 2800 rpm to collect the nanoparticles. The particles were washed 2 times with 5 mL hexane and 4 times with 5 mL acetone with centrifuging after each wash to remove the organic phase components. The particles were dried under high vacuum overnight. To resuspend the gels in aqueous solution, 1 mL water was added to the particles and sonicated in 30 s intervals until the solution was homogenous.

Mice

C57BL/6 (denoted as B6) female mice were purchased from Charles River Laboratories (Wilmington, MA.) All mice were housed in an animal facility at the University of Southern California (Los Angeles, CA) in accordance with institute regulations.

In vivo immunization of naive mice

OVA-ND and OVA-furin (0.7 mg/mL) were concentrated in 200 μl of PBS by ultracentrifugation. The concentrated nanoparticles (140 μg) were injected into the lower two footpads of C57BL/6 mice. The immunized mice were analyzed for immune responses 2 weeks postinjection.

Surface marker and intracellular staining

Mouse lymphocytes were collected and washed in PBS. The prepared cells were stained with anti-mouse CD16/32 to block Fc receptors. For intracellular staining, splenocytes were restimulated for 6 h with OVAp1 (1 mg/ml) or OVAp2 (10 mg/ml), with GolgiPlug (BD Biosciences) to inhibit IFN-γ secretion. The cell surface markers were stained with anti-mouse CD8–FITC. Cells were then permeabilized and stained with anti-mouse IFN-γ–PE. Stained cells were analyzed by flow cytometry (FACSort; BD Biosciences). All monoclonal staining antibodies were from BD Biosciences or from BioLegend (San Diego, CA).

Enzyme-linked immunosorbent spot assay (ELISPOT)

T cells were harvested from spleens and cocultured with either OVAp1 or OVAp2 peptide (GeneScript, Piscataway, NJ) overnight. The next day, restimulated T cells were counted and transferred to a MultiScreen plate (Millipore, Billerica, MA) coated with anti-mouse IFN-γ antibody (BD Biosciences). The plate was incubated at 37℃ and 5% CO_2 for 18–22 h. On the third day, biotinylated anti-mouse IFN-γ (BD Biosciences) was added to the plate, followed by the addition of streptavidin–alkaline phosphatase (Millipore) and BCIP/NBTplus substrate (Chemicon International, Temecula, CA) to develop spots. Spot development was stopped by rinsing thoroughly with deionized water. The plate was air dried and read with a Zeiss ELISPOT reader (Carl Zeiss MicroImaging, Göttingen, Germany). The number of spot-forming counts (SFCs) per 10^6 cells was used to plot results.

Table S2. Hydrodynamic Size and Zeta Potential for Protein NPs synthesized using inverse microemulsion procedures.

PROTEIN	CROSSLINKER	SIZE (nm)	ZETA POTENTIAL (mV)
eGFP	None	5.4	-7.2
eGFP	Furin-degradable (Ahx-RVRRSK)	120.5	19
eGFP	Non-degradable (*N,N'*-Methylene bisacrylamide)	60	20
CP3	None	5.4	-4.1
CP3	Furin-degradable (Ahx-RVRRSK)	70	14
CP3	Non-degradable (*N,N'*-Methylene bisacrylamide)	90	11
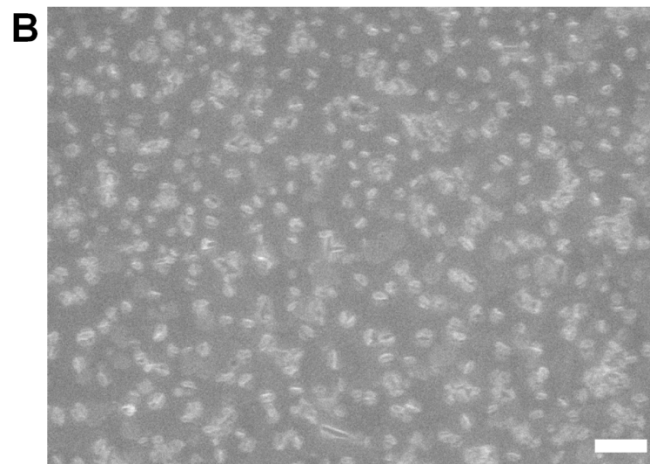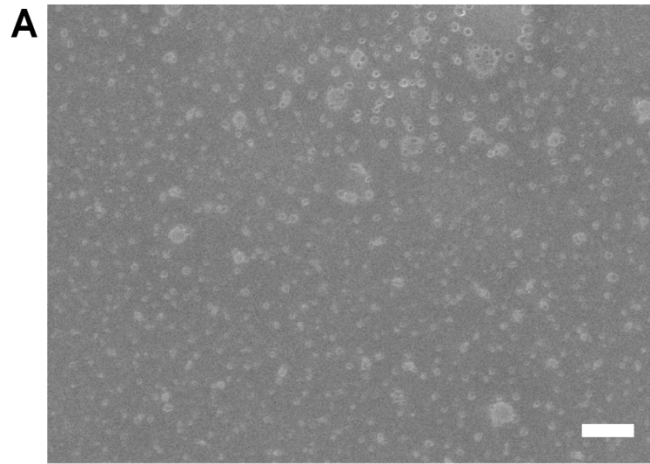
Figure S10. Scanning electron microscopy images of Caspase-3 NPs. (A) Non-degradable Caspase-3 NPs and (B) Furin-degradable Caspase-3 NPs

7.3. Supplementary Information for Engineered Biocompatible Degradable Polymeric Nanocapsules and Functional Delivery of a Differentiation Transcription Factor, MyoD

Materials

All chemicals were purchased from Sigma Aldrich unless noted otherwise. *N*-(3-aminopropyl) methacrylamide hydrochloride was purchased from Polymer Science, Inc. CellTiter 96® AQ$_{ueous}$ One Solution Cell Proliferation Assay (MTS) reagent was purchased from Promega Corporation. The furin-degradable peptide was synthesized as previously described [58]. Deionized water was prepared using a Millipore NanoPure purification system.

Instruments

Bradford assay absorbances were measured in a Thermo Scientific GENESYS 20 spectrometer. TEM images of nanoparticles were obtained on a Philips EM-120 TEM instrument. Zeta potential and particle size distribution were measured on the Malvern particle sizer Nano-ZS. Peptides were synthesized on a C S Bio Co. CS336X solid phase peptide synthesizer. Fluorescent images of cells were obtained with either a Zeiss Axio Observer Z1 Inverted Microscope or Leica one-photon *confocal* laser scanning *microscope* (Leica Microsystems, Heidelberg).

Protein expression and purification

NLS-eGFP was expressed and purified as previously reported [58]. For expression of MyoD, *pET-His-MyoD* (a gift from Dr. Kobatake) was transformed into BL21 cells by electroporation. Transformed cells were inoculated overnight at 37℃ with shaking in Luria-Bertani medium containing 100 μg/mL ampicillin. Overnight cultures were diluted 1:200 and grown in Fernbach flasks containing 1 liter of LB medium with 100 μg/mL ampicillin at 37℃ with shaking at 270 rpm. When the cultures reached an absorbance *A*600 ~0.8, isopropyl β-D-thiogalactopyranoside was added to a final concentration of 1 mM to induce protein expression, and the cells were incubated for 3 h at 37℃. The cells were harvested by centrifugation (3500g, 4℃, 15 min),

resuspended in 30 mL Buffer A (50 mM Tris–HCl, pH 8.0, 2 mM DTT, 2 mM EDTA), and lysed by sonication. The insoluble fraction was collected by centrifugation (15,000g, 4°C, 30 min) and dissolved in 8 M urea overnight at 4°C. After centrifugation at 14,000g, 4°C, 10 min, the solubilized fraction was filtered with a 0.45 μm filter and incubated with 3 mL of Ni-NTA resin (Qiagen) for 3 hours at 4°C. The protein was then purified using a step gradient of Buffer A with 8 M urea with increasing concentrations of imidazole (10, 20, and 250 mM). MyoD protein was eluted with 15 mL Buffer A containing 250 mM imidazole. The protein concentration was qualitatively assessed by SDS-PAGE and quantitatively determined by the Bradford protein assay. MyoD was dialyzed three times in refolding buffer (1xPBS, 1 M urea, 400 mM arginine, 40 μM glutathione (reduced), 4 μM glutathione (oxidized)) and then three times in 1xPBS. Far-UV circular dichroism (CD) spectra of MyoD protein (0.1 mg/mL in PBS) before and after refolding were obtained at 20°C with a JASCO J-715 Circular Dichroism Spectrometer. Optical rotation was measured from 190-250 nm with a bandwidth of 1 nm.

Preparation of protein NCs

1 mg protein was diluted in 500 μL of 5 mM pH 9 NaHCO$_3$ buffer after which PEG methyl ether acrylate (M$_n$~480) was added with stirring for 10 min at 4°C. Next, *N*-(3-aminopropyl) methacrylamide (APMAAm) was added with stirring for 5 min. Afterwards, the furin-degradable, redox-responsive (*N,N'*-Bis(acryloyl)cystamine) or non-degradable crosslinker (*N,N'*-methylene bisacrylamide) was added. The polymerization was immediately initiated by adding 3 mg of ammonium persulfate and 3 μL of *N,N,N',N'*-tetramethylethylenediamine. The polymerization was allowed to proceed for 60 min at 4°C. Finally, buffer exchange with 100 mM HEPES, 1 mM CaCl$_2$, pH 7.5 (furin-degradable NCs) or 1xPBS (redox-responsive and non-degradable NCs) was performed to remove unreacted monomers and initiators.

Cell-free protein release assay from NCs

150 nmol of NLS-eGFP furin-degradable NC was added to 100 mM HEPES, 1 mM CaCl$_2$, pH 7.5 buffer into a total volume of 50 μL. 10 units of furin enzyme was added to the reaction mixture and incubated at 37℃ for various times. 1 unit of enzyme is defined by Sigma as the amount of enzyme needed to release 1 pmole from flourogenic peptide Boc-RVRR-AMC in 1 min at 30℃. 10 μg NLS-eGFP redox-responsive NC was incubated with 1 mM GSH in 200 μL PBS buffer at 37℃ for various times. Samples from specific time points were appropriately diluted for the GFP ELISA assay.

Enzyme-linked Immunosorbant Assay (ELISA)

To quantify native eGFP protein released, a GFP ELISA kit was obtained from Cell Biolabs, Inc., San Diego, CA. We constructed a standard curve using known eGFP amounts with the kit's standard eGFP sample and by performing the assay. Briefly, samples were centrifuged for 10 min at 7000 rpm with a 30 kDa MWCO filter to isolate native eGFP protein. Then, the samples were loaded into anti-GFP rabbit antibody coated wells and incubated at 4℃ overnight. After careful washing, a detection antibody (anti-GFP mouse antibody) was added to each well and incubated at room temperature for 2 hours. Next, an anti IgG mouse-HRP conjugate antibody was added. After one hour, TMB substrate was added and incubated for 30 minutes. After the addition of stop solution to each well, absorbance at 450 nm was measured.

Cell culture.

HeLa and HFF (ATCC, Manassas, VA) were cultured in Dulbecco's Modified Eagle's Medium (Invitrogen) or DMEM supplemented with 10% bovine growth serum (Hyclone, Logan, UT) or BGS, 1.5 g/L sodium bicarbonate, 100 μg/mL streptomycin and 100 U/mL penicillin. Mouse C2C12 myoblast cells (a gift from Dr. Rachelle Crosbie, UCLA) were cultured in DMEM with 20% bovine growth serum, 1.5 g/L sodium bicarbonate, 100 μg/mL streptomycin and 100 U/mL penicillin. All cells were cultured at 37℃, in 98% humidity and 5% CO$_2$. Cells were regularly subcultured using 0.25% trypsin-EDTA.

Cytotoxicity study using 3-(4,5-dimethylthiazol-2-yl)-5-(3-carboxymethoxyphenyl)-2-(4-sulfophenyl)-2H-tetrazolium) (MTS) assay

Cells were seeded into 96-well plates at a density of 5,000 cells per well and cultivated in 100 µL of DMEM with 10 % BGS. The plates were then incubated in 5% CO_2 and at 37℃ for 12 h to reach 70-80% confluency before addition of protein/NCs. After 24 h or 48 h incubation with protein NCs, the cells were washed with PBS solution and incubated with 100 µL fresh DMEM and 20µL MTS solution (CellTiter 96® AQueous One Solution Cell Proliferation Assay, Invitrogen). The plates were incubated for an additional 3 h. The absorbance of the plates was read at 550 nm and a reference wavelength of 690 nm using a microplate reader (PowerWave X, Bio-tek Instruments, USA).

Imaging and quantification of nuclear localization

Cells were seeded into 48 well plates at a density of 10,000 cells/well and cultured in 250 µL DMEM with 10% BGS. The plates were incubated for 12 h before being treated with 400 nM NCs. After 24 h, cells were washed 3x with PBS and fixed for 15 min with 4% paraformaldehyde. Nuclei were stained with 1 µg/mL DAPI. Cells were imaged using Z-stack imaging and Image J was used for quantification of eGFP and nuclear overlap.

Nuclear and cytoplasmic fractionation

Cells were seeded into 6-well plates at a density of 1×10^5 cells per well and cultivated in 1.5 mL of DMEM with 10% BGS. The plates were incubated for 12 h before being treated with 400 nM of appropriate NCs. Cells were collected by trypsin-EDTA and centrifugation after 24 hours. A Nuclear/Cytosol Fractionation Kit (BioVision, Inc., Mountain View, CA) was used to separate cytosolic and nuclear extracts from NC-treated cells. Fractions were obtained per the manufacturer's instructions. All procedures were performed at 4℃. Extracts were stored at -80 ℃ until the GFP-ELISA assay was performed (Cell Bi olabs, Inc., San Diego, CA)

MyoD-Rhodamine conjugation

NHS-rhodamine (Thermo Scientific Pierce) was reacted with MyoD protein in a 5 molar excess in 50 mM NaHCO$_3$ buffer, pH 9 for 2 hours at 4℃. After the reactio n, MyoD-rho was purified by extensive buffer exchange using PBS with 30,000 MWCO filters. MyoD-rho NCs were synthesized and cellular uptake was subsequently imaged as previously described.

MyoD luciferase reporter construct cloning

A MyoD firefly luciferase reporter plasmid was constructed using pGL3-promoter vector (Promega) as a template. Four copies of the E-box promoter sequence upstream of the firefly luciferase gene was PCR amplified using the specific primers I (5'-CTCTT<u>ACGCGT</u>CACCTGCACCTGCACCTGCACCTGCTCGAGATCTGCGATCTGC-3' with an underlined *Mlu*I site) and II (5'CAGTACCGGAATGCC<u>AAGCTT</u>TTTGCAAAAGCCTAGGCCTCC-3' with an underlined *Hind*III site). This fragment was amplified and inserted between the *Mlu*I and *Hind*III sites of pGL3-promoter, thus resulting in *MyoD-luc*. After sequence confirmation, the plasmid was transformed into *E. coli* XL1 cells and subsequently purified by miniprep (Zymo Research).

Dual-luciferase assay

C2C12 cells were plated at a density of 10,000 cells per well in 96-well plates and incubated for 16 h. Cells were transfected with Lipofectamine per the manufacturer's instructions with 50 ng *pRL-TK* Renilla luciferase (Promega) and 0.1 µg *MyoD-luc*. For MyoD DNA transfected cells, 0.1 µg *pORFMyoD* (a gift from Dr. Derrick Rossi) was also transfected. Cells were incubated in antibiotic-free media for 4 hours, after which 400 nM MyoD protein/NCs were added into fresh media with antibiotics. After 16 h, another 400 nM MyoD protein/NCs were added to cells. After a total 48 h, cells were washed three times with PBS and lysed with 80 µL Passive Lysis Buffer (Promega) for 15 minutes at 25℃. Cell lysate was c entrifuged at 4℃ at 3500 rpm and 10 µL was plated in a 96 well plate and luciferase activity was monitored using the Dual-Luciferase Reporter Assay system (Promega) with the GloMax Multi+ Detection System.

Myoblast differentiation treatment

C2C12 cells were plated in 24 well plates (3000 cells/well) for immunostaining or 6 well plates (10,000 cells/well) for qPCR and cultured in DMEM + 20%BGS. After 24 hours, cells were treated with 400 nM MyoD protein/ NCs for 3 subsequent days. For MyoD transfected cells, 1 μg or 3 μg *pORFMyoD* was transfected using Lipofectamine using the manufacturer's protocol for 24 well or 6 well plates, respectively. Media was changed each day thereafter for a total of 7 days after which cells were either fixed or harvested for further experiments. For proteinase K treatment assays, 10 μg protein/NCs were treated with 50 μg/mL proteinase K in 50 mM Tris-HCl, 5 mM $CaCl_2$ pH 7.5 buffer for 1 h at 37°C before incubation wi th cells.

Immunostaining

Treated C2C12 cells were washed with PBS and fixed by 4% paraformaldehyde in PBS. Immunostaining was performed with mouse anti-MyHC antibody (1:400, Millipore) and an Alexa Flour 488 conjugated secondary Ab. DAPI (0.1 mg/mL) was used for nuclear counterstaining. Positively-stained cells were counted using Image J.

Quantitative Real-Time PCR for MyoD-treated cells

Treated C2C12 cells were trypsinized, collected by centrifugation and homogenized using QIAshredder and total RNA was extracted using the RNeasy mini kit (Qiagen). RNA samples (1 µg) were treated with DNase I (Invitrogen) and reverse transcription was performed using the iScript RT kit (Bio-Rad). The SybrGreen supermix kit (Bio-Rad) was used for real-time PCR. Threshold cycle (Ct) was determined on the linear phase. Results were normalized by Ct of 18 s. Relative gene expression fold difference was calculated by $2^{-\Delta normalized\ Ct}$. PCR primers are listed in Table S2.
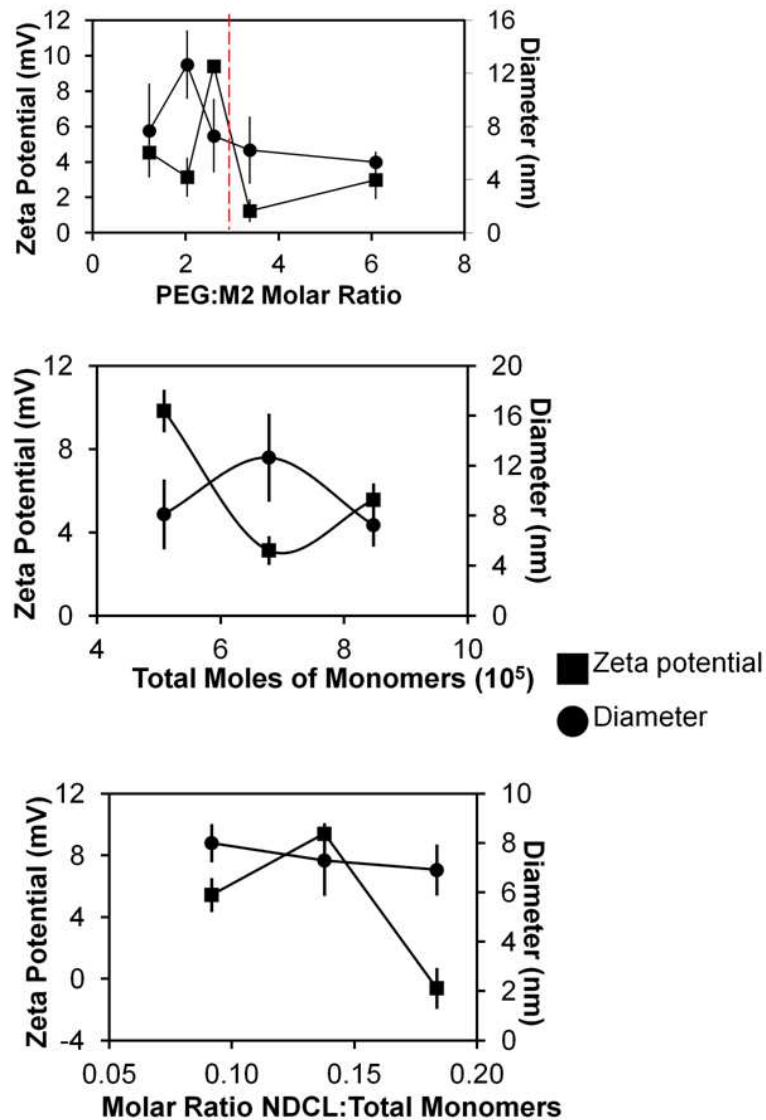
Figure S11. Physical characterization curves of PEG NCs used for optimization. *(Top)* **Hydrodynamic size and zeta potential of NLS-eGFP non-degradable NCs prepared with varying PEG:M2 molar ratios. NCs did not enter cells right of the red line. Data represents average values and standard deviation from six measurements.** *(Center)* **Total amount of monomers was adjusted by keeping the molar ratio between PEG:M2 the same at 2.03.** *(Bottom)* **The crosslinking ratio of non-degradable crosslinker was adjusted while the total number of monomers was the same (7.07×10^5 moles).**
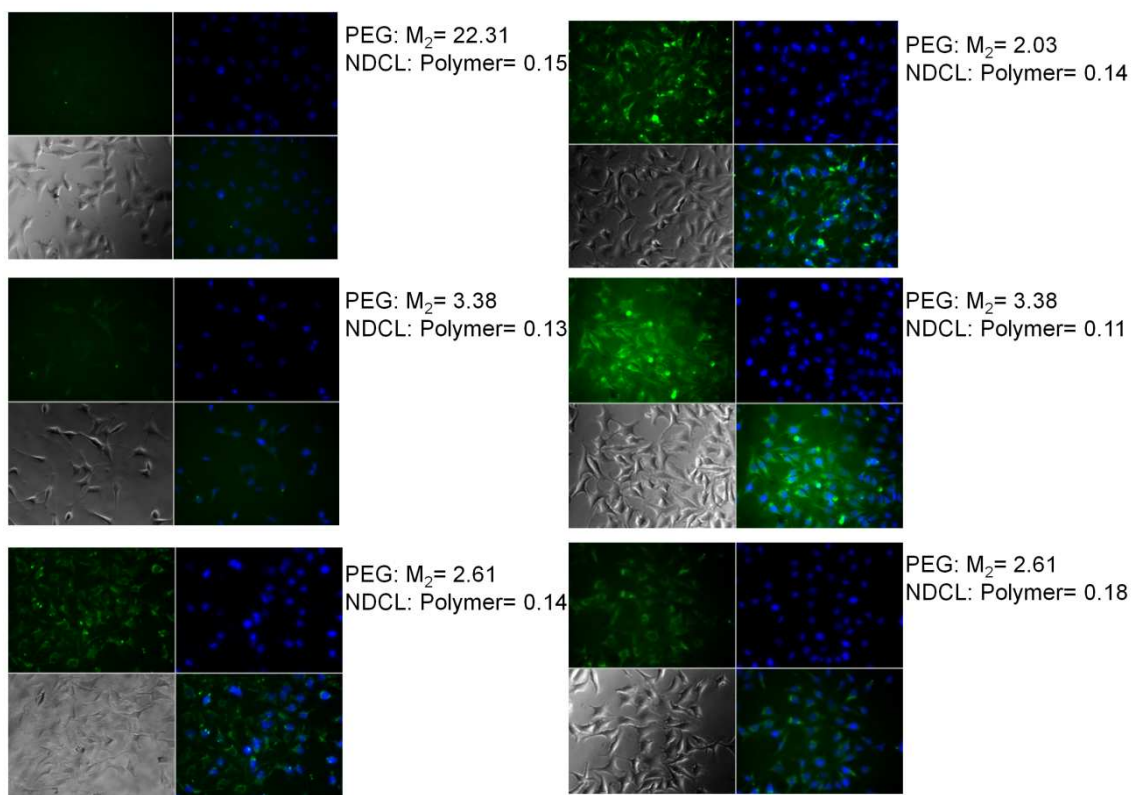
Figure S12. Representative images of PEG NLS-eGFP NCs used for optimization. NCs were synthesized using non-degradable crosslinkers and then incubated with HeLa cells for 24 h with 400 nM NCs before being fixed and stained. (green:eGFP; blue: DAPI-stained nuclei)

Table S3. Optimized PEG NLS-eGFP NCs using various crosslinkers

Protein	Crosslinker type	PEG:M2 (molar ratio)	Crosslinking Ratio (molar)	Size (nm)	Zeta Potential (mV)
NLS-eGFP	non-deg	2.6	0.16	6.5	1.3
NLS-eGFP	furin-deg	2.6	0.16	6.3	2.9
NLS-eGFP	redox-resp	2.6	0.16	7.0	1.2
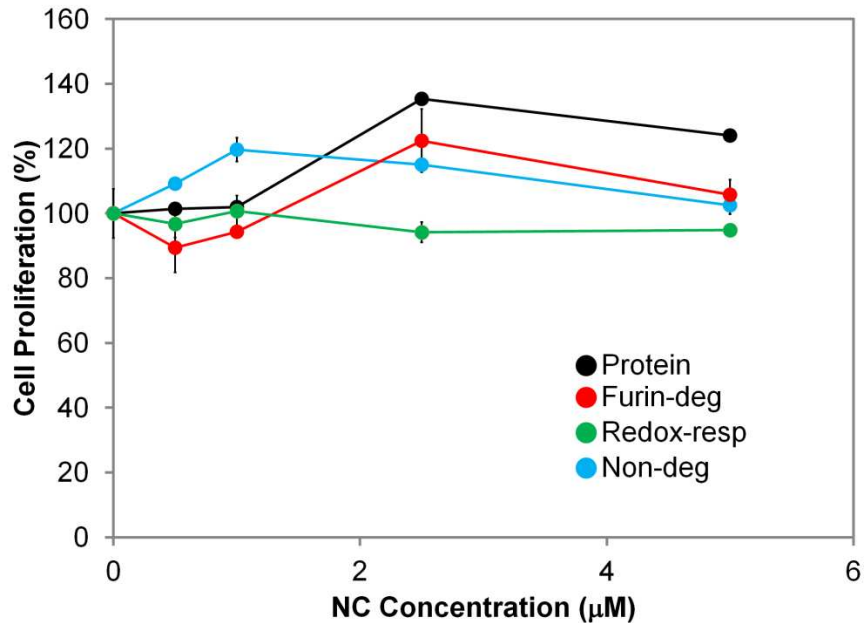
Figure S13. proliferation profiles of various concentrations of NLS-eGFP PEG NCs delivered to HeLa cells for 24 h and quantified by the MTS assay.
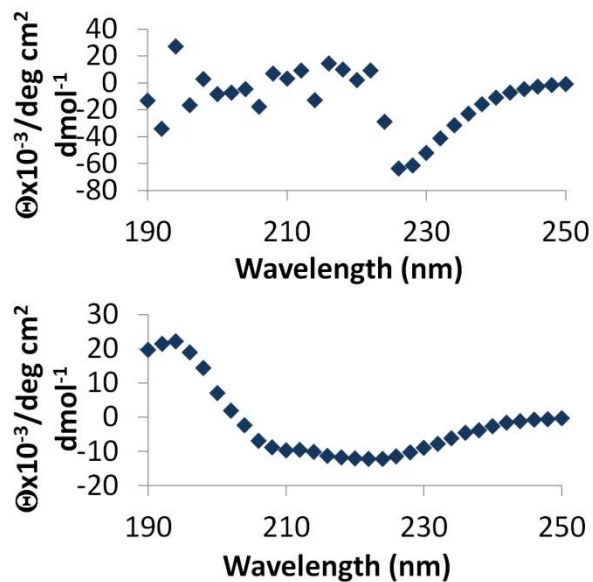
Figure S14. Circular dichroism (CD) curves of MyoD protein before (top) and after (bottom) refolding. Far-UV CD spectra of MyoD protein (0.1 mg/mL in PBS) were obtained at 20℃ with a JASCO J- 715 Circular Dichroism Spectrometer. Optical rotation was measured from 190-250 nm with a bandwidth of 1 nm.
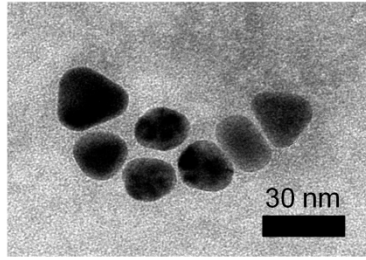
Figure S15. Image of redox-responsive MyoD PEG NCs.

Table S4. Primers for Real-Time PCR for MyoD-treated C2C12 Cells

Primer Name	Primer Sequence
HPRT F	AAGGACCTCTCGAAGTGTTGGATA
HPRT R	CATTTAAAAGGAACTGTTGACAACG
Myog F	CTACAGGCCTTGCTCAGCTCC
Myog R	TCTAACACCCGCAGACATCC
MyHC F	AAAGGTCTGCGCAAACACGGAGAGAC
MyHC R	ACAACCTAACAAGGAGTCGGAGGAG
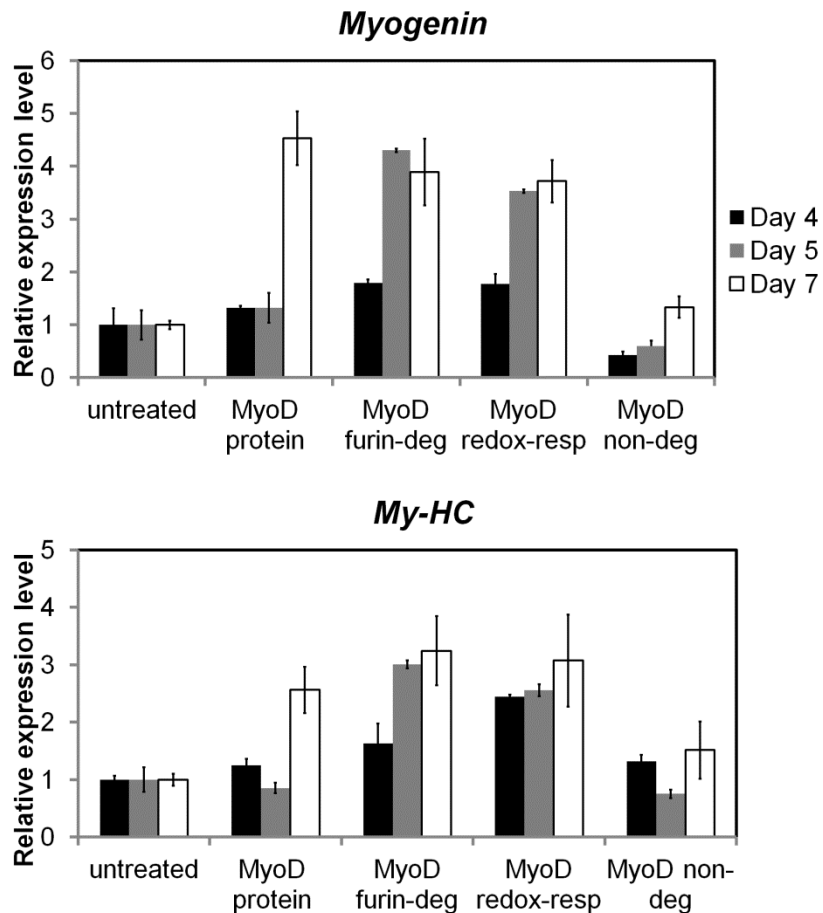
Figure S16. Real-time PCR analysis of the relative expression of muscle-specific genes *Myogenin* and *My-HC* in treated C2C12 cells at day 4, 5 and 7 of treatment. (n=2).
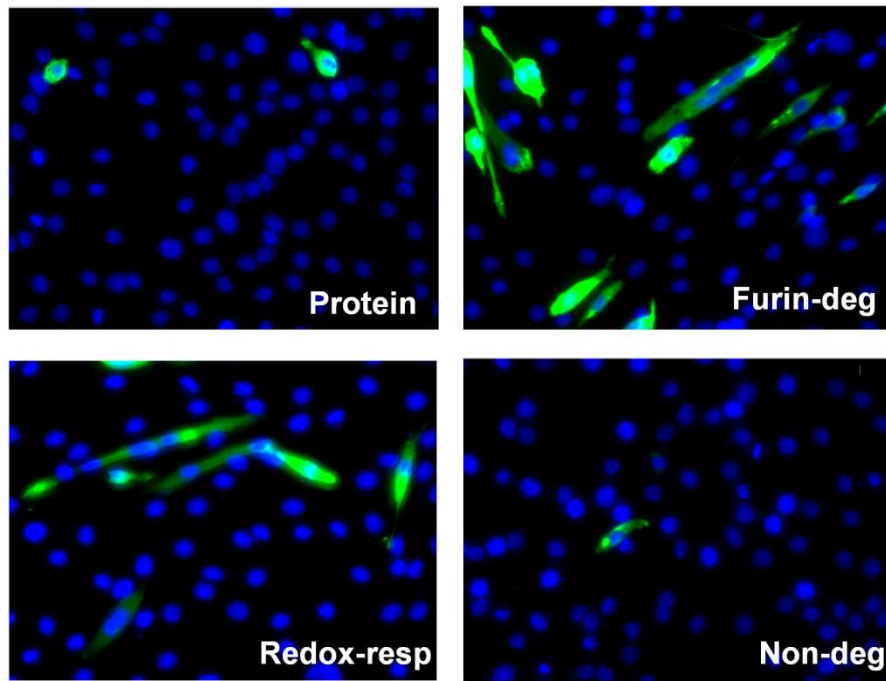
Figure S17. Fluorescent images of My-HC immunostaining in treated C2C12 myoblasts with MyoD protein/NCs which were first treated with 50 μg/mL proteinase K for 1 h at 37℃. (green: Alexa- Fluor 488 conjugated My-HC antibody; blue: DAPI-stained nuclei)

7.4. Supplementary Information for Functional Delivery of a Transdifferentiation Transcription Factor, Pdx1

Protein Purification of rPdx1

pET28a-Pdx1 was generously provided by Dr. Li-Jung Yang from the University of Florida. Plasmid was transfected into BL21 (DE3) cells using electroporation and grown in LB supplemented with kanamycin. After growth at 37℃ t o an optical density (OD600) of 0.8, cells were incubated at room temperature for another 18 h in the presence of 0.5 mM isopropyl β-d-1-thiogalactopyranoside. Bacteria were lysed by pulse sonication in buffer A (20 mM Tris/HCl pH 8.0, 500 mM NaCl, and 0.1% Triton X-100) containing 5 mM imidazole and proteinase inhibitors (Roche Diagnostics, Basel, Switzerland). After centrifugation, the cell-free supernatant was applied to a column of Ni-NTA resin for 1 hour and washed with several volumes of buffer A containing 25 mM imidazole. The protein was eluted by buffer A containing 250 mM imidazole and dialyzed in PBS.

Cell culture of HepG2, Fetal liver cells and AR42J cells

HepG2 cells were cultured in Eagle's Minimum Essential Medium supplemented with 10% FBS. AR42J-B13 cells were cultured in low glucose DMEM, 10% FBS and 1x anti-anti solution. Fetal liver cells were cultured in Williams' medium E (ICN Biomedicals Inc., Aurora, OH) supplemented with 10% fetal bovine serum (FBS, Sigma-Aldrich, St. Louis, MO), hormones (dexamethasone, 0.1 µmol/L; insulin, 0.1 µmol/L; aprotinin, 5,000 KIU/L (5.8 TIU/L); Sigma-Aldrich) and antibiotics (penicillin G, 50,000 IU/L; streptomycin, 50 µg/L; amphotericin B, 125 µg/L; Gibco BRL, Grand Island, NY).

Pdx1-Rhodamine conjugation

NHS-rhodamine (Thermo Scientific Pierce) was reacted with Pdx1 protein in a 5 molar excess in 50 mM NaHCO₃ buffer, pH 9 for 2 hours at 4℃. After the reactio n, Pdx1-rho was purified by extensive buffer exchange using PBS with 30,000 MWCO filters. Pdx1-rho NCs were synthesized and cellular uptake was subsequently imaged as previously described.

Insulin promoter activated dual-luciferase assay

HepG2 or AR42J-B13 cells were plated at a density of 10,000 cells per well in 96-well plates and incubated for 16 h. Cells were transfected with Lipofectamine per the manufacturer's instructions with 50 ng *pRL-TK* Renilla luciferase (Promega) and 0.1 μg *RIP-luc*. In some studies, 1 μg NeuroD plasmid was also transfected. Cells were incubated in antibiotic-free media for 24 hours, after which 400 nM, 800 nM or 1600 nM Pdx1 protein/NCs were added into fresh media with antibiotics. After a total 48 h, cells were washed three times with PBS and lysed with 80 μL Passive Lysis Buffer (Promega) for 15 minutes at 25°C. Cell lysate was centrifuged at 4°C at 3500 rpm and 10 μL was plated in a 96 well plate and luciferase activity was monitored using the Dual-Luciferase Reporter Assay system (Promega) with the GloMax Multi+ Detection System.

Pdx1 transdifferentiation treatment on fetal liver cells or AR42J-B13 cells

Fetal liver cells and AR42J-B13 cells were plated in 6 well plates (10,000 cells/well) for qPCR and cultured in appropriate media. After 24 hours, cells were treated with 400 nM MyoD protein/ NCs for 3 subsequent days. Media was changed each day thereafter for a total of 7 days after which cells were harvested for further experiments.

Pancreatic Gene Expression Quantitative Real-Time PCR

Treated fetal liver cells or AR42J cells were trypsinized, collected by centrifugation and homogenized using QIAshredder and total RNA was extracted using the RNeasy mini kit (Qiagen). RNA samples (1 µg) were treated with DNase I (Invitrogen) and reverse transcription was performed using the iScript RT kit (Bio-Rad). The SybrGreen supermix kit (Bio-Rad) was used for real-time PCR. Threshold cycle (Ct) was determined on the linear phase. Results were normalized by Ct of 18 s. Relative gene expression fold difference was calculated by $2^{-\Delta normalized\ Ct}$. PCR primers are listed in Table S5.

A250   A40   A20   FT   A250

Optimization

Protease Inhibitor
Low nickel resin
binding time
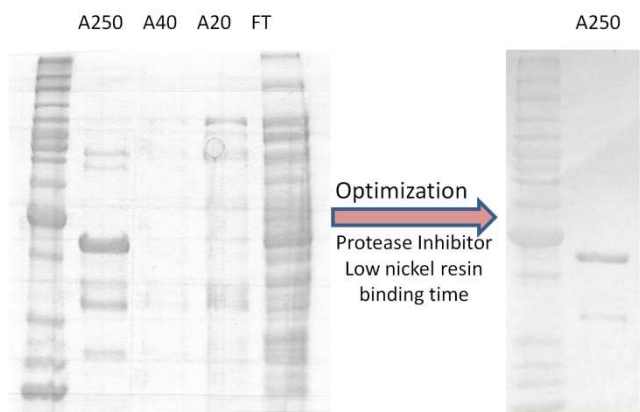
Figure S18. Optimization of Pdx1 protein expression using protease inhibitor and a lower nickel resin binding time. A250, A40 and A20 refer to 250 mM, 40 mM and 20 mM imidazole concentration, respectively. FT refers to the flowthrough of unbound protein to nickel.

Table S5. Primers used for qPCR assays in Fetal liver cells or AR42J-B13 rat cells treated with Pdx1 NCs

Species	Primer Name	Sequence
Human	GADPH F	5'-AGCCACATCGCTCAGACACC-3'
Human	GADPH R	5'-GTACTCAGCGGCCAGCATCG-3'
Human	Pdx1 F	5'-AAAGCTCACGCGTGGAAAGG-3'
Human	Pdx1 R	5'-TCAACATGACAGCCAGCTCCA-3'
Human	IAPP F	5'-TGTGCTCTCTGTTGCATTGAACC-3'
Human	IAPP R	5'-TGGATCCCACGTTGGTAGATGA-3'
Human	Insulin F	5'-TACCTAGTGTGCGGGGAACGA-3'
Human	Insulin R	5'-CCAGCTGGTAGAGGGAGCAGA-3'
Rat	GADPH F	5'-TCCAGTATGACTCTACCCACG-3'
Rat	GADPH R	5'-CACGACATACTCAGCACCAG-3'
Rat	Insulin1 F	5'-CAATCATAGACCATCAGCAAGC-3'
Rat	Insulin1 R	5'-AGAAACCACGTTCCCCAC-3'
Rat	Insulin2 F	5'-CCCAGGCTTTTGTCAAACAG-3'
Rat	Insulin2 R	5'-GTGCCAAGGTCTGAAGGTC-3'
Rat	IAPP F	5'-CCACTGAAAGGGATCTTGAGAC-3'
Rat	IAPP R	5'-TTCCGTTTGTCCACCTGAG-3'
Rat	Pax4 F	5'-GGGCAGTATCCAGATTCAGTTG-3'
Rat	Pax4 R	5'-GGCATCTGTGTTTCCCATTTC-3'
Rat	NeuroD1 F	5'-ATGTCTTCCACGTCAAGCC-3'
Rat	NeuroD1 R	5'-GAGAAGTTGCCATTGATGCTG-3'
Rat	Nkx2.2 F	5'-GGTCAAGATCTGGTTCCAAAAC-3'
Rat	Nkx2.2 R	5'-GTCACCTCCATACCTTTCTCAG-3'
Rat	Pcsk2 F	5'-GCATAAAGACGGAGAGGAAGAG-3'

S34

Rat	Pcsk2 R	5'-TGGTAAAAGTGGTACAGGCC-3'
Rat	Pdx1 F	5'-CCCGAGCTTCTGAAAACTTTG-3'
Rat	Pdx1 R	5'-CTTTTCATTGTCCTCAGTTGGG-3'

7.5. Supplementary Information for Delivery of a Combination of Transcription Factors for Formation of iPS Cells

Cloning of luciferase reporter plasmids

Reporter inserts were amplified from the pGL3 promoter vector (Promega) with the following forward primers and unversal reverse primer containing MluI site in green, SacI site in red, and HindIII site in orange.

Oct4-F2	5'-CTCTTACGCGTATTGTAATGCAAATCATTGTAATGCAAA TCATTGTAATGCAAATCATCGAGATCTGCGATCTGC-3'
Klf4-F2	5'-CTCTTACGCGT GGGTGTGGCCAGGGTGTGGCCAGGGTGTGGCCACTCGAGATCTCGA TCTGC
Myc-F2	5'CTCTTACGCGTGCACGTGGCCGCACGTGGCCGCACGT GGCCTCGAGATCTGCGATCTGC-3'
Rv2	5'-CAGTACCGGAATGCCAAGCTTTTTGCAAAAGCCTAGGCCTCC-3'.

PCR products and pLG3 promoter were digested with MluI and HindIII and ligated to form reporter plasmids. Constructs were verified with sequencing.

OSKM-specific activated dual-luciferase assay

293T or HFF cells were plated at a density of 10,000 cells per well in 96-well plates and incubated for 16 h. Cells were transfected with Lipofectamine per the manufacturer's instructions with 50 ng *pRL-TK* Renilla luciferase (Promega) and 0.1 μg *pGL3-O/S, pGL3-M or pGL3-K*. In some studies, 1 μg pMX-OSKM plasmids were also transfected. Cells were incubated in antibiotic-free media for 4 hours, after which 400 nM OSKM protein/NCs were added into fresh media with antibiotics. After a total 48 h, cells were washed three times with

PBS and lysed with 80 μL Passive Lysis Buffer (Promega) for 15 minutes at 25°C. Cell lysate was centrifuged at 4°C at 3500 rpm and 10 μL was plated in a 96 well plate and luciferase activity was monitored using the Dual-Luciferase Reporter Assay system (Promega) with the GloMax Multi+ Detection System.

Treatment of Neural Stem Cells with OSKM Nanocapsules

NSCs were seeded in 6 well plates at a density of 5×10^4 cells per well and were treated with 400 nM of each furin-degradable OSKM NC every alternate day for a total of 4 treatments. NSCs were cultured in MEM/F12 w/o HEPES, w/ L-Glutamine (CHEMICON Cat. No. DF-042-B), L-glutamine (CHEMICON Cat. No. TMS-002-C), human serum albumin, human transferrin, putrescine dihydrochloride, human recombinant insulin, L-thyroxine, Tri-iodo-thyronine, progesterone, sodium selenite, heparin, corticosterone. After 30 days, the cells were transferred to a MEF feeder layer and cultured in ESC medium for observation of iPS colonies. ESC medium consisted of DMEM high glucose, 10% FBS, P/S, 1 M HEPS, 100 mM sodium pyruvate, 200 mM L-glutamine, 55 mM β-mercaptoethanol and 50 mg/mL gentamicin.

7.6. Supplementary Information for Delivery of mRNA Using Degradable Polymeric NCs

mRNA Synthesis

Venus linearized DNA was under the control of the Sp6 promoter. 25 mM of NTP mixture was prepared: 100 mM ATP, 100 mM GTP, 100 mM 5-mC, and 100 mM pSU along with RNase free water. The *in vitro* transcription reaction was intiated using 4 μg linearized Venus DNA, 5x Sp6 buffer, 25 mM NTP, 32 mM Cap, Sp6 enzyme mix and incubated for 5 hours at 37°C. DNase (Invitrogen) was added to the mixture for 30 minutes at 37°C and then incubated at 65 C to inactivate the enzyme. 2 mL antarctic phosphatase was added at 37°C for 20 min. RNA was purified with a kit. For fluorescent mRNA, AlexaFluor-UTP was added at a concentration of 1 mM along with the NTP mixture.

Stability studies for mRNA NCs

Naked mRNA and mRNA NCs were subjected to physiological conditions of 37℃, 10% serum and pH 5 for 4 hours or 24 hours. Naked mRNA and mRNA NCs were also tested for stability in various storage/handling conditions using 3 or 7 freeze/thaw cycles from -80℃ and with storage at 4℃ for 4 or 24 hours. After treatment, mRNA NCs were treated with 2 mM GSH for 2 hours and all samples were assessed on a 1% agarose gel.

REFERENCES

1. Leader, B., Baca, Q.J. & Golan, D.E. Protein therapeutics: A summary and pharmacological classification. *Nature Reviews Drug Discovery* **7**, 21-39 (2008).

2. Walsh, G. Biopharmaceutical benchmarks 2010. *Nat Biotechnol* **28**, 917-924 (2010).

3. Walsh, G. Biopharmaceutical benchmarks 2006. *Nat Biotechnol* **24**, 769-U765 (2006).

4. Kabanov, A.V. & Vinogradov, S.V. Nanogels as Pharmaceutical Carriers: Finite Networks of Infinite Capabilities. *Angewandte Chemie-International Edition* **48**, 5418-5429 (2009).

5. Leader, B., Baca, Q.J. & Golan, D.E. Protein therapeutics: a summary and pharmacological classification. *Nat Rev Drug Discov* **7**, 21-39 (2008).

6. Peer, D. et al. Nanocarriers as an emerging platform for cancer therapy. *Nature Nanotechnology* **2**, 751-760 (2007).

7. Pack, D.W., Hoffman, A.S., Pun, S. & Stayton, P.S. Design and development of polymers for gene delivery. *Nature Reviews Drug Discovery* **4**, 581-593 (2005).

8. Petros, R.A. & DeSimone, J.M. Strategies in the design of nanoparticles for therapeutic applications. *Nat Rev Drug Discov* **9**, 615-627 (2010).

9. Whitehead, K.A., Langer, R. & Anderson, D.G. Knocking down barriers: advances in siRNA delivery. *Nat Rev Drug Discov* **8**, 129-138 (2010).

10. Bareford, L.M. & Swaan, P.W. Endocytic mechanisms for targeted drug delivery. *Adv. Drug Deliv. Rev.* **59**, 748-758 (2007).

11. Sawant, R. & Torchilin, V. Intracellular transduction using cell-penetrating peptides. *Mol Biosyst* **6**, 628-640.

12. Schwarze, S.R., Hruska, K.A. & Dowdy, S.F. Protein transduction: unrestricted delivery into all cells? *Trends in Cell Biology* **10**, 290-295 (2000).

13. Patel, L.N., Zaro, J.L. & Shen, W.C. Cell penetrating peptides: Intracellular pathways and pharmaceutical perspectives. *Pharmaceutical Research* **24**, 1977-1992 (2007).

14. Green, I., Christison, R., Voyce, C.J., Bundell, K.R. & Lindsay, M.A. Protein transduction domains: are they delivering? *Trends in Pharmacological Sciences* **24**, 213-215 (2003).

15. Murriel, C. & Dowdy, S. Influence of protein transduction domains on intracellular delivery of macromolecules. *Expert Opinion on Drug Delivery* **3**, 739-746 (2006).

16. Shi, J.J., Votruba, A.R., Farokhzad, O.C. & Langer, R. Nanotechnology in Drug Delivery and Tissue Engineering: From Discovery to Applications. *Nano Lett* **10**, 3223-3230 (2010).

17. Doeppner, T.R. et al. TAT-Hsp70-mediated neuroprotection and increased survival of neuronal precursor cells after focal cerebral ischemia in mice. *J Cereb Blood Flow Metab* **29**, 1187-1196 (2009).

18. Kameyama, S. et al. Effects of cell-permeating peptide binding on the distribution of I-125-labeled Fab fragment in rats. *Bioconjugate Chem* **17**, 597-602 (2006).

19. Shuai, K., Liu, B., Gross, M. & ten Hoeve, J. A transcriptional corepressor of Stat1 with an essential LXXLL signature motif. *P Natl Acad Sci USA* **98**, 3203-3207 (2001).

20. Zhang, Y.E. et al. In Vivo protein transduction: Delivery of PEP-1-SOD1 fusion protein into myocardium efficiently protects against ischemic insult. *Mol Cells* **27**, 159-166 (2009).

21. Mitsui, H., Inozume, T., Kitamura, R., Shibagaki, N. & Shimada, S. Polyarginine-mediated protein delivery to dendritic cells presents antigen more efficiently onto MHC class I and class II and elicits superior antitumor immunity. *J Invest Dermatol* **126**, 1804-1812 (2006).

22. Padari, K. et al. Cell transduction pathways of transportans. *Bioconjugate Chem* **16**, 1399-1410 (2005).

23. Gu, Z., Biswas, A., Zhao, M.X. & Tang, Y. Tailoring nanocarriers for intracellular protein delivery. *chem Soc Rev* **40**, 3638-3655 (2011).

24. Faraji, A.H. & Wipf, P. Nanoparticles in cellular drug delivery. *Bioorg Med Chem* **17**, 2950-2962 (2009).

25. Gao, J.H. & Xu, B. Applications of nanomaterials inside cells. *Nano Today* **4**, 37-51 (2009).

26. Lee, K.Y. & Yuk, S.H. Polymeric protein delivery systems. *Progress in Polymer Science* **32**, 669-697 (2007).

27. Chou, L.Y., Ming, K. & Chan, W.C. Strategies for the intracellular delivery of nanoparticles. *chem Soc Rev* (2010).

28. Gaberc-Porekar, V., Zore, I., Podobnik, B. & Menart, V. *Curr Opin Drug Disc* **11**, 242-250 (2008).

29. Stuart, M.A. et al. Emerging applications of stimuli-responsive polymer materials. *Nat Mater* **9**, 101-113 (2010).

30. Solaro, R. Targeted Delivery of Proteins by Nanosized Carriers. *J Polym Sci: Part A: Polym Chem* **46**, 1-11 (2008).

31. Roberts, M.J., Bentley, M.D. & Harris, J.M. Chemistry for peptide and protein PEGylation. *Adv Drug Deliv Rev* **54**, 459-476 (2002).

32. Francesco M. Veronese, A.M.a.G.P. in PEGylated Protein Drugs: Basic Science and Clinical Applications, Vol. 1. (ed. F.M. Veronese) (Birkhäuser Basel, 2009).

33. Futami, J. et al. Intracellular delivery of proteins into mammalian living cells by polyethylenimine-cationization. *Journal of Bioscience and Bioengineering* **99**, 95-103 (2005).

34. Murata, H. et al. Intracellular delivery of glutathione S-transferase-fused proteins into mammalian cells by polyethylenimine-glutathione conjugates. *Journal of Biochemistry* **144**, 447-455 (2008).

35.   Futami, J. & Yamada, H. Design of cytotoxic ribonucleases by cationization to enhance intracellular protein delivery. *Current Pharmaceutical Biotechnology* **9**, 180-184 (2008).

36.   Murata, H. et al. Denatured and reversibly cationized p53 readily enters cells and simultaneously folds to the functional protein in the cells. *Biochemistry* **45**, 6124-6132 (2006).

37.   Kitazoe, M. et al. Protein transduction assisted by polyethylenimine-cationized carrier proteins. *Journal of Biochemistry* **137**, 693-701 (2005).

38.   Murata, H. et al. Transient cell proliferation with polyethylenimine-cationized N-terminal domain of simian virus 40 large T-antigen. *Journal of Bioscience and Bioengineering* **105**, 34-38 (2008).

39.   Lackey, C.A., Press, O.W., Hoffman, A.S. & Stayton, P.S. A biomimetic pH-responsive polymer directs endosomal release and intracellular delivery of an endocytosed antibody complex. *Bioconjugate Chem* **13**, 996-1001 (2002).

40.   Foster, S., Duvall, C.L., Crownover, E.F., Hoffman, A.S. & Stayton, P.S. Intracellular Delivery of a Protein Antigen with an Endosomal-Releasing Polymer Enhances CD8 T-Cell Production and Prophylactic Vaccine Efficacy. *Bioconjugate Chem* **21**, 2205-2212 (2010).

41.   Jung, S., Huh, S., Cheon, Y.P. & Park, S. Intracellular protein delivery by glucose-coated polymeric beads. *Chem Commun (Camb)*, 5003-5005 (2009).

42.   Maier, K., Martin, I. & Wagner, E. Sequence Defined Disulfide-Linked Shuttle for Strongly Enhanced Intracellular Protein Delivery. *Mol Pharmaceut* **9**, 3560-3568 (2012).

43.   Maier, K. & Wagner, E. Acid-Labile Traceless Click Linker for Protein Transduction. *J Am Chem Soc* **134**, 10169-10173 (2012).

44.   Schaffert, D. et al. Solid-Phase Synthesis of Sequence-Defined T-, i-, and U-Shape Polymers for pDNA and siRNA Delivery. *Angew Chem Int Edit* **50**, 8986-8989 (2011).

45.   Tong, J. et al. Conjugates of Superoxide Dismutase 1 with Amphiphilic Poly(2-oxazoline) Block Copolymers for Enhanced Brain Delivery: Synthesis, Characterization and Evaluation in Vitro and in Vivo. *Mol Pharmaceut* **10**, 360-377 (2013).

46.   Didenko, V.V., Ngo, H. & Baskin, D.S. Polyethyleneimine as a transmembrane carrier of fluorescently labeled proteins and antibodies. *Anal Biochem* **344**, 168-173 (2005).

47.   Hu, Y. et al. Cytosolic delivery of membrane-impermeable molecules in dendritic cells using pH-responsive core-shell nanoparticles. *Nano Lett* **7**, 3056-3064 (2007).

48.   Ayame, H., Morimoto, N. & Akiyoshi, K. Self-assembled cationic nanogels for intracellular protein delivery. *Bioconjugate Chem* **19**, 882-890 (2008).

49.   Nochi, T. et al. Nanogel antigenic protein-delivery system for adjuvant-free intranasal vaccines. *Nat Mater* **9**, 572-578.

50.   Morimoto, N. et al. Self-Assembled pH-Sensitive Cholesteryl Pullulan Nanogel As a Protein Delivery Vehicle. *Biomacromolecules* **14**, 56-63 (2013).

51.   Rosenbaugh, E.G. et al. The attenuation of central angiotensin II-dependent pressor response and intra-neuronal signaling by intracarotid injection of nanoformulated copper/zinc superoxide dismutase. *Biomaterials* **31**, 5218-5226 (2010).

52.   Murthy, N. et al. A macromolecular delivery vehicle for protein-based vaccines: Acid-degradable protein-loaded microgels. *Proc Natl Acad Sci U S A* **100**, 4995-5000 (2003).

53.   Bachelder, E.M. et al. Acid-degradable polyurethane particles for protein-based vaccines: biological evaluation and in vitro analysis of particle degradation products. *Molecular pharmaceutics* **5**, 876-884 (2008).

54.   Bachelder, E.M., Beaudette, T.T., Broaders, K.E., Dashe, J. & Frechet, J.M. Acetal-derivatized dextran: an acid-responsive biodegradable material for therapeutic applications. *J Am Chem Soc* **130**, 10494-10495 (2008).

55.   Jewell, C.M., Lopez, S.C.B. & Irvine, D.J. In situ engineering of the lymph node microenvironment via intranodal injection of adjuvant-releasing polymer particles. *P Natl Acad Sci USA* **108**, 15745-15750 (2011).

56.   Yan, M. et al. A novel intracellular protein delivery platform based on single-protein nanocapsules. *Nat Nanotechnol* **5**, 48-53 (2010).

57.   Gu, Z. et al. Protein nanocapsule weaved with enzymatically degradable polymeric network. *Nano Lett* **9**, 4533-4538 (2009).

58.   Biswas, A. et al. Endoprotease-Mediated Intracellular Protein Delivery Using Nanocapsules. *Acs Nano* **5**, 1385-1394 (2011).

59.   Lee, Y. et al. Charge-conversional polyionic complex micelles-efficient nanocarriers for protein delivery into cytoplasm. *Angew Chem Int Ed Engl* **48**, 5309-5312 (2009).

60.   Lee, Y. et al. Efficient Delivery of Bioactive Antibodies into the Cytoplasm of Living Cells by Charge-Conversional Polyion Complex Micells. *Angew Chem Int Ed* **49**, 1-5 (2010).

61.   Akagi, T., Wang, X., Uto, T., Baba, M. & Akashi, M. Protein direct delivery to dendritic cells using nanoparticles based on amphiphilic poly(amino acid) derivatives. *Biomaterials* **28**, 3427-3436 (2007).

62.   Chong, S.F. et al. A paradigm for peptide vaccine delivery using viral epitopes encapsulated in degradable polymer hydrogel capsules. *Biomaterials* **30**, 5178-5186 (2009).

63.   De Rose, R. et al. Binding, Internalization, and Antigen Presentation of Vaccine-Loaded Nanoengineered Capsules in Blood. *Adv Mater* **20**, 4698-+ (2008).

64.   Lee, A.L. et al. Efficient intracellular delivery of functional proteins using cationic polymer core/shell nanoparticles. *Biomaterials* **29**, 1224-1232 (2008).

65.   Hasadsri, L., Kreuter, J., Hattori, H., Iwasaki, T. & George, J.M. Functional Protein Delivery into Neurons Using Polymeric Nanoparticles. *J Biol Chem* **284**, 6972-6981 (2009).

66.   Cohen, J.A. et al. T-cell activation by antigen-loaded pH-sensitive hydrogel particles in vivo: the effect of particle size. *Bioconjug Chem* **20**, 111-119 (2009).

67.   Beaudette, T.T. et al. Chemoselective Ligation in the Functionalization of Polysaccharide-Based Particles. *J Am Chem Soc* **131**, 10360-10361 (2009).

68.   Standley, S.M. et al. Incorporation of CpG oligonucleotide ligand into protein-loaded particle vaccines promotes antigen-specific CD8 T-cell immunity. *Bioconjug Chem* **18**, 77-83 (2007).

69.   Cohen, J.L. et al. Enhanced cell penetration of acid-degradable particles functionalized with cell-penetrating peptides. *Bioconjugate chemistry* **19**, 876-881 (2008).

70.   Bershteyn, A. et al. Polymer-supported lipid shells, onions, and flowers. *Soft Matter* **4**, 1787-1791 (2008).

71.   Diwan, M. & Park, T.G. Pegylation enhances protein stability during encapsulation in PLGA microspheres. *J Control Release* **73**, 233-244 (2001).

72.   Utama, R.H., Guo, Y., Zetterlund, P.B. & Stenzel, M.H. Synthesis of hollow polymeric nanoparticles for protein delivery via inverse miniemulsion periphery RAFT polymerization. *Chem Commun* **48**, 11103-11105 (2012).

73.   Du, J. et al. Quantum-dot-decorated robust transductable bioluminescent nanocapsules. *J Am Chem Soc* **132**, 12780-12781 (2010).

74.   Gu, Z. et al. Probing protease activity by single-fluorescent-protein nanocapsules. *Chem Commun (Camb)* **46**, 6467-6469.

75.   Zhao, M.X. et al. Redox-responsive nanocapsules for intracellular protein delivery. *Biomaterials* **32**, 5223-5230 (2011).

76.   Heffernan, M.J. & Murthy, N. Disulfide-Crosslinked Polyion Micelles for Delivery of Protein Therapeutics. *Ann Biomed Eng* **37**, 1993-2002 (2009).

77. Hwa Kim, S., Hoon Jeong, J., Joe, C.O. & Gwan Park, T. Folate receptor mediated intracellular protein delivery using PLL-PEG-FOL conjugate. *J Control Release* **103**, 625-634 (2005).

78. Rivera-Gil, P., De Koker, S., De Geest, B.G. & Parak, W.J. Intracellular Processing of Proteins Mediated by Biodegradable Polyelectrolyte Capsules. *Nano Letters* **9**, 4398-4402 (2009).

79. She, S.J., Zhang, X.G., Wu, Z.M., Wang, Z. & Li, C.X. Gradient cross-linked biodegradable polyelectrolyte nanocapsules for intracellular protein drug delivery. *Biomaterials* **31**, 6039-6049 (2010).

80. Latchman, D.S. Transcription factors: An overview. *Int J Biochem Cell B* **29**, 1305-1312 (1997).

81. Farnham, P.J. Insights from genomic profiling of transcription factors. *Nat Rev Genet* **10**, 605-616 (2009).

82. Lobe, C.G. Transcription Factors and Mammalian Development. *Curr Top Dev Biol* **27**, 351-383 (1992).

83. Vaquerizas, J.M., Kummerfeld, S.K., Teichmann, S.A. & Luscombe, N.M. A census of human transcription factors: function, expression and evolution. *Nat Rev Genet* **10**, 252-263 (2009).

84. Blelloch, R. Regenerative medicine - Short cut to cell replacement. *Nature* **455**, 604-605 (2008).

85. Jopling, C., Boue, S. & Belmonte, J.C.I. Dedifferentiation, transdifferentiation and reprogramming: three routes to regeneration. *Nat Rev Mol Cell Bio* **12**, 79-89 (2011).

86. Thomson, J.A. Embryonic stem cell lines derived from human blastocysts (vol 282, pg 1147, 1998). *Science* **282**, 1827-1827 (1998).

87.   Ying, Q.L., Nichols, J., Chambers, I. & Smith, A. BMP induction of Id proteins suppresses differentiation and sustains embryonic stem cell self-renewal in collaboration with STAT3. *Cell* **115**, 281-292 (2003).

88.   Mountford, J.C. Human embryonic stem cells: origins, characteristics and potential for regenerative therapy. *Transfusion Med* **18**, 1-12 (2008).

89.   Zeng, X.M. et al. Dopaminergic differentiation of human embryonic stem cells. *Stem Cells* **22**, 925-940 (2004).

90.   D'Amour, K.A. et al. Production of pancreatic hormone-expressing endocrine cells from human embryonic stem cells. *Nat Biotechnol* **24**, 1392-1401 (2006).

91.   Zheng, J.K. et al. Skeletal myogenesis by human embryonic stem cells. *Cell Res* **16**, 713-722 (2006).

92.   Olivier, E.N., Qiu, C.H., Velho, M., Hirsch, R.E. & Bouhassira, E.E. Large-scale production of embryonic red blood cells from human embryonic stem cells. *Exp Hematol* **34**, 1635-1642 (2006).

93.   Nisbet, M.C., Brossard, D. & Kroepsch, A. Framing science - The stem cell controversy in an age of press/politics. *Harv Int J Press-Pol* **8**, 36-70 (2003).

94.   Power, C. & Rasko, J.E.J. Will Cell Reprogramming Resolve the Embryonic Stem Cell Controversy? A Narrative Review. *Ann Intern Med* **155**, 114-121 (2011).

95.   Takahashi, K. & Yamanaka, S. Induction of pluripotent stem cells from mouse embryonic and adult fibroblast cultures by defined factors. *Cell* **126**, 663-676 (2006).

96.   Madonna, R. Human-Induced Pluripotent Stem Cells: In Quest of Clinical Applications. *Mol Biotechnol* **52**, 193-203 (2012).

97.   Okita, K., Ichisaka, T. & Yamanaka, S. Generation of germline-competent induced pluripotent stem cells. *Nature* **448**, 313-U311 (2007).

98.   Wernig, M. et al. In vitro reprogramming of fibroblasts into a pluripotent ES-cell-like state. *Nature* **448**, 318-U312 (2007).

99. Maherali, N. et al. Directly reprogrammed fibroblasts show global epigenetic remodeling and widespread tissue contribution. *Cell Stem Cell* **1**, 55-70 (2007).

100. Takahashi, K. et al. Induction of pluripotent stem cells from adult human fibroblasts by defined factors. *Cell* **131**, 861-872 (2007).

101. Park, I.H. et al. Reprogramming of human somatic cells to pluripotency with defined factors. *Nature* **451**, 141-U141 (2008).

102. Yu, J.Y. et al. Induced pluripotent stem cell lines derived from human somatic cells. *Science* **318**, 1917-1920 (2007).

103. Kim, J.B. et al. Pluripotent stem cells induced from adult neural stem cells by reprogramming with two factors. *Nature* **454**, 646-U654 (2008).

104. Silva, J. et al. Promotion of Reprogramming to Ground State Pluripotency by Signal Inhibition. *Plos Biol* **6**, 2237-2247 (2008).

105. Aoi, T. et al. Generation of pluripotent stem cells from adult mouse liver and stomach cells. *Science* **321**, 699-702 (2008).

106. Stadtfeld, M., Brennand, K. & Hochedlinger, K. Reprogramming of pancreatic beta cells into induced pluripotent stem cells. *Curr Biol* **18**, 890-894 (2008).

107. Hanna, J. et al. Direct reprogramming of terminally differentiated mature B lymphocytes to pluripotency (vol 133, pg 250, 2008). *Cell* **134**, 365-365 (2008).

108. Yamanaka, S. A Fresh Look at iPS Cells. *Cell* **137**, 13-17 (2009).

109. Hanna, J. et al. Treatment of sickle cell anemia mouse model with iPS cells generated from autologous skin. *Science* **318**, 1920-1923 (2007).

110. Wernig, M. et al. Neurons derived from reprogrammed fibroblasts functionally integrate into the fetal brain and improve symptoms of rats with Parkinson's disease. *P Natl Acad Sci USA* **105**, 5856-5861 (2008).

111. Xu, D. et al. Phenotypic correction of murine hemophilia A using an iPS cell-based therapy. *P Natl Acad Sci USA* **106**, 808-813 (2009).

112. Dimos, J.T. et al. Induced pluripotent stem cells generated from patients with ALS can be differentiated into motor neurons. *Science* **321**, 1218-1221 (2008).

113. Park, I.H. et al. Disease-specific induced pluripotent stem cells. *Cell* **134**, 877-886 (2008).

114. Ebert, A.D. et al. Induced pluripotent stem cells from a spinal muscular atrophy patient. *Nature* **457**, 277-U271 (2009).

115. Spence, J.R. et al. Directed differentiation of human pluripotent stem cells into intestinal tissue in vitro. *Nature* **470**, 105-U120 (2011).

116. Zhao, X.Y. et al. iPS cells produce viable mice through tetraploid complementation. *Nature* **461**, 86-U88 (2009).

117. Narsinh, K.H. et al. Single cell transcriptional profiling reveals heterogeneity of human induced pluripotent stem cells. *Journal of Clinical Investigation* **121**, 1217-1221 (2011).

118. Stadtfeld, M. et al. Aberrant silencing of imprinted genes on chromosome 12qF1 in mouse induced pluripotent stem cells. *Nature* **465**, 175-U155 (2010).

119. Hu, B.Y. et al. Neural differentiation of human induced pluripotent stem cells follows developmental principles but with variable potency. *P Natl Acad Sci USA* **107**, 4335-4340 (2010).

120. Feng, Q. et al. Hemangioblastic Derivatives from Human Induced Pluripotent Stem Cells Exhibit Limited Expansion and Early Senescence. *Stem Cells* **28**, 704-712 (2010).

121. Urbach, A., Bar-Nur, O., Daley, G.Q. & Benvenisty, N. Differential Modeling of Fragile X Syndrome by Human Embryonic Stem Cells and Induced Pluripotent Stem Cells. *Cell Stem Cell* **6**, 407-411 (2010).

122. Lister, R. et al. Hotspots of aberrant epigenomic reprogramming in human induced pluripotent stem cells. *Nature* **471**, 68-U84 (2011).

123. Kim, K. et al. Epigenetic memory in induced pluripotent stem cells. *Nature* **467**, 285-U260 (2010).

124. Parkinson, D.B. et al. c-Jun is a negative regulator of myelination. *J Cell Biol* **181**, 625-637 (2008).

125. Crocker, S.J. et al. c-Jun mediates axotomy-induced dopamine neuron death in vivo. *Proc Natl Acad Sci U S A* **98**, 13385-13390 (2001).

126. Lattanzi, L. et al. High efficiency myogenic conversion of human fibroblasts by adenoviral vector-mediated MyoD gene transfer - An alternative strategy for ex vivo gene therapy of primary myopathies. *Journal of Clinical Investigation* **101**, 2119-2128 (1998).

127. Davis, R.L., Weintraub, H. & Lassar, A.B. Expression of a Single Transfected Cdna Converts Fibroblasts to Myoblasts. *Cell* **51**, 987-1000 (1987).

128. Weintraub, H. et al. Activation of Muscle-Specific Genes in Pigment, Nerve, Fat, Liver, and Fibroblast Cell-Lines by Forced Expression of Myod. *P Natl Acad Sci USA* **86**, 5434-5438 (1989).

129. Choi, J. et al. Myod Converts Primary Dermal Fibroblasts, Chondroblasts, Smooth-Muscle, and Retinal Pigmented Epithelial-Cells into Striated Mononucleated Myoblasts and Multinucleated Myotubes. *P Natl Acad Sci USA* **87**, 7988-7992 (1990).

130. Kulessa, H., Frampton, J. & Graf, T. Gata-1 Reprograms Avian Myelomonocytic Cell-Lines into Eosinophils, Thromboblasts, and Erythroblasts. *Gene Dev* **9**, 1250-1262 (1995).

131. Szabo, E. et al. Direct conversion of human fibroblasts to multilineage blood progenitors. *Nature* **468**, 521-U191 (2010).

132. Feng, R. et al. PU.1 and C/EBPalpha/beta convert fibroblasts into macrophage-like cells. *Proc Natl Acad Sci U S A* **105**, 6057-6062 (2008).

133. Vierbuchen, T. et al. Direct conversion of fibroblasts to functional neurons by defined factors. *Nature* **463**, 1035-U1050 (2010).

134. Ieda, M. et al. Direct Reprogramming of Fibroblasts into Functional Cardiomyocytes by Defined Factors. *Cell* **142**, 375-386 (2010).

135. Kajimura, S. et al. Initiation of myoblast to brown fat switch by a PRDM16-C/EBP-beta transcriptional complex. *Nature* **460**, 1154-1158 (2009).

136. Huang, P. et al. Induction of functional hepatocyte-like cells from mouse fibroblasts by defined factors. *Nature* **475**, 386-389 (2011).

137. Xie, H.F., Ye, M., Feng, R. & Graf, T. Stepwise reprogramming of B cells into macrophages. *Cell* **117**, 663-676 (2004).

138. Cobaleda, C., Jochum, W. & Busslinger, M. Conversion of mature B cells into T cells by dedifferentiation to uncommitted progenitors. *Nature* **449**, 473-U478 (2007).

139. Laiosa, C.V., Stadtfeld, M., Xie, H.F., de Andres-Aguayo, L. & Graf, T. Reprogramming of committed T cell progenitors to macrophages and dendritic cells by C/EBP alpha and PU.1 transcription factors. *Immunity* **25**, 731-744 (2006).

140. Hori, S., Nomura, T. & Sakaguchi, S. Control of regulatory T cell development by the transcription factor Foxp3. *Science* **299**, 1057-1061 (2003).

141. Ferber, S. & Meivar-Levy, I. New organs from our own tissues: liver-to-pancreas transdifferentiation. *Trends in Endocrinology and Metabolism* **14**, 460-466 (2003).

142. Zhou, Q., Brown, J., Kanarek, A., Rajagopal, J. & Melton, D.A. In vivo reprogramming of adult pancreatic exocrine cells to beta-cells. *Nature* **455**, 627-U630 (2008).

143. Shen, C.N., Slack, J.M. & Tosh, D. Molecular basis of transdifferentiation of pancreas to liver. *Nat Cell Biol* **2**, 879-887 (2000).

144. Rapino, F. et al. C/EBPalpha Induces Highly Efficient Macrophage Transdifferentiation of B Lymphoma and Leukemia Cell Lines and Impairs Their Tumorigenicity. *Cell Rep* **3**, 1153-1163 (2013).

145. Iwasaki, H. et al. The order of expression of transcription factors directs hierarchical specification of hematopoietic lineages. *Gene Dev* **20**, 3010-3021 (2006).

146. Ferber, S. et al. Functional, persistent, and extended liver to pancreas transdifferentiation. *J Biol Chem* **278**, 31950-31957 (2003).

147. Bian, J. et al. Effect of cell-based intercellular delivery of transcription factor GATA4 on ischemic cardiomyopathy. *Circ Res* **100**, 1626-1633 (2007).

148. Zaret, K.S. & Grompe, M. Generation and Regeneration of Cells of the Liver and Pancreas. *Science* **322**, 1490-1494 (2008).

149. Hacein-Bey-Abina, S. et al. LMO2-associated clonal T cell proliferation in two patients after gene therapy for SCID-X1. *Science* **302**, 415-419 (2003).

150. Kane, N.M. et al. Lentivirus-mediated Reprogramming of Somatic Cells in the Absence of Transgenic Transcription Factors. *Mol Ther* **18**, 2139-2145 (2010).

151. Stadtfeld, M., Nagaya, M., Utikal, J., Weir, G. & Hochedlinger, K. Induced Pluripotent Stem Cells Generated Without Viral Integration. *Science* **322**, 945-949 (2008).

152. Okita, K., Nakagawa, M., Hong, H.J., Ichisaka, T. & Yamanaka, S. Generation of Mouse Induced Pluripotent Stem Cells Without Viral Vectors. *Science* **322**, 949-953 (2008).

153. Kaji, K. et al. Virus-free induction of pluripotency and subsequent excision of reprogramming factors. *Nature* **458**, 771-U112 (2009).

154. Woltjen, K. et al. piggyBac transposition reprograms fibroblasts to induced pluripotent stem cells. *Nature* **458**, 766-U106 (2009).

155. Huangfu, D.W. et al. Induction of pluripotent stem cells by defined factors is greatly improved by small-molecule compounds. *Nat Biotechnol* **26**, 795-797 (2008).

156. Shi, Y. et al. A combined chemical and genetic approach for the generation of induced pluripotent stem cells (vol 2, pg 525, 2008). *Cell Stem Cell* **3**, 119-119 (2008).

157. Warren, L. et al. Highly Efficient Reprogramming to Pluripotency and Directed Differentiation of Human Cells with Synthetic Modified mRNA. *Cell Stem Cell* **7**, 618-630 (2010).

158. Zhou, H.Y. et al. Generation of Induced Pluripotent Stem Cells Using Recombinant Proteins (vol 4, pg 381, 2009). *Cell Stem Cell* **4**, 581-581 (2009).

159. Kim, D. et al. Generation of Human Induced Pluripotent Stem Cells by Direct Delivery of Reprogramming Proteins. *Cell Stem Cell* **4**, 472-476 (2009).

160. Gu, Z. et al. Protein Nanocapsule Weaved with Enzymatically Degradable Polymeric Network. *Nano Lett* **9**, 4533-4538 (2009).

161. Seidah, N.G., Day, R., Marcinkiewicz, M. & Chretien, M. Precursor convertases: An evolutionary ancient, cell-specific, combinatorial mechanism yielding diverse bioactive peptides and proteins. *Trends in Comparative Endocrinology and Neurobiology* **839**, 9-24 (1998).

162. Krysan, D.J., Rockwell, N.C. & Fuller, R.S. Quantitative characterization of furin specificity - Energetics of substrate discrimination using an internally consistent set of hexapeptidyl methylcoumarinamides. *J Biol Chem* **274**, 23229-23234 (1999).

163. Thomas, G. Furin at the cutting edge: From protein traffic to embryogenesis and disease. *Nat Rev Mol Cell Bio* **3**, 753-766 (2002).

164. Anderson, E.D. et al. The ordered and compartment-specific autoproteolytic removal of the furin intramolecular chaperone is required for enzyme activation. *J Biol Chem* **277**, 12879-12890 (2002).

165. Roebroek, A.J.M. et al. Failure of ventral closure and axial rotation in embryos lacking the proprotein convertase Furin. *Development* **125**, 4863-4876 (1998).

166. Henrich, S. et al. The crystal structure of the proprotein processing proteinase furin explains its stringent specificity (vol 10, pg 520, 2003). *Nature Structural Biology* **10**, 669-669 (2003).

167. Lee, R., Kermani, P., Teng, K.K. & Hempstead, B.L. Regulation of cell survival by secreted proneurotrophins. *Science* **294**, 1945-1948 (2001).

168.   Kim, S.H. et al. Furin mediates enhanced production of fibrillogenic ABri peptides in familial British dementia. *Nature Neuroscience* **2**, 984-988 (1999).

169.   Kim, S.H., Creemers, J.W.M., Chu, S., Thinakaran, G. & Sisodia, S.S. Proteolytic processing of familial British dementia-associated BRI variants - Evidence for enhanced intracellular accumulation of amyloidogenic peptides. *J Biol Chem* **277**, 1872-1877 (2002).

170.   Chen, Y.W. et al. Mutations within a furin consensus sequence block proteolytic release of ectodysplasin-A and cause X-linked hypohidrotic ectodermal dysplasia. *P Natl Acad Sci USA* **98**, 7218-7223 (2001).

171.   Kang, T.B., Nagase, H. & Pei, D.Q. Activation of membrane-type matrix metalloproteinase 3 zymogen by the proprotein convertase furin in the trans-Golgi network. *Cancer Res* **62**, 675-681 (2002).

172.   Gordon, V.M., Klimpel, K.R., Arora, N., Henderson, M.A. & Leppla, S.H. Proteolytic Activation of Bacterial Toxins by Eukaryotic Cells Is Performed by Furin and by Additional Cellular Proteases. *Infection and Immunity* **63**, 82-87 (1995).

173.   Lea, N., Lord, J.M. & Roberts, L.M. Proteolytic cleavage of the A subunit is essential for maximal cytotoxicity of Escherichia coli O157 : H7 Shiga-like toxin-1. *Microbiology-Uk* **145**, 999-1004 (1999).

174.   Jean, F. et al. alpha(1)-antitrypsin Portland, a bioengineered serpin highly selective for furin: Application as an antipathogenic agent. *P Natl Acad Sci USA* **95**, 7293-7298 (1998).

175.   Moulard, M. & Decroly, E. Maturation of HIV envelope glycoprotein precursors by cellular endoproteases. *Biochimica Et Biophysica Acta-Reviews on Biomembranes* **1469**, 121-132 (2000).

176. Richards, R.M., Lowy, D.R., Schiller, J.T. & Day, P.M. Cleavage of the papillomavirus minor capsid protein, L2, at a furin consensus site is necessary for infection. *P Natl Acad Sci USA* **103**, 1522-1527 (2006).

177. Youker, R.T., Shinde, U., Day, R. & Thomas, G. At the crossroads of homoeostasis and disease: roles of the PACS proteins in membrane traffic and apoptosis. *Biochem J* **421**, 1-15 (2009).

178. Plunkett, K.N., Berkowski, K.L. & Moore, J.S. Chymotrypsin responsive hydrogel: Application of a disulfide exchange protocol for the preparation of methacrylamide containing peptides. *Biomacromolecules* **6**, 632-637 (2005).

179. OBrienSimpson, N.M., Ede, N.J., Brown, L.E., Swan, J. & Jackson, D.C. Polymerization of unprotected synthetic peptides: A view toward synthetic peptide vaccines. *J Am Chem Soc* **119**, 1183-1188 (1997).

180. Gu, Z. et al. Probing protease activity by single-fluorescent-protein nanocapsules. *Chem Commun* **46**, 6467-6469 (2010).

181. Mansouri, S. et al. Characterization of folate-chitosan-DNA nanoparticles for gene therapy. *Biomaterials* **27**, 2060-2065 (2006).

182. Jin, R.C., Wu, G.S., Li, Z., Mirkin, C.A. & Schatz, G.C. What controls the melting properties of DNA-linked gold nanoparticle assemblies? *J Am Chem Soc* **125**, 1643-1654 (2003).

183. Mei, B.C., Susumu, K., Medintz, I.L. & Mattoussi, H. Polyethylene glycol-based bidentate ligands to enhance quantum dot and gold nanoparticle stability in biological media. *Nat Protoc* **4**, 412-423 (2009).

184. Hodel, M.R., Corbett, A.H. & Hodel, A.E. Dissection of a nuclear localization signal. *J Biol Chem* **276**, 1317-1325 (2001).

185. Page, R.E. et al. Increased expression of the pro-protein convertase furin predicts decreased survival in ovarian cancer. *Cellular Oncology* **29**, 289-299 (2007).

186. Torchilin, V.P. Recent approaches to intracellular delivery of drugs and DNA and organelle targeting. *Annual Review of Biomedical Engineering* **8**, 343-375 (2006).

187. Hoffman, A.S. et al. Design of "smart" polymers that can direct intracellular drug delivery. *Polymers for Advanced Technologies* **13**, 992-999 (2002).

188. Toda, A., Okabe, M., Yoshida, T. & Nikaido, T. The potential of amniotic membrane/amnion-derived cells for regeneration of various tissues. *Journal of Pharmacological Sciences* **105**, 215-228 (2007).

189. Li, C.L. et al. Pluripotency can be rapidly and efficiently induced in human amniotic fluid-derived cells. *Human Molecular Genetics* **18**, 4340-4349 (2009).

190. Cotter, T.G. Apoptosis and cancer: the genesis of a research field. *Nat Rev Cancer* **9**, 501-507 (2009).

191. Riedl, S.J. et al. Structural basis for the inhibition of caspase-3 by XIAP. *Cell* **104**, 791-800 (2001).

192. Gavrieli, Y., Sherman, Y. & Bensasson, S.A. Identification of Programmed Cell-Death Insitu Via Specific Labeling of Nuclear-DNA Fragmentation. *J Cell Biol* **119**, 493-501 (1992).

193. Bale, S.S. et al. Nanoparticle-Mediated Cytoplasmic Delivery of Proteins To Target Cellular Machinery. *Acs Nano* **4**, 1493-1500 (2010).

194. Cheng, M. et al. Pro-protein convertase gene expression in human breast cancer. *International Journal of Cancer* **71**, 966-971 (1997).

195. Bassi, D.E. et al. Elevated furin expression in aggressive human head and neck tumors and tumors cell lines. *Molecular Carcinogenesis* **31**, 224-232 (2001).

196. Mercapide, J. et al. Inhibition of furin-mediated processing results in suppression of astrocytoma cell growth and invasiveness. *Clin Cancer Res* **8**, 1740-1746 (2002).

197. Schalken, J.A. et al. Fur Gene-Expression as a Discriminating Marker for Small-Cell and Nonsmall Cell Lung Carcinomas. *Journal of Clinical Investigation* **80**, 1545-1549 (1987).

198. Aguilera, T.A., Olson, E.S., Timmers, M.M., Jiang, T. & Tsien, R.Y. Systemic in vivo distribution of activatable cell penetrating peptides is superior to that of cell penetrating peptides. *Integrative Biology* **1**, 371-381 (2009).

199. Rowland, B.D. & Peeper, D.S. KLF4, p21 and context-dependent opposing forces in cancer. *Nat Rev Cancer* **6**, 11-23 (2006).

200. Wei, D.Y., Kanai, M., Huang, S.Y. & Xie, K.P. Emerging role of KLF4 in human gastrointestinal cancer. *Carcinogenesis* **27**, 23-31 (2006).

201. Matsui, H., Tomizawa, K., Lu, Y.F. & Matsushita, M. Protein therapy: In vivo protein transduction by polyarginine (11R) PTD and subcellular targeting delivery. *Current Protein & Peptide Science* **4**, 151-157 (2003).

202. Joliot, A. & Prochiantz, A. Transduction peptides: from technology to physiology. *Nat Cell Biol* **6**, 189-196 (2004).

203. Ormo, M. et al. Crystal structure of the Aequorea victoria green fluorescent protein. *Science* **273**, 1392-1395 (1996).

204. Katz, J.P. et al. The zinc-finger transcription factor Klf4 is required for terminal differentiation of goblet cells in the colon. *Development* **129**, 2619-2628 (2002).

205. Nicholson, D.W. Caspase structure, proteolytic substrates, and function during apoptotic cell death. *Cell Death and Differentiation* **6**, 1028-1042 (1999).

206. Murthy, N. et al. A macromolecular delivery vehicle for protein-based vaccines: Acid-degradable protein-loaded microgels. *P Natl Acad Sci USA* **100**, 4995-5000 (2003).

207. Corish, P. & Tyler-Smith, C. Attenuation of green fluorescent protein half-life in mammalian cells. *Protein Eng* **12**, 1035-1040 (1999).

208. Coyne, J.S. & Hilsenrath, P. The World Health report 2000. *Am J Public Health* **92**, 30-+ (2002).

209. Yan, W. & Huang, L. Recent advances in liposome-based nanoparticles for antigen delivery. *Polym Rev* **47**, 329-344 (2007).

210. O'Hagan, D.T. & Valiante, N.M. Recent advances in the discovery and delivery of vaccine adjuvants. *Nature Reviews Drug Discovery* **2**, 727-735 (2003).

211. Rosenberg, S.A., Yang, J.C. & Restifo, N.P. Cancer immunotherapy: moving beyond current vaccines. *Nat Med* **10**, 909-915 (2004).

212. Nguyen, D.N., Green, J.J., Chan, J.M., Longer, R. & Anderson, D.G. Polymeric Materials for Gene Delivery and DNA Vaccination. *Adv Mater* **21**, 847-867 (2009).

213. Steinman, R.M. Dendritic cells in vivo: A key target for a new vaccine science. *Immunity* **29**, 319-324 (2008).

214. Yang, L. & Baltimore, D. Long-term in vivo provision of antigen-specific T cell immunity by programming hematopoietic stem cells. *P Natl Acad Sci USA* **102**, 4518-4523 (2005).

215. Dai, B.B. et al. HIV-1 Gag-specific immunity induced by a lentivector-based vaccine directed to dendritic cells. *P Natl Acad Sci USA* **106**, 20382-20387 (2009).

216. Steinman, R.M. & Banchereau, J. Taking dendritic cells into medicine. *Nature* **449**, 419-426 (2007).

217. Zhao, M. et al. Redox-responsive nanocapsules for intracellular protein delivery. *Biomaterials* **32**, 5223-5230 (2011).

218. Thomas, G. Furin at the cutting edge: from protein traffic to embryogenesis and disease. *Nat Rev Mol Cell Biol* **3**, 753-766 (2002).

219. Meister, A. & Tate, S.S. Glutathione and Related Gamma-Glutamyl Compounds - Biosynthesis and Utilization. *Annual Review of Biochemistry* **45**, 559-604 (1976).

220. Knop, K., Hoogenboom, R., Fischer, D. & Schubert, U.S. Poly(ethylene glycol) in Drug Delivery: Pros and Cons as Well as Potential Alternatives. *Angew Chem Int Edit* **49**, 6288-6308 (2010).

221. Karakoti, A.S., Das, S., Thevuthasan, S. & Seal, S. PEGylated inorganic nanoparticles. *Angew Chem Int Ed Engl* **50**, 1980-1994 (2011).

222. Govender, T. et al. Defining the drug incorporation properties of PLA-PEG nanoparticles. *Int J Pharm* **199**, 95-110 (2000).

223. Webster, R. et al. PEGylated proteins: evaluation of their safety in the absence of definitive metabolism studies. *Drug Metab Dispos* **35**, 9-16 (2007).

224. Gratton, S.E. et al. The effect of particle design on cellular internalization pathways. *Proc Natl Acad Sci U S A* **105**, 11613-11618 (2008).

225. Ledent, V. & Vervoort, M. The basic helix-loop-helix protein family: comparative genomics and phylogenetic analysis. *Genome Res* **11**, 754-770 (2001).

226. Weintraub, H. et al. The myoD gene family: nodal point during specification of the muscle cell lineage. *Science* **251**, 761-766 (1991).

227. Tapscott, S.J. The circuitry of a master switch: Myod and the regulation of skeletal muscle gene transcription. *Development* **132**, 2685-2695 (2005).

228. Starovasnik, M.A., Blackwell, T.K., Laue, T.M., Weintraub, H. & Klevit, R.E. Folding topology of the disulfide-bonded dimeric DNA-binding domain of the myogenic determination factor MyoD. *Biochemistry* **31**, 9891-9903 (1992).

229. Anthonycahill, S.J. et al. Molecular Characterization of Helix-Loop-Helix Peptides. *Science* **255**, 979-983 (1992).

230. Yaffe, D. & Saxel, O. Serial passaging and differentiation of myogenic cells isolated from dystrophic mouse muscle. *Nature* **270**, 725-727 (1977).

231. Noda, T., Fujino, T., Mie, M. & Kobatake, E. Transduction of MyoD protein into myoblasts induces myogenic differentiation without addition of protein transduction domain. *Biochem Biophys Res Commun* **382**, 473-477 (2009).

232. Lassar, A.B. et al. MyoD is a sequence-specific DNA binding protein requiring a region of myc homology to bind to the muscle creatine kinase enhancer. *Cell* **58**, 823-831 (1989).

233. Seward, D.J., Haney, J.C., Rudnicki, M.A. & Swoap, S.J. bHLH transcription factor MyoD affects myosin heavy chain expression pattern in a muscle-specific fashion. *Am J Physiol Cell Physiol* **280**, C408-413 (2001).

234. Muroya, S., Nakajima, I. & Chikuni, K. Related expression of MyoD and Myf5 with myosin heavy chain isoform types in bovine adult skeletal muscles. *Zoolog Sci* **19**, 755-761 (2002).

235. Charge, S.B. & Rudnicki, M.A. Cellular and molecular regulation of muscle regeneration. *Physiol Rev* **84**, 209-238 (2004).

236. Armand, A.S. et al. Cooperative synergy between NFAT and MyoD regulates myogenin expression and myogenesis. *J Biol Chem* **283**, 29004-29010 (2008).

237. Hamamori, Y., Wu, H.Y., Sartorelli, V. & Kedes, L. The basic domain of myogenic basic helix-loop-helix (bHLH) proteins is the novel target for direct inhibition by another bHLH protein, Twist. *Mol Cell Biol* **17**, 6563-6573 (1997).

238. Shklover, J. et al. MyoD uses overlapping but distinct elements to bind E-box and tetraplex structures of regulatory sequences of muscle-specific genes. *Nucleic Acids Res* **35**, 7087-7095 (2007).

239. Bengal, E. et al. Positive control mutations in the MyoD basic region fail to show cooperative DNA binding and transcriptional activation in vitro. *Proc Natl Acad Sci U S A* **91**, 6221-6225 (1994).

240. Ishibashi, J., Perry, R.L., Asakura, A. & Rudnicki, M.A. MyoD induces myogenic differentiation through cooperation of its NH2- and COOH-terminal regions. *J Cell Biol* **171**, 471-482 (2005).

241. Etzioni, S. et al. Homodimeric MyoD preferentially binds tetraplex structures of regulatory sequences of muscle-specific genes. *J Biol Chem* **280**, 26805-26812 (2005).

242. Lluis, F., Ballestar, E., Suelves, M., Esteller, M. & Munoz-Canoves, P. E47 phosphorylation by p38 MAPK promotes MyoD/E47 association and muscle-specific gene transcription. *EMBO J* **24**, 974-984 (2005).

243. Ebeling, W. et al. Proteinase K from Tritirachium album Limber. *Eur J Biochem* **47**, 91-97 (1974).

244. Wild, S.H., Roglic, G., Green, A., Sicree, R. & King, H. Global prevalence of diabetes: Estimates for the year 2000 and projections for 2030 - Response to Rathman and Giani. *Diabetes Care* **27**, 2569-2569 (2004).

245. Prevention, C.f.D.C.a. National diabetes fact sheet: national estimates and general information on diabetes and prediabetes in the United States, 2011. *Atlanta, GA: U.S. Department of Health and Human Services, Centers for Disease Control and Prevention* (2011).

246. Alberti, K.G.M.M., Zimmet, P.Z. & Consultation, W. Definition, diagnosis and classification of diabetes mellitus and its complications part 1: Diagnosis and classification of diabetes mellitus - Provisional report of a WHO consultation. *Diabetic Medicine* **15**, 539-553 (1998).

247. Sarwar, N. et al. Diabetes mellitus, fasting blood glucose concentration, and risk of vascular disease: a collaborative meta-analysis of 102 prospective studies. *Lancet* **375**, 2215-2222 (2010).

248. Pambianco, G. et al. The 30-year natural history of type 1 diabetes complications - The Pittsburgh epidemiology of diabetes complications study experience. *Diabetes* **55**, 1463-1469 (2006).

249. Cooke, D.W. & Plotnick, L. Type 1 Diabetes Mellitus in Pediatrics. *Pediatrics in Review* **29**, 374-385 (2008).

250. Kitabchi, A.E., Umpierrez, G.E., Murphy, M.B. & Kreisberg, R.A. Hyperglycemic crises in adult patients with diabetes. *Diabetes Care* **29**, 2739-2748 (2006).

251. Gomez-Perez, F.J. & Rull, J.A. Insulin therapy: Current alternatives. *Archives of Medical Research* **36**, 258-272 (2005).

252. Weir, G.C. & BonnerWeir, S. Scientific and political impediments to successful islet transplantation. *Diabetes* **46**, 1247-1256 (1997).

253. Paty, B.W., Ryan, E.A., Shapiro, A.M.J., Lakey, J.R.T. & Robertson, R.P. Intrahepatic islet transplantation in type 1 diabetic patients does not restore hypoglycemic hormonal counterregulation or symptom recognition after insulin independence. *Diabetes* **51**, 3428-3434 (2002).

254. Zaret, K.S., Deutsch, G., Jung, J.N., Zheng, M.H. & Lora, J. A bipotential precursor population for pancreas and liver within the embryonic endoderm. *Development* **128**, 871-881 (2001).

255. Slack, J.M.W. Metaplasia and transdifferentiation: from pure biology to the clinic. *Nat Rev Mol Cell Bio* **8**, 369-378 (2007).

256. Gu, G.Q., Dubauskaite, J. & Melton, D.A. Direct evidence for the pancreatic lineage: NGN3+cells are islet progenitors and are distinct from duct progenitors. *Development* **129**, 2447-2457 (2002).

257. Baeyens, L. et al. In vitro generation of insulin-producing beta cells from adult exocrine pancreatic cells. *Diabetologia* **48**, 49-57 (2005).

258. Minami, K. et al. Lineage tracing and characterization of insulin-secreting cells generated from adult pancreatic acinar cells. *P Natl Acad Sci USA* **102**, 15116-15121 (2005).

259. Akinci, E., Banga, A., Greder, L.V., Dutton, J.R. & Slack, J.M.W. Reprogramming of pancreatic exocrine cells towards a beta (beta) cell character using Pdx1, Ngn3 and MafA. *Biochem J* **442**, 539-550 (2012).

260. Lima, M.J., Docherty, H.M., Chen, Y.X. & Docherty, K. Efficient differentiation of AR42J cells towards insulin-producing cells using pancreatic transcription factors in combination with growth factors. *Mol Cell Endocrinol* **358**, 69-80 (2012).

261. McKinnon, C.M. & Docherty, K. Pancreatic duodenal homeobox-1, PDX-1, a major regulator of beta cell identity and function. *Diabetologia* **44**, 1203-1214 (2001).

262. Longo, A., Guanga, G.P. & Rose, R.B. Structural basis for induced fit mechanisms in DNA recognition by the Pdx1 homeodomain. *Biochemistry* **46**, 2948-2957 (2007).

263. Jonsson, J., Carlsson, L., Edlund, T. & Edlund, H. Insulin-Promoter-Factor-1 Is Required for Pancreas Development in Mice. *Nature* **371**, 606-609 (1994).

264. Perfetti, R. & Hui, H.X. Pancreas duodenum homeobox-1 regulates pancreas development during embryogenesis and islet cell function in adulthood. *European Journal of Endocrinology* **146**, 129-141 (2002).

265. Stoffers, D.A., Ferrer, J., Clarke, W.L. & Habener, J.F. Early-onset type-II diabetes mellitus (MODY4) linked to IPF1. *Nat Genet* **17**, 138-139 (1997).

266. Ferber, S. et al. Pancreatic and duodenal homeobox gene 1 induces expression of insulin genes in liver and ameliorates streptozotocin-induced hyperglycemia. *Nat Med* **6**, 568-572 (2000).

267. Efrat, S., Zalzman, M. & Anker-Kitai, L. Differentiation of human liver-derived, insulin-producing cells toward the beta-cell phenotype. *Diabetes* **54**, 2568-2575 (2005).

268. Ferber, S. et al. Cell-replacement therapy for diabetes: Generating functional insulin-producing tissue from adult human liver cells. *P Natl Acad Sci USA* **102**, 7964-7969 (2005).

269. Fodor, A. et al. Adult rat liver cells transdifferentiated with lentiviral IPF1 vectors reverse diabetes in mice: an ex vivo gene therapy approach. *Diabetologia* **50**, 121-130 (2007).

270. Horb, M.E., Shen, C.N., Tosh, D. & Slack, J.M.W. Experimental conversion of liver to pancreas. *Curr Biol* **13**, 105-115 (2003).

271. Moon, S.Y. et al. Cellular manipulation of human embryonic stem cells by TAT-PDX1 protein transduction. *Mol Ther* **12**, 28-32 (2005).

272. Yang, L.J. et al. Reversal of streptozotocin-induced diabetes in mice by cellular transduction with recombinant pancreatic transcription factor pancreatic duodenal homeobox-1 - A novel protein transduction domain-based therapy. *Diabetes* **57**, 757-769 (2008).

273. Murtaugh, L.C. & Melton, D.A. Genes, signals, and lineages in pancreas development. *Annu Rev Cell Dev Bi* **19**, 71-89 (2003).

274. Vanderford, N.L., Andrali, S.S. & Ozcan, S. Glucose induces MafA expression in pancreatic beta cell lines via the hexosamine biosynthetic pathway. *J Biol Chem* **282**, 1577-1584 (2007).

275. Naya, F.J., Stellrecht, C.M.M. & Tsai, M.J. Tissue-Specific Regulation of the Insulin Gene by a Novel Basic Helix-Loop-Helix Transcription Factor. *Gene Dev* **9**, 1009-1019 (1995).

276. Desmet, I.A.J.L.B.F.C.V.J. Liver: Biology and Pathobiology The: Organizational principles, Vol. 4. (Lippincott Williams & Wilkins, Philadelphia; 2001).

277. Wilson, J.M. A History Lesson for Stem Cells. *Science* **324**, 727-728 (2009).

278. Chan, L. et al. NeuroD-betacellulin gene therapy induces islet neogenesis in the liver and reverses diabetes in mice. *Nat Med* **9**, 596-603 (2003).

279. Bonner-Weir, S., Noguchi, H., Kaneto, H. & Weir, G.C. PDX-1 protein containing its own antennapedia-like protein transduction domain can transduce pancreatic duct and islet cells. *Diabetes* **52**, 1732-1737 (2003).

280. Noguchi, H. et al. PDX-1 protein is internalized by lipid raft-dependent macropinocytosis. *Cell Transplant* **14**, 637-645 (2005).

281. Swart, A.M.C., Burdett, S., Ledermann, J., Mook, P. & Parmar, M.K.B. Why i.p. therapy cannot yet be considered as a standard of care for the first-line treatment of ovarian cancer: a systematic review. *Ann Oncol* **19**, 688-695 (2008).

282. Guillouzo, A. et al. The human hepatoma HepaRG cells: A highly differentiated model for studies of liver metabolism and toxicity of xenobiotics. *Chemico-Biological Interactions* **168**, 66-73 (2007).

283. Carlotti, F. et al. The 45-kDa form of Pdx-1 does not result from post-translational modifications. *Biochem Bioph Res Co* **370**, 225-229 (2008).

284. Higham, C.E. et al. Processing of synthetic pro-islet amyloid polypeptide (proIAPP) 'amylin' by recombinant prohormone convertase enzymes, PC2 and PC3, in vitro. *European Journal of Biochemistry* **267**, 4998-5004 (2000).

285. Noguchi, H. et al. Induction of pancreatic stem/progenitor cells into insulin-producing cells by adenoviral-mediated gene transfer technology. *Cell Transplant* **15**, 929-938 (2006).

286. Naya, F.J. et al. Diabetes, defective pancreatic morphogenesis, and abnormal enteroendocrine differentiation in BETA2/NeuroD-deficient mice. *Gene Dev* **11**, 2323-2334 (1997).

287. Schwitzgebel, V.M. et al. Expression of neurogenin3 reveals an islet cell precursor population in the pancreas. *Development* **127**, 3533-3542 (2000).

288. Kojima, H. et al. NeuroD-betacellulin gene therapy induces islet neogenesis in the liver and reverses diabetes in mice. *Nat Med* **9**, 596-603 (2003).

289. Song, Y.D. et al. Islet cell differentiation in liver by combinatorial expression of transcription factors Neurogenin-3, BETA2, and RIPE3b1. *Biochem Bioph Res Co* **354**, 334-339 (2007).

290. Kaneto, H. et al. PDX-1/VP16 fusion protein, together with NeuroD or Ngn3, markedly induces insulin gene transcription and ameliorates glucose tolerance. *Diabetes* **54**, 1009-1022 (2005).

291. Appavoo, M. & Tuch, B.E. Effect of upregulation of NeuroD in insulin-producing liver cells. *Islets* **1**, 55-61 (2009).

292. Huang, Y. et al. Reversal of hyperglycemia by protein transduction of NeuroD in vivo. *Acta Pharmacol Sin* **28**, 1181-1188 (2007).

293. Sharma, A. & Stein, R. Glucose-Induced Transcription of the Insulin Gene Is Mediated by Factors Required for Beta-Cell-Type-Specific Expression. *Mol Cell Biol* **14**, 871-879 (1994).

294. German, M.S. & Wang, J.H. The Insulin Gene Contains Multiple Transcriptional Elements That Respond to Glucose. *Mol Cell Biol* **14**, 4067-4075 (1994).

295. Babu, D.A., Chakrabarti, S.K., Garmey, J.C. & Mirmira, R.G. Pdx1 and BETA2/NeuroD1 participate in a transcriptional complex that mediates short-range DNA looping at the insulin gene. *J Biol Chem* **283**, 8164-8172 (2008).

296. Kaneto, H., Matsuoka, T., Katakami, N. & Matsuhisa, M. Combination of MafA, PDX-1 and NeuroD is a Useful Tool to Efficiently Induce Insulin-Producing Surrogate beta-Cells. *Curr Med Chem* **16**, 3144-3151 (2009).

297. Do Kwon, Y. et al. Cellular manipulation of human embryonic stem cells by TAT-PDX1 protein transduction. *Mol Ther* **12**, 28-32 (2005).

298. Lima, M.J., Docherty, H.M., Chen, Y.X., Vallier, L. & Docherty, K. Pancreatic Transcription Factors Containing Protein Transduction Domains Drive Mouse Embryonic Stem Cells towards Endocrine Pancreas. *Plos One* **7** (2012).

299. Liang, Q.L., Mo, Z.Y., Li, X.F., Wang, X.X. & Li, R.M. Pdx1 protein induces human embryonic stem cells into the pancreatic endocrine lineage. *Cell Biol Int* **37**, 2-10 (2013).

300. Schuit, F., Flamez, D., De Vos, A. & Pipeleers, D. Glucose-regulated gene expression maintaining the glucose-responsive state of beta-cells. *Diabetes* **51**, S326-S332 (2002).

301. Bonner-Weir, S. & Weir, G.C. New sources of pancreatic beta-cells. *Nat Biotechnol* **23**, 857-861 (2005).

302. Slack, J.M.W. Developmental Biology of the Pancreas. *Development* **121**, 1569-1580 (1995).

303. Bardeesy, N. & DePinho, R.A. Pancreatic cancer biology and genetics. *Nat Rev Cancer* **2**, 897-909 (2002).

304. Gmyr, V. et al. Adult human cytokeratin 19-positive cells reexpress insulin promoter factor 1 in vitro - Further evidence for pluripotent pancreatic stem cells in humans. *Diabetes* **49**, 1671-1680 (2000).

305. Rooman, I., Heremans, Y., Heimberg, H. & Bouwens, L. Modulation of rat pancreatic acinoductal transdifferentiation and expression of PDX-1 in vitro. *Diabetologia* **43**, 907-+ (2000).

306. Todorov, I. et al. Generation of human islets through expansion and differentiation of non-islet pancreatic cells discarded (pancreatic discard) after islet isolation. *Pancreas* **32**, 130-138 (2006).

307. Longnecker, D.S., Lilja, H.S., French, J., Kuhlmann, E. & Noll, W. Transplantation of Azaserine-Induced Carcinomas of Pancreas in Rats. *Cancer Lett* **7**, 197-202 (1979).

308. Mashima, H. et al. Betacellulin and activin A coordinately convert amylase-secreting pancreatic AR42J cells into insulin-secreting cells. *Journal of Clinical Investigation* **97**, 1647-1654 (1996).

309. Wallace, K., Fairhall, E.A., Charlton, K.A. & Wright, M.C. AR42J-B-13 cell: An expandable progenitor to generate an unlimited supply of functional hepatocytes. *Toxicology* **278**, 277-287 (2010).

310. Pinho, A.V. et al. Adult pancreatic acinar cells dedifferentiate to an embryonic progenitor phenotype with concomitant activation of a senescence programme that is present in chronic pancreatitis. *Gut* **60**, 958-966 (2011).

311. Vila, M.R., Lloreta, J. & Real, F.X. Normal human pancreas cultures display functional ductal characteristics. *Lab Invest* **71**, 423-431 (1994).

312.   Aldibbiat, A. et al. Inability to process and store proinsulin in transdifferentiated pancreatic acinar cells lacking the regulated secretory pathway (vol 196, pg 33, 2005). *J Endocrinol* **199**, 149-149 (2008).

313.   Mashima, H., Shibata, H., Mine, T. & Kojima, I. Formation of insulin-producing cells from pancreatic acinar AR42J cells by hepatocyte growth factor. *Endocrinology* **137**, 3969-3976 (1996).

314.   Palgi, J., Stumpf, E. & Otonkoski, T. Transcription factor expression and hormone production in pancreatic AR42J cells. *Mol Cell Endocrinol* **165**, 41-49 (2000).

315.   Zhang, Y.Q., Mashima, H. & Kojima, I. Changes in the expression of transcription factors in pancreatic AR42J cells during differentiation into insulin-producing cells. *Diabetes* **50**, S10-S14 (2001).

316.   Umezawa, K. et al. Induction of insulin production in rat pancreatic acinar carcinoma cells by conophylline. *Biomed Pharmacother* **57**, 341-350 (2003).

317.   Tosh, D. & Slack, J.M.W. How cells change their phenotype. *Nat Rev Mol Cell Bio* **3**, 187-194 (2002).

318.   Bernardo, A.S., Hay, C.W. & Docherty, K. Pancreatic transcription factors and their role in the birth, life and survival of the pancreatic beta cell. *Mol Cell Endocrinol* **294**, 1-9 (2008).

319.   Yu, J.Y. et al. Human Induced Pluripotent Stem Cells Free of Vector and Transgene Sequences. *Science* **324**, 797-801 (2009).

320.   Chen, X. et al. Integration of external signaling pathways with the core transcriptional network in embryonic stem cells. *Cell* **133**, 1106-1117 (2008).

321.   Episkopou, V. SOX2 functions in adult neural stem cells. *Trends Neurosci* **28**, 219-221 (2005).

322.   Miyagi, S. et al. The Sox-2 regulatory regions display their activities in two distinct types of multipotent stem cells. *Mol Cell Biol* **24**, 4207-4220 (2004).

323.	Gordan, J.D., Thompson, C.B. & Simon, M.C. HIF and c-Myc: sibling rivals for control of cancer cell metabolism and proliferation. *Cancer Cell* **12**, 108-113 (2007).

324.	Shi, Y. et al. Induction of Pluripotent Stem Cells from Mouse Embryonic Fibroblasts by Oct4 and Klf4 with Small-Molecule Compounds. *Cell Stem Cell* **3**, 568-574 (2008).

325.	Loh, Y.H. et al. The Oct4 and Nanog transcription network regulates pluripotency in mouse embryonic stem cells. *Nat Genet* **38**, 431-440 (2006).

326.	Viswanathan, S.R., Daley, G.Q. & Gregory, R.I. Selective blockade of MicroRNA processing by Lin28. *Science* **320**, 97-100 (2008).

327.	Yamamoto, A., Kormann, M., Rosenecker, J. & Rudolph, C. Current prospects for mRNA gene delivery. *Eur J Pharm Biopharm* **71**, 484-489 (2009).

328.	Parker, A.L. & Seymour, L.W. Targeting of polyelectrolyte RNA complexes to cell surface integrins as an efficient cytoplasmic transfection mechanism. *J Bioact Compat Pol* **17**, 229-238 (2002).

329.	Rolland, A. Nuclear gene delivery: the Trojan horse approach. *Expert Opin Drug Deliv* **3**, 1-10 (2006).

330.	Khalil, I.A., Kogure, K., Akita, H. & Harashima, H. Uptake pathways and subsequent intracellular trafficking in nonviral gene delivery. *Pharmacol Rev* **58**, 32-45 (2006).

331.	Rabinovich, P.M. et al. Synthetic messenger RNA as a tool for gene therapy. *Hum Gene Ther* **17**, 1027-1035 (2006).

332.	Probst, J. et al. Spontaneous cellular uptake of exogenous messenger RNA in vivo is nucleic acid-specific, saturable and ion dependent. *Gene Ther* **14**, 1175-1180 (2007).

333.	Mockey, M. et al. mRNA transfection of dendritic cells: Synergistic effect of ARCA mRNA capping with Poly(A) chains in cis and in trans for a high protein expression level. *Biochem Bioph Res Co* **340**, 1062-1068 (2006).

334. Holtkamp, S. et al. Modification of antigen-encoding RNA increases stability, translational efficacy, and T-cell stimulatory capacity of dendritic cells. *Blood* **108**, 4009-4017 (2006).

335. McIvor, R.S. Therapeutic Delivery of mRNA: The Medium Is the Message. *Mol Ther* **19**, 822-823 (2011).

336. Urnov, F.D., Rebar, E.J., Holmes, M.C., Zhang, H.S. & Gregory, P.D. Genome editing with engineered zinc finger nucleases. *Nat Rev Genet* **11**, 636-646 (2010).

337. Wilber, A. et al. Messenger RNA as a source of transposase for Sleeping Beauty transposon-mediated correction of hereditary tyrosinemia type I. *Mol Ther* **15**, 1280-1287 (2007).

338. Wolff, J.A. et al. Direct Gene-Transfer into Mouse Muscle Invivo. *Science* **247**, 1465-1468 (1990).

339. Hoerr, I., Obst, R., Rammensee, H.G. & Jung, G. In vivo application of RNA leads to induction of specific cytotoxic T lymphocytes and antibodies. *Eur J Immunol* **30**, 1-7 (2000).

340. Malone, R.W., Felgner, P.L. & Verma, I.M. Cationic Liposome-Mediated Rna Transfection. *P Natl Acad Sci USA* **86**, 6077-6081 (1989).

341. Zohra, F.T., Chowdhury, E.H. & Akaike, T. High performance mRNA transfection through carbonate apatite-cationic liposome conjugates. *Biomaterials* **30**, 4006-4013 (2009).

342. Martinon, F. et al. Induction of Virus-Specific Cytotoxic T-Lymphocytes in-Vivo by Liposome-Entrapped Messenger-Rna. *Eur J Immunol* **23**, 1719-1722 (1993).

343. Bettinger, T., Carlisle, R.C., Read, M.L., Ogris, M. & Seymour, L.W. Peptide-mediated RNA delivery: a novel approach for enhanced transfection of primary and post-mitotic cells. *Nucleic Acids Research* **29**, 3882-3891 (2001).

344. Read, M.L. et al. A versatile reducible polycation-based system for efficient delivery of a broad range of nucleic acids. *Nucleic Acids Research* **33** (2005).

345. Qiu, P., Ziegelhoffer, P., Sun, J. & Yang, N.S. Gene gun delivery of mRNA in situ results in efficient transgene expression and genetic immunization. *Gene Ther* **3**, 262-268 (1996).

346. Vassilev, V.B., Gil, L.H.V.G. & Donis, R.O. Microparticle-mediated RNA immunization against bovine viral diarrhea virus. *Vaccine* **19**, 2012-2019 (2001).

347. Kyte, J.A. et al. Phase I/II trial of melanoma therapy with dendritic cells transfected with autologous tumor-mRNA. *Cancer Gene Ther* **13**, 905-918 (2006).

348. Van Driessche, A. et al. Clinical-grade manufacturing of autologous mature mRNA-electroporated dendritic cells and safety testing in acute myeloid leukemia patients in a phase I dose-escalation clinical trial. *Cytotherapy* **11**, 653-668 (2009).

349. Van Tendeloo, V.F.I. et al. Highly efficient gene delivery by mRNA electroporation in human hematopoietic cells: superiority to lipofection and passive pulsing of mRNA and to electroporation of plasmid cDNA for tumor antigen loading of dendritic cells. *Blood* **98**, 49-56 (2001).

350. Kawai, T. & Akira, S. The role of pattern-recognition receptors in innate immunity: update on Toll-like receptors. *Nat Immunol* **11**, 373-384 (2010).

351. Hornung, V. et al. 5 '-triphosphate RNA is the ligand for RIG-I. *Science* **314**, 994-997 (2006).

352. Pichlmair, A. et al. RIG-I-mediated antiviral responses to single-stranded RNA bearing 5 '-phosphates. *Science* **314**, 997-1001 (2006).

353. Nallagatla, S.R., Toroney, R. & Bevilacqua, P.C. A brilliant disguise for self RNA 5 '-end and internal modifications of primary transcripts suppress elements of innate immunity. *Rna Biol* **5**, 140-144 (2008).

354. Kariko, K., Buckstein, M., Ni, H.P. & Weissman, D. Suppression of RNA recognition by Toll-like receptors: The impact of nucleoside modification and the evolutionary origin of RNA. *Immunity* **23**, 165-175 (2005).

355. Nallagatla, S.R. & Bevilacqua, P.C. Nucleoside modifications modulate activation of the protein kinase PKR in an RNA structure-specific manner. *Rna* **14**, 1201-1213 (2008).

356. Nagai, T. et al. A variant of yellow fluorescent protein with fast and efficient maturation for cell-biological applications. *Nat Biotechnol* **20**, 87-90 (2002).

357. Nilsen, T.W. & Rio, D.C. In vitro transcription of labeled RNA: synthesis, capping, and substitution. *Cold Spring Harb Protoc* **2012**, 1181-1186 (2012).

358. Kormann, M.S.D. et al. Expression of therapeutic proteins after delivery of chemically modified mRNA in mice. *Nat Biotechnol* **29**, 154-U196 (2011).